Università degli studi di Napoli “Federico II”

Università degli studi di Napoli ‘Parthenope’

Stratospheric dust collection by DUSTER (Dust in The Upper Stratosphere Tracking Experiment and Retrieval), a balloon-borne instrument, and laboratory analyses of collected dust.

Submitted for the degree of

Philosophiae Doctor in Aerospace Engineering

Alessandra Ciucci

Advisor: Prof. Pasquale Palumbo

Co-advisor: Prof. Frans J. M. Rietmeijer

Coordinator : Prof. Antonio Moccia

“Everything is determined, the beginning as well as the end, by forces over which we have no control. It is determined for insects as well as for the stars. Human beings, vegetables or cosmic dust, we all dance to a mysterious tune, intoned in the distance by an invisible piper”

Albert Einstein

Abstract

The subject of this work is focused on the study of stratospheric dust with DUSTER (Dust in the Upper Stratosphere Tracking Experiment and Retrieval) a balloon-borne instrument.

The stratospheric environment is an atmospheric layer placed in the range altitude 20-50 km. The stratosphere is composed of aerosols (mostly H_2SO_4 and NO_x) and refractory dust of different nature: natural terrestrial dust, anthropogenic dust, and natural extraterrestrial dust (see Chapter 1 for more details).

The DUSTER project is aimed at uncontaminated collection of stratospheric dust particles, in the submicron/micron range. The submicron/micron size range was chosen because: 1) it is poorly studied so far; 2) particles of natural terrestrial origin in this size range are responsible of local and global climate changing; 3) particles of natural extraterrestrial origin in submicron/micron range suffer less the heating due to the entry in the Earth atmosphere and subsequently they are less altered in the original physico-chemical characteristics.

The DUSTER scientific aim is to derive the size distribution, the concentration and the composition of stratospheric dust, to study the natural and the extraterrestrial component. To reach its aim DUSTER implies in-situ collection and sample recovering to perform laboratory analyses without sample manipulation.

The technical requirement of the instrument are: capability to work autonomously during the balloon flight in the range altitude of 30 – 40 km; capability to work at temperatures in the range -40°C < T < 80°C and pressure in the range 3 – 10 mbar; sampling at least 20 m^3 of air for at least 24 h of continuous working; samples storage and retrieval under contamination controlled conditions (see Chapter 2 for more details).

The particles are captured based on the principle of inertial impact collection (without the use of sticking materials) by a continuous flow created through the chamber.

DUSTER had a qualification flight in January 2006 from Kiruna (Sweden) and two scientific flights from Svalbard (Norway) in June 2008 and July 2009.

This work is a report of the two scientific flights from the sample holder preparation to the analyses of collected samples. In particular, it will deal with:

- the sample holders structure, how to assemble them (see Chapter 2 for more details) and their implementation for DUSTER 2009 campaign (see Chapter 6 for more details);
- the instrument characteristics for DUSTER 2008 campaign and the improvements for DUSTER 2009 campaign;
- the curation, to ensure the contamination control, and the characterization of the sample holders, to identify the particles actually collected from the spurious contamination (see Chapter 4 for more details);
- the techniques used to characterize the sample holder before and after the flights and to analyze the sample collected (see Chapter 3 for more details);
- the procedure to recognize the collected particles from the spurious contamination;
- the sources of contamination due to the environment and to the sample holders materials (see Chapter 4 for more details);
- the data reduction of the analyses performed on samples collected during DUSTER 2008 campaign (see Chapter 5 for more details);
- a very preliminary analysis to identify particles collected during DUSTER 2009 campaign (see Chapter 6 for more details).

The strength of DUSTER is to collect particles in a boundary layer in which could be found particles coming from extraterrestrial (e.g. interplanetary dust particles) and terrestrial environment (e.g. volcanic ash) mixed in an environment clean by human pollution.

1 Stratospheric particles

The terrestrial atmosphere is divided into different layers diverse each other for altitude, pressure and temperature. From the ground to the space environment there are: troposphere, stratosphere, mesosphere, thermosphere and exosphere.

The troposphere and stratosphere extend from the ground until 50 km. In the troposphere the temperature decreases with the altitude until -60 °C, in the stratosphere the temperature increases until 0 °C (Figure 1.1) due to the presence of an ozone layer that absorbs the ultraviolet radiation coming from the Sun.

In the mesosphere layer the temperature decreases until -90 °C; in this layer the destruction of meteors that enter Earth's atmosphere occurs and the light elements relative abundances slowly increase to the detriment of the heaviest. In the thermosphere the temperature increases; this is considered the last atmospheric layer. Above 100 km, the environment is very rarefied and it is possible to put a spacecraft in orbit around Earth. The exosphere is a range in which there is a gradual passage from atmosphere to the space environment.

This work is focuses on stratosphere. It contains aerosols typically in the size range 0.1 – 1 µm, and a solid component (hereinafter, particles) that can be larger than 1 µm. The stratospheric particles can be of different origins: natural terrestrial, anthropogenic and extraterrestrial. Stratosphere is relatively accessible and close to the surface and at the same time it is a clean environment where to collect particles for laboratory studies with a significant fraction of extraterrestrial materials. Finally, stratospheric particles are relatively poorly studied, having in any case strong impact on atmosphere physical status and chemical processes.

In this chapter the different kind of particles populating the stratosphere are presented together with the experiments performed up to now in situ or through sample return to study the stratospheric environment.

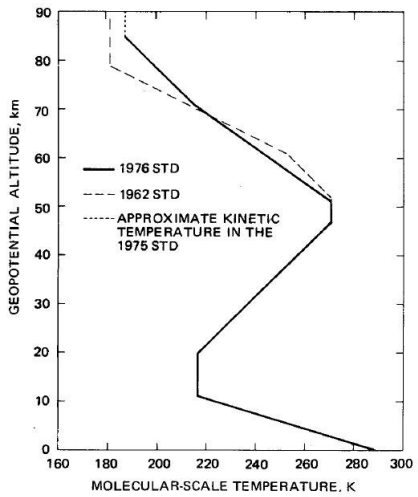

Figure 1.1 Molecular-scale temperature as a function of geopotential altitude (US Standard Atmosphere 1976)

1.1 Aerosols in stratosphere

The US Standard Atmosphere model defines the typical value for temperature, pressure, density and composition of the different layers of Earth's atmosphere. In Table 1.1 the typical concentration of troposphere constituents near the Earth's surface are reported, but that values change with altitude and latitude.

The Nitrous Oxide is between 250 – 100 ppbv in the altitude range of 13 -18 km. The Nitric Oxide and the Nitrogen Dioxide have a similar behavior: the NO has an estimated mixing ratio varying from about 0.1 ppbv at 16 km and 5 ppv at 40 km; the NO_2 goes from 1 – 10 ppbv in the altitude range 12 - 28 km and increase from 20 -28 km. The Nitric Acid vapor is 2 ppbv at about 18 km and 5 ppbv at 24 km maintaining an high concentration until 30 km. Instead Hydrogen reaches the highest value at 28 km and decreases above it. Carbon Monoxide has both anthropogenic and natural sources, it has been found in troposphere, while CO_2 can be found in stratosphere too, but 0.6 ppmv less than in troposphere (US Standard Atmosphere 1976).

In Figure 1.2 the Ozone model density is shown; it reaches the maximum concentration in lower stratosphere, the high presence of Ozone in unpolluted regions near the Earth's surface is probably formed in stratosphere and brought down by the vertical transport process; the presence of water vapor in stratosphere is attribute to this process.

A study of aerosol type, concentration and size distribution that combined theoretical data with observations was done using two balloon-born instruments: Spectroscopie d'Absorpion Lunaire pour l'Observation des Minoritaires Ozone et NO_x (SALOMON), and Laboratiorie de Météorologie Dynamique (LMD).

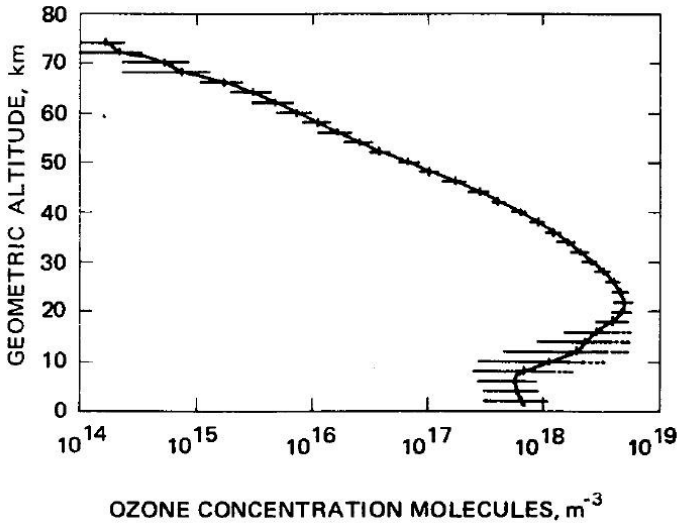

Figure 1.2 Mid-latitude ozone model density as a function of height

Constituent	Typical concentration in parts per billion per volume (ppbv)
N_2O	270
NO	0.5
NO_2	1
H_2S	0.05
NH_3	4
H_2	500
CH_4	1500
SO_2	1
CO	190
CO_2	3.22×10^5
O_3	40

Table1.1 Concentration of tropospheric constituent near the Earth's surface (US Standard Atmosphere data)

These experiments confirmed the presence of aerosols around 30 km. The unexpected results were: particles with a size dimensions bigger than 1 μm (Figure 1.3); particles composed of a mixture of H_2SO_4 and water vapor, typical of aerosol present in lower stratosphere and not suppose to be at that altitude (Renard et al. 2005). They hypothesized that the identified particles can be soot of terrestrial or extraterrestrial origin, from coagulation process or from vaporization of micrometeorites during entry in atmosphere respectively. The data provided by SALOMON and LMD suggested that the main population of solid particles present in middle stratosphere can be originated by interplanetary medium.

At any given time in stratosphere there are different kinds of solid particles: some are originated at the Earth's surface due to natural and anthropogenic processes, others are of extraterrestrial origins, viz. (1) a wide range of different interplanetary dust particles, (2) condensed meteoric dust from sublimating meteors that so far has eluded collection, (3) residues of meteorite and micrometeorite ablation in the mesosphere or cometary fragments.

The alteration of Stratospheric Aerosol (SA) population may cause alteration in the global stratospheric dynamics (Pitari et al. 1993), the ozone depletion (Hofmann et al. 1993, Chandra 1993), the stratospheric heating (Angell 1997, Parker e Brownscombe 1983) and solar radiance

variations (as during Pinatubo eruption of June 1991 (Dutton and Christy 1992)). For these reasons it is important to study and characterize stratospheric particles and their dynamics.

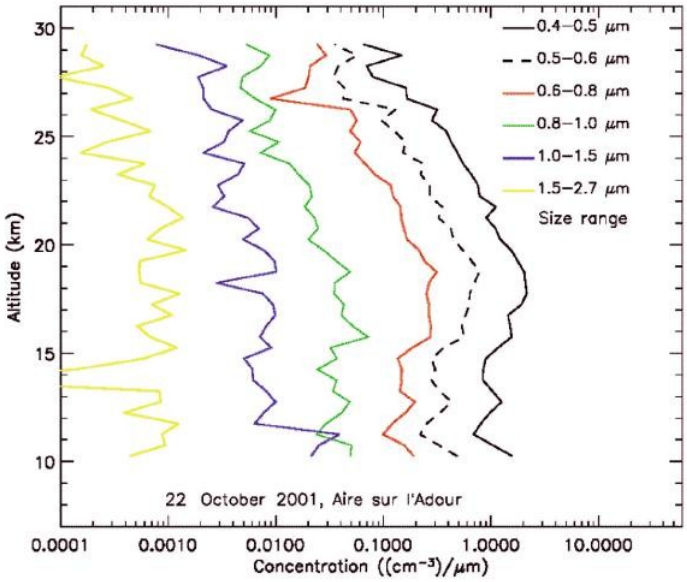

Figure 1.3 Vertical distribution of six diameter class of aerosols obtained on 22 October 2001 by the LMD counter (after Renard et al. 2005)

1.1.1 Terrestrial natural and anthropogenic particles

The particles of natural terrestrial origins are typically volcanic ashes, wind-blown dust and condensed aerosols. The Stratospheric Sulfate Aerosols (SSA) are produced by the interaction between SO_2 and water condensed particles; sulfur dioxide can be transported from the tropical tropopause, or photochemically produced in the mid-stratosphere after ultraviolet photolysis of carbonyl sulfide (Rodhe et al. 1985).

The presence of volcanic ashes in the stratosphere and their effects were studied after Fuego (14°N, October 1974, 3–6 Tg of aerosol) eruption and especially during the El Chichòn (17°N, April 1982, 12 Tg of aerosols) and Pinatubo eruptions (15 °N, June 1991, 30 Tg of aerosols) (McCormick et al., 1995). Following Kerr (1983), the volcanic cloud after El Chichòn eruption extended in the latitude range of 10°S and 30°N; a temperature rise of 3°C was measured around 26 km and its cause was almost entirely attributed to sunlight absorption. After Pinatubo eruption the enhancement of stratospheric aerosol caused a disturbance of the twilight sky radiative field (Mateshvili et al. 2005) and the increasing of the temperature (Saxena et al. 1997).

A size distribution of SA after Pinatubo eruption and its changing with years was provided by Deshler (2008). One year lather the eruption, the SA were well mixed, particles > 0.78 μm were observed over 20 km; 15 years lather particles > 0.5 μm were observed in stratosphere and there

is a difference in concentration of Condensation Nuclei (CN) in particles > 0.15 µm and increasing with size (Figure 1.4).

The changing of size distribution during time and the removal of same particles from stratosphere is due to the gravitational settling; the nucleation and condensation of aerosols increase the size and the heaviest particles are moved close to the tropopause and subsequently moved in the troposphere by the exchange process between troposphere and stratosphere.

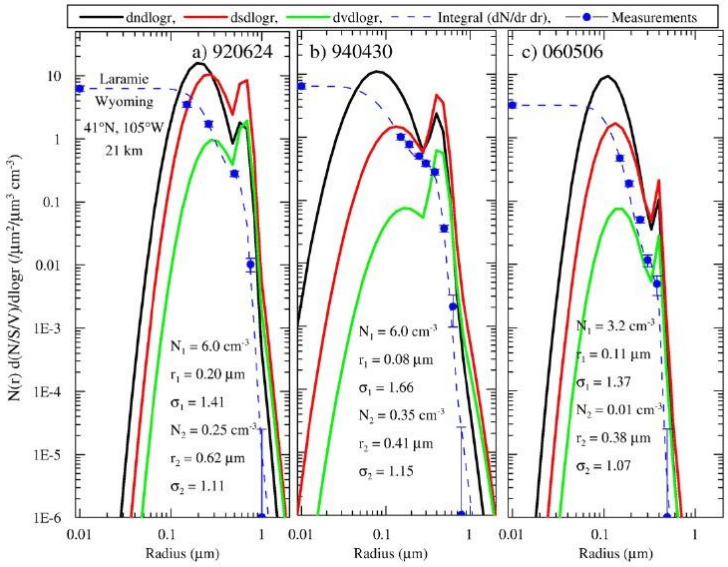

Figure 1.4 Differential number (cm^{-3}), surface area ($\mu m^2\ cm^{-3}$), and volume ($\mu m^3\ cm^{-3}$) distributions, as a function of $dlog_{10}(r)$ derived from fitting bimodal lognormal size distributions to in situ optical particle counter measurements at 21 km above Laramie, Wyoming (Deshler et al., 2003). The cumulative number distribution (the blue data points), and the fitted distribution (the blue dashed line). The size distributions are representative of measurements a) one year, b) 3 years, and c) 15 years after the Pinatubo eruption.

During volcanically quiescent periods SA (in particular sulfuric acid and water vapor) affect the budget of several trace of gases, in particular NO_x, while after volcanic activity SA may increase the abundance of chlorine (Hanson and Lovejoy, 1995).

Particles of anthropogenic origins are typically residual of solid-fuel rocket exhaust, coal- and oil-burning and power plants residuals. Evidences of propellant residuals particles came from the first experiment of collection in stratosphere (at 34 km) performed by Brownlee in 1970. The majority of the particles collected by that experiment in the size range 3 – 8 µm were spheres of Al_2O_3 originated by fuel residuals (Brownlee et al. 1973).

The others typical sources of particles of anthropogenic origin are power plant combustion and coal combustion products (CCP). In Svalbard Islands there are coal power plants that produce coal fly ash and heavy metal pollution in the region, as found studying sediments of the iced Lake of Bolterskardet (Qing et al. 2006). In China, where coal is the basic energy source (about 84% of total production), the presence of Fluorine pollution was studied because of its harmful effects; when the coal is burnt at mid-low temperature (800 - 1200 °C) power station, only 20% of

Fluorine remain in the cinder and the rest is divided between 5% trapped in coal fly ash and 75% directly injected in the atmosphere (Luo et al. 2002).

All these components could be found on stratosphere because of the convective upward transport from tropical tropopause (Pitari et al. 1993).

1.1.2 Extraterrestrial particles

The sources of dust population are comets and asteroids (from the inner Solar System), Kuiper belt dust and interstellar dust (from outer Solar System).

Meteorites or Interplanetary Dust Particles (IDPs) are fragment of rocks and metals from other bodies in the Solar System that have fallen to the Earth and survive to the passage through the atmosphere. The difference is mainly the size, the IDPs being typically 10 – 100 μm while meteorites can reach several meters. The IDPs can be originated by collision between small bodies, such as bodies in the main asteroid belt, meteoroids impact on the asteroids and interaction with near Earth asteroids, or by sublimation of active comet nuclei during the perihelion transit (Rietmeijer 2000).

These particles are the responsible of the Zodiacal light. It is the diffuse light in the night sky, enhanced in the ecliptic, also called Zodiacal line (from which the name of the effect). The light is actually extended across the entire night sky, but being the particles distributed principally in the Sun equatorial plane the light is stronger in the ecliptic line. Due to the Pointing-Robertson effect, these particles has a spiral motion toward to the Sun; for this reason the density of particles between 0.1 – 100 μm increases with decreasing distance from the Sun proportional to r^{-1} (where r is the distance from the Sun).

The particles in this size range are the most abundant in 1 AU range from the Sun (Rietmeijer 2002). The heating and melting of the particle during the deceleration is function of the size, density, mineralogy, entry angle and entry velocity (Love and Brownlee 1994). Being the IDPs very small (<100 μm), they are able to survive to the atmospheric entry with some thermal alteration; instead the meteoroids (in a size range from 100 μm up to same meters) will not survive to the atmospheric entry and typically produced ablation debris.

The interstellar dust is originated by the loosing mass of stars that are in the last evolutionary stage or by supernovae explosion. The gas flux from the stars, during the expansion, cools down and reaches the condition to allow solid dust particles condensation. Interstellar dust was identified at 5 AU by the Ulysses dust detector (Grün et al., 1993), and inside 1AU it is estimated less abundant than in the outer Solar System (Grün et al., 1994). In particular at 1AU the interstellar dust component is less than 3% of the interplanetary component (McDonnel & Berg, 1975).

The IDPs collected in stratosphere are classified combining the chemical composition and the morphological class (Figure 1.5). They can be chondritic or non chondritic IDPs.

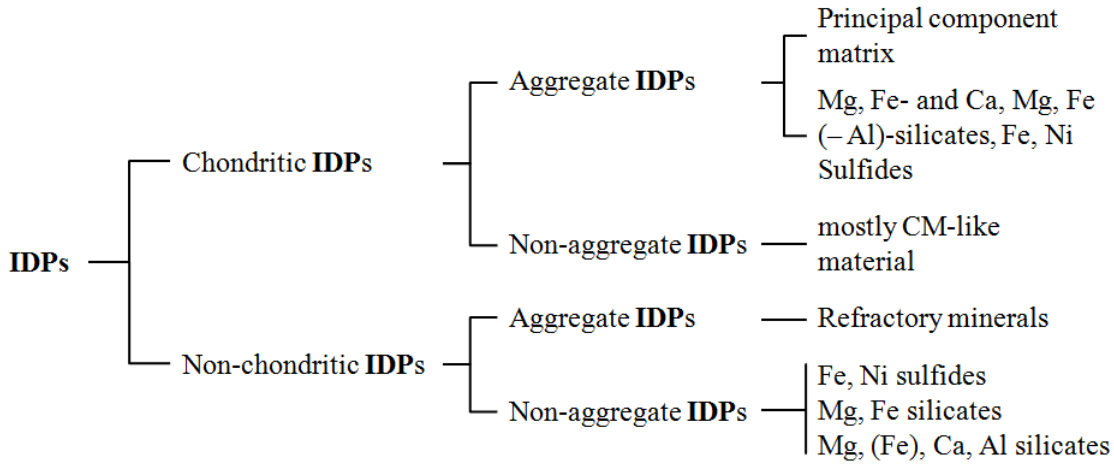

Figure 1.5 Chemical and morphological classification of interplanetary dust particles collected in Earth's lower stratosphere (Rietmeijer 2002).

Chondrites are aggregate of dust or small grains formed in oxygen-rich regions of the early solar system so that most of the metal is not found in its free form but as silicates, oxides, or sulfides. Chondrites are divided into different class differentiated by composition, the most primitive are the CI type (Table 1.2).

Chondritic IDPs can be Aggregate or non-aggregate. In the first case they are a matrix of principal components (< 1µm) with embedded grains (~ 5 µm) compose of Ca, Mg, Fe-silicates, iron dioxide or amorphous materials. The non-aggregate types are typical CM-like materials (Table 1.2) compose of Silicates (Mg, Fe-silicates or Mg(Fe), Ca, Al-silicates), Sulfides (Ni-free or low-Ni pyrrhotite) or refractory (Ca, Ti, Al-rich) (Rietmeijer 2002).

1.2 Studies of stratospheric aerosols

Stratospheric dust has been studied in-situ (e.g. Optical Particle Counters), by remote sensing (e.g. twilight method, spectrometric methods or LIDAR) or in-situ sample collection (e.g. using flat plate collectors mounted underneath the wings of high-flying aircraft, or air aspiration systems). Usually the OPC (Optical Particle Counter) are easily mounted on the balloon-born instruments, so they could be present in remote sensing or in-situ experiments. In the next sections the experiments performed in stratosphere until now and the results obtained are shown.

Species	*CI type*	*CM type*
SiO_2	22.69	28.97
TiO_2	0.07	0.13
Al_2O_3	1.70	2.17
Cr_2O_3	0.32	0.43
Fe_2O_3	13.55	-
FeO	4.63	22.14
MnO	0.21	0.25
MgO	15.87	19.88
CaO	1.36	1.89
Na_2O	0.76	0.43
K_2O	0.06	0.06
P_2O_5	0.22	0.24
H_2O^+	10.80	8.73
H_2O^-	6.10	1.67
Fe^0	-	0.14
FeS	9.08	5.76
C	2.80	1.82
S (element)	0.10	-
NiO	1.33	1.71
CoO	0.08	0.08
SO_3	5.63	1.59
CO_2	1.50	0.78
TOTAL	98.86	99.82

Table 1.2 Average chemical compositions of chondrites CI and CM type.

1.2.1 Remote sensing

From late 1979 two similar experiments studied the atmosphere with remote sensing techniques: the SAGE I (Stratospheric Areosol Gas Experiment 1979-1981) and SAM II (Stratospheric Aerosol Measurements 1978-1993). They are satellite experiments based on Sun photometers to measure the extinction of solar radiation produced by aerosol in the Earth atmosphere (McCormick et al.1979). Because of the attenuation of tropospheric clouds, data are available above 5 km; the variation of 1 µm tropospheric aerosol with latitude, season and altitude as well as changes due to volcanic injection of material into the stratosphere has been highlighted (Kent et al. 1988).

From 1981 to 1985, during a period of strong volcanic activity (El Chichòn and Pinatubo eruptions), the stratospheric dust was tracked using the twilight sounding method (TSM) capable of covering an altitude range between 20 and 140 km (Mateshvili and Rietmeijer 2002). This method allowed to study the distribution of volcanic dust and the life time of that particles into the stratosphere. The volcanic ash had the maximum concentration in stratosphere immediately after the eruption and decays in few months; instead the condensed aerosols have the maximum few months after the volcanic event.

A campaign of LIDAR (Light Detection and Ranging) observations was performed from Thule in Greenland through the period 1990-1997 to study the Polar Stratospheric Clouds (PSCs). They observed that the PSC formation depends by the evolution of polar vortex, altitude, temperature and on the variable structure (they noted that a kind of PSC formed mainly after Pinatubo eruption). From the observation it was derived that the PSCs were made of crystals less than 2 µm in size (more than 2 µm appears unlikely) with a water (more than expected) and nitric acid composition (Di Sarra et al. 2002).

The two balloon borne instruments AMON (Absorbition by the Minor components Ozone and Nox 1991-2003) and SALOMON (Spectroscopie d'Absorbition Lunaire pour l'Observation des Minoritaries), are designed to perform measurements of stratospheric trace-gas species (O_3, NO_2, NO) in the polar vortex in UV-VIS range. They concluded that each flight had its own peculiarity depending on events, such as volcanic injections, and that most spectral signatures differ significantly from the background aerosol (Berthet 2002).

During the same period (April - May 1998 and September 1999) there were same experiments on stratospheric aerosol managed with a laser ion mass spectrometer on board of an aircraft from 5 to 19 km. The instrument collected more than 2500 spectrum of aerosol between 0.2 - 3 µm. Those spectra suggest that many particles may contain extraterrestrial material coming from meteoritic ablation, confirming the descending of material from mesosphere to stratosphere, and the presence of mercury at 19 km altitude, showing that the terrestrial emission come up into the lower stratosphere (Murphy et al. 1998). Taking into consideration the composition of typical chondrites and the ablation phenomena, it results that in lower stratosphere until the sulphates layer the material is mostly of terrestrial origin, and in upper stratosphere the sulphate is dominated by the extraterrestrial component (Figure1.6) coming from ablation of micrometeorites (Cziczo et al. 2001).

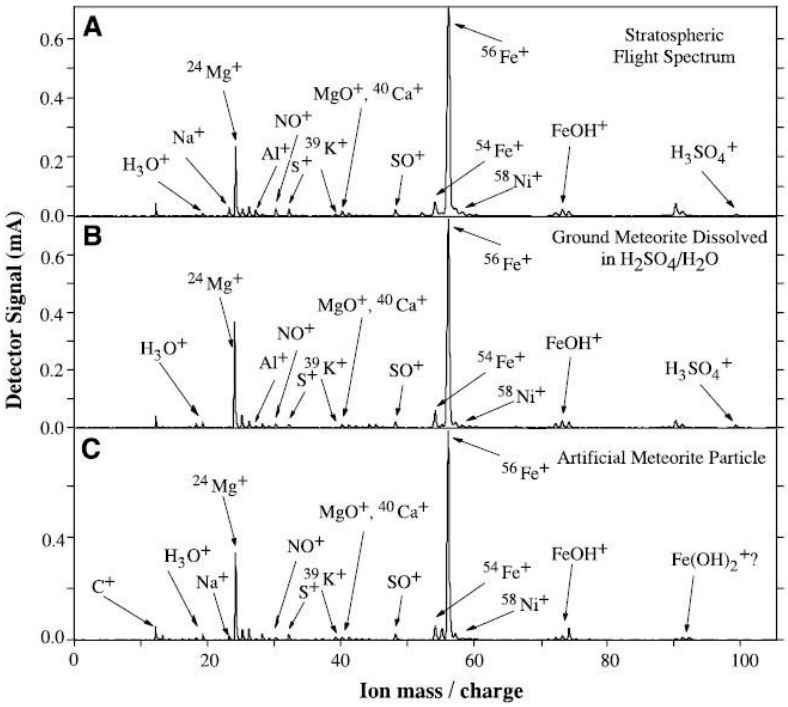

Figure 1.6 Typical positive ion mass spectra. (A) Stratospheric aerosol particle that contained meteoritic material. (B) Ground meteorite particle composed of H-group chondritic matter (Field Museum of Natural History sample Me 2076) dissolved in 65 wt % sulfuric acid such that there was ≤ 1.0 wt% Fe in solution (some fraction, possibly SiO2, remained visibly undissolved). (C) Artificial meteorite particle prepared in the laboratory that was 65 wt % sulfuric acid, 0.75 wt % Fe, 0.23 wt % Mg, and minor species in the abundance found in chondritic meteorites with respect to the given iron concentration. Particle mass is balanced by H_2O in all cases. (Courtesy of Cziczo et al 2001).

In-situ observations of lower stratosphere were done within the Arctic and Antarctic polar vortexes. In 1987 a balloon-borne instrument with condensation nucleus counter (CNC) and eight channel aerosol detectors were flown from McMurdo station in Antarctic until 22 km altitude, and in 1989 the same instrument was flown from Kiruna (Sweden 68°N) until 31 km altitude. The results from Antarctic zone show two different aerosol types, large particles of nitric acid (~1 µm) and small sulphate particles; under -79°C the two types are melted, and under -85°C the concentration of the two distributions grow up suggesting the simultaneous nucleation and growth phenomena (Hofmann et al. 1989). The results of Arctic zone are very similar to the Antarctic zone, they found strong level of CN above 18 km suggesting homogeneous and ionic nucleation (Hofmann et al. 1990). In the Arctic zone also flown on January and February 1989 an air-borne instrument, compose of a passive cavity aerosol spectrometer and CNC. The results showed that it seems to exist, in upper troposphere and lower stratosphere, a region of newly formed small (0.02 – 1 µm) particles (Wilson et al. 1992), moreover the CN particles production is important for Polar Stratospheric Clouds (PSC) formation and the concentration can affect PSC properties (Wilson et al. 1990). More recently, from January to March 2003, an aircraft-borne instrument was flown from Kiruna (Sweden) for in-situ measurements of Arctic lower stratosphere (10 - 20.5 km altitude) inside and outside the polar vortex. The instrument was composed of a two channel aerosol counter COPAS (COndensation PArticle counter System) with

a cut off of 0.01 µm and a modified Forward Scattering Spectrometer Probe FSSP-300 able to measure aerosol particles between 0.4 - 23 µm. The COPAS experiment confirmed the aerosol nucleation above 19 km, and detect a fraction of 58-76% of non-volatile particles inside the vortex and 12-45% outside. This difference was attributed to the vertical transport of meteoritic material from mesosphere to the lowest level of polar vortex (Curtius et al. 2005).

1.2.2 In-Situ collection

During the last 50 years there have been research projects aimed at study aerosol and stratospheric dust in laboratory, so they need sample return experiment. For this reason several balloon born instruments and special collector for rockets and airplanes were developed.

Junge at al. (1961) sampled the atmosphere until 30 km of altitude with a cascade inertial impactor carried aloft on a stratospheric balloon, and used an optical particle counter (OPC) to determine the concentration and the vertical profile of aerosol particle <0.1 µm. The experiment collected particles in a constant size distribution, with a maximum in the range between 0.01-0.1 µm. The particles can be divided into three major classes: (1) particles <0.1µm from the troposphere; (2) particles in the range (0.1-1.0) µm formed within the troposphere, the analyses shown composition based on sulphur with traces of iron and silicon; (3) particle >1.0 µm of extraterrestrial origin (this last had a low frequency and for this reason less studied in this experiment).

Brownlee et al. (1973) collected stratospheric particles at about 35 km of altitude using a rocket, mostly Al_2O_3 spherical particles and a 10% of IDPs; the spheres are anthropogenic particles produced by burning fuel rockets and lying in the altitude range 25-35 km with a density of $10^{-2}m^{-3}$ (Brownlee et al. 1976).

NASA has a long-term stratospheric dust collection program using high-flying (WB and U2) aircraft fitted with inertial-impact, flat-plate collectors coated by high viscosity silicon oil layer to collect dust particles at about 20 km altitude (Zolensky and Warren 1994). The collected solid dust particles range between ~2 and 150 µm of natural extraterrestrial (comic dust) and terrestrial origins and anthropogenic origins, e.g. aluminium or aluminium oxide spheres that are solid rocket effluents (Mackinnon et al. 1982, Zolensky and Mackinnon 1985, Zolensky et al. 1989). The collected particles receive a provisional identification based on their morphological, optical and chemical properties (Figure1.7) and are then listed in the NASA Johnson Space Center catalogues (Cosmic Dust Catalogues, volumes 1 through 17).

Testa et al. (1990) developed a balloon-borne instrument, with a collecting area made of a nuclepore membrane filter (NMF) and nine TEM grids made of beryllium and carbon film. The NMF was spattered with silver to make the surface more conductive and useful for Scanning Electron Microscope (SEM) and Analytical Transmission Electron Microscope (ATEM) analyses. The particles collected are in the size range 0.045-1.0 µm, mostly of particles from volcanic injections (Rietmeijer, 1993). The measured particles density was much higher (10-10^5 times) than the concentrations predicted by models of Hunten et al. (1980) but they were close to the in-situ

observations (Zolensky and Mackinnon 1985). The higher concentration of particle density respect to the model may be due to a major contribution from volcanic particles (Testa et al 1990).

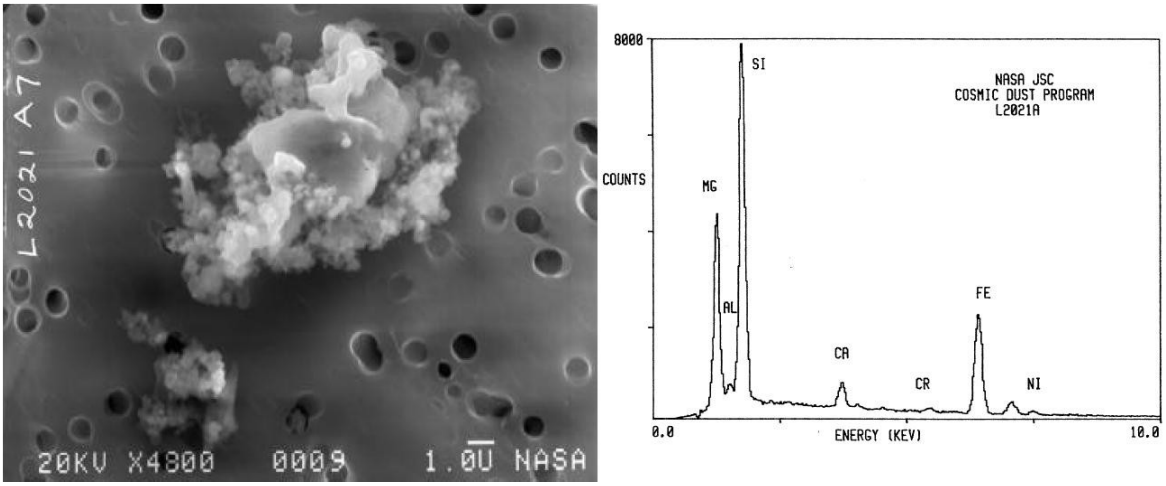

Figure 1.7 An example of IDP collected in stratosphere by NASA program. On the left the Scanning Electron Microscope image; on the right the Energy Dispersive X-rays spectrum. (Cosmic Dust Catalogue, vol.15, July 1997)

Another balloon born instrument to study aerosol composition was projected by Xu et al. (2001). They collected particles with a balloon born instrument studied for analyses with Transmission Electron Microscope (TEM) technique and OPC to have a vertical profile. From EDS analyses of particles in the size range of 0.1 - 0.5 µm emerged that: (1) between 4 - 6 km the 80% of particle collected were compose of sulphate; (2) between 8 – 21 km were predominant particles compose of sulphuric acid; (3) S-rich particles are present in troposphere and lower stratosphere; (4) 20 - 30% of particle in lower stratosphere contain sulphuric acid; (5) particles composed of minerals were present at 5 – 6 km of altitude, indicating a vertical transport to the upper troposphere; (6) mineral with sulphuric acid suggest formation of it in a tropospheric environment; (7) as a demonstration of vertical transport, sea-salt particles were found on upper troposphere and lower stratosphere.

In 1999 a new project, CARIBIC (Civil Aircraft for Regular Investigation of the atmosphere was born. Based on an Instrument Container), to sampling aerosols and trace gases in the upper troposphere and lower stratosphere (8.2 – 12 km). Until April 2002 they had data from 60 intercontinental flights with Boeing 767-300 ER from LTU Airways (Brenninkmeijer et al. 1998); since December 2004 they use the Lufthansa support. The on board instrumentation consist of a container with a dedicated aerosol sampler used to collect particles in the size range 0.07 – 1.5 µm based on impaction technique. There are two separate inlet for aerosol collection and gas traces, they are mounted at 8 m from the nose of the aircraft and protruding 20 cm from the fuselage to avoid the influence from the air layers connected to the aircraft. The particles were collected on a polyimide film analysed for elemental composition using a PIXE (Particle-Induced X-ray emission).

They investigated potassium, iron and sulphur concentration in relation to potential vorticity (PV) of the air mass and respect to the seasons. The results were that iron and potassium shown no measurable change with the increasing of PV, but had a peak in concentration during March-June; instead sulphur increase with the increasing of PV and shown a peak of concentration in the same months but not as strong for the other elements. The sulphur at this altitude is produced by three sources: the sulphur particulate by carbonyl sulphide (OCS) contribution, particulate made up of sulphur dioxide transported across the tropical tropopause and extratropical tropopause (Martinsson et al. 2005).

Conclusions

From all those experiment managed into troposphere and stratosphere we learn that: there is a mutual exchange from mesosphere to upper stratosphere and from troposphere to lower stratosphere; volcanoes ejecta arrive until upper stratosphere; stratosphere aerosol are mixed with extraterrestrial materials coming from micrometeoroids ablation and evaporation.

The tracking and monitoring experiments in the Arctic and Antarctic polar vortex regions provided a wealth of information on the upper stratospheric and mesospheric interactions, and about PSCs formation and composition, but they did not collected particles for detailed laboratory characterization. Dust particles could provide substrates for atmospheric chemistry of condensable gases and they may play a role in the removal of sulphuric acid above ~40 km altitude (Plane 2003). Meteoroid and other dust reach their maximum concentrations in the mesosphere of the Arctic and Antarctic polar vortexes during the wintertime by moving dust from one to the other region back and forth.

From the literature few collection experiments emerge and the NASA long term program does not operate in the upper stratosphere. This left a gap in our understanding of the upper stratosphere for what concern the solid particulates, their size, morphology, surface properties, chemistry, the proportions of glass to mineral ratio, and their mineralogy. For this reasons the upper stratosphere remains poorly sampled.

Any dust sampling instruments functioning in these environments needs to operate in an autonomous operation mode, must have a efficient and reliable contamination control system and the collected nanometer- to micrometer-scale dust must be stored safely during the period of collector retrieval in the field and opening in the laboratory. In this frame the DUSTER (Dust in the Upper Stratosphere Tracking Experiment and Retrieval) experiment was designed, with the aim to collect dust in the boundary layer in which there is material coming up (from Earth's surface) and coming down from mesosphere.

2 DUSTER (Dust in the Upper Stratosphere Tracking Experiment and Retrieval)

In this chapter I will discussed the DUSTER experiment from the first idea, in 2006, to perform a long term project for stratospheric aerosols collection, to the successful flight performed in June 2008 Svalbard campaign.

Aims, scientific and technical requirements who brought to the DUSTER2oo8 instrument will be discussed. The instrument from the mechanical and functional points of view will be described.

Particular attention will be given to the core of DUSTER2008, the collecting chamber, the sample holders and their accommodation inside the chamber. For what concerns the sample holders, the details will be discussed in the last section, together with the mounting and contamination control procedure.

Finally, the conclusions will describe the goals of DUSTER2008 and the related scientific and technical requirements and their relation with the previous experiment for stratospheric aerosol study.

2.1 Aims

DUSTER is a balloon-borne experiment developed to collect the stratospheric aerosol in the poorly studied region in the elevation range of *30 – 40 km*. The principal aim is to detect and study the different typology of particles (natural - volcanic, anthropogenic, extraterrestrial - micrometeorites and IDPs) present in that stratospheric region.

DUSTER has to be light, little and totally autonomous; it has to collect particle in the size range *0.1 - 10 μm* without contamination and manipulation; and, possibly, it has to be cheap.

Good results have been obtained for what concern the miniaturization; it goes from the prototype DUSTER2006 *(0.6x0.6x0.46) m^3* in size and *65 kg* in weight, to the operative versions DUSTER2008 that is almost ¼ in volume of the prototype, *(0.41x0.41x0.31) m^3* in size and *30 kg* in weight. It is able to fly autonomously, with a little balloon (*10.000 m^3*), or as a piggyback of another instrument and in both cases it can be autonomous. This is important to ensure a doable and repeatable program to collect particles in different areas and season.

The first scientific flight (DUSTER2008) collected particles in the size range *0.5 – 150 μm*, and they are uncontaminated and well distinguishable from potential accidental contamination present on collection substrate. Preliminary analyses can be done successfully without manipulation of the samples. As we will see for specific analyses the samples need to be manipulated, but it can be done under contamination control.

All DUSTER versions are totally designed and assembled in laboratory, with customized commercial elements and tools developed for vacuum environment. This allows to create a very cheap and autonomous instrument.

2.2 Scientific and technical requirements

To have a successful collection flight, the instrument has to meet some scientific and technical requirement.

It needs to work in autonomous operation mode, must have a reliable contamination control system and the collected nanometer to micrometer scale dust must be stored safely during the period of instrument retrieval and opening in laboratory.

It has to be able to work in a wide range of temperature (*-40°C <T< 50°C)* at the altitude between *30 and 40 km*. Last but not least, DUSTER has to be compatible with collection of aerosols in the size range between *0.1* and *10 μm*; to allow the collection of hundreds of those particles, an air volume collection of about *20 m^3* is required.

The collection is focused on the given size range for the following reasons:

- it is a size range poorly study especially with laboratory instrumentation;

- the IDPs on this size range have the peculiarity to suffer lower heating during entry in atmosphere with respect to larger particles and in this manner they are not processed. The probability of surviving unaltered during entry is significantly higher for particle in the size range 0.1 – 1 µm (Flynn 1997), and this allows to study the particles in their original status;

- it is demonstrated by the in-situ data of Ulysses and Galileo missions that, for interstellar grains, smaller particles are dominant in number and mass with respect to the large particles (Landgraf et al., 2000) (Figure 2.1);

- aerosol density measured in this conditions allow to collect 10^{-1} particles/*cm*3 in the size range of 0.1 - 1 µ*m* (Renard et al. 2005), and about $2x10^{-4}$ particles/*cm*3 for the solid component greater than 10 µm (Pueschel et al. 1995, Biermann et al. 1996).

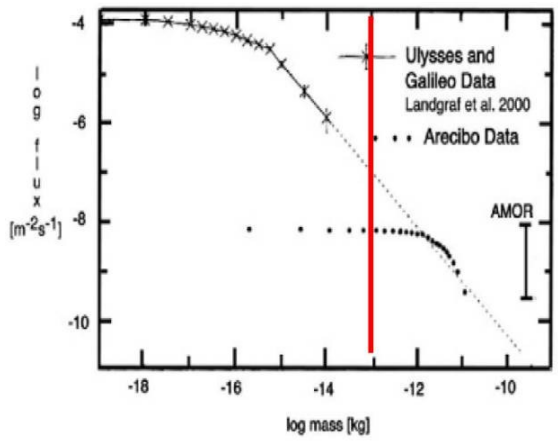

Figure 2.1 Ulysses and Galileo Data (Landgraf et al. 2000). The red line is the expected from DUSTER collection.

2.3 DUSTER2008: the instrument

DUSTER prototype was developed looking at the previous experience of Testa et al. (1990). DUSTER2006 (Figure 2.2) had a qualification flight on January 2006 from Kiruna (Sweden) thanks to CNES (Centre National d'Etudes Spatiales) and Esrange Space Centre balloon campaign. It was in operative mode for *2h* at the floating altitude of *28-29 km*. The aim of the flight was to test the operation and the capability of retrieval. Inside the instrument, the sample holders were present too, but there were no significant scientific data due to the very short collection time and insufficient characterization of contamination before the flight.

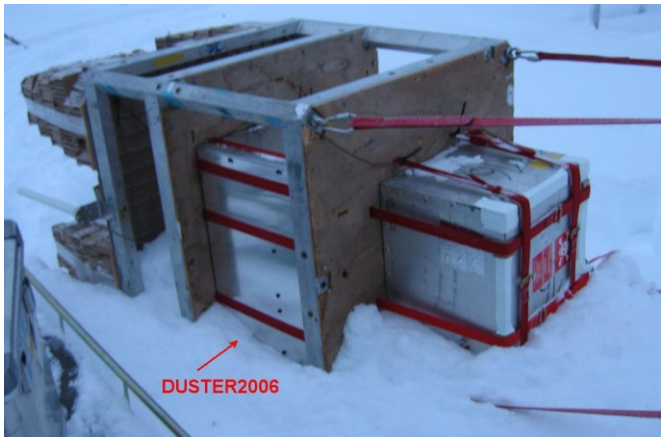

Figure 2.2 DUSTER2006 recovery.

The new miniaturized instrument, DUSTER2008, was launched from Longyearbyen (Svalbard Islands) on June 2008 in a dedicated ASI (Italian Space Agency) balloon campaign (Figure 2.3). It flew for *3.5 days* and remained in operative mode for *55h* at a floating altitude of about *37 km* with a flow rate of *1* m^3/h before being recovered in Thule (Greenland) (Figure 2.3). From this flight we were able to collect particles for following scientific analyses.

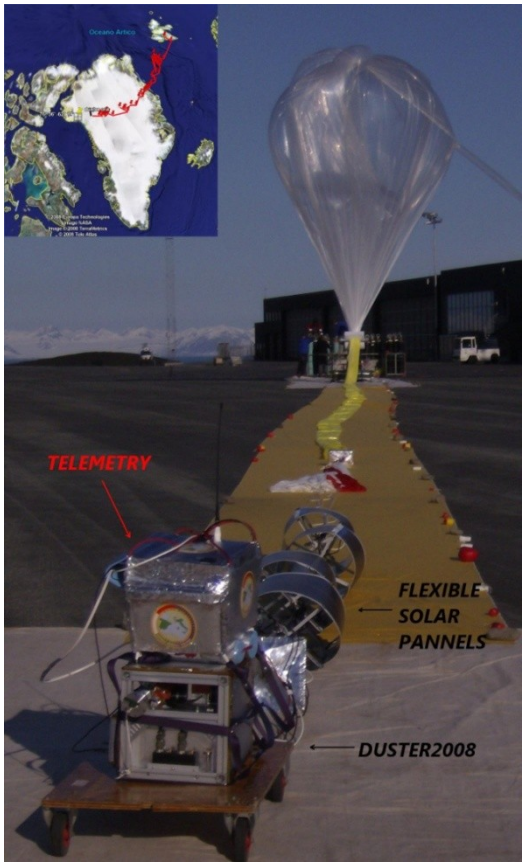

Figure 2.3 Launch chain (the big image) and trajectory (the little image on left) of DUSTER2008 instrument.

The instrument structure is a box realized with aluminium bars Bosh Rexroth and an aluminium plates that divided the box in two ambient; the box is covered with *5* aluminium panels, *4* of them wrapped with thermal isolation material.

In the bottom part of the box the battery and the main electronics are fixed. The electrical power required for instrument operations is *20 W*. It is provided by a combination of a rechargeable battery with capacity of *20 Ah* and *4* solar array connected in parallel to the battery. The solar arrays are flexible and assembled in four cylinders in order to have always the equivalent of one panel surface expose to the sun (Figure 2.3).

In the upper floor of the box there are the mechanical parts of the instrument. They are designed and realized with high vacuum standards to minimize the contamination and to ensure the sealing of the collected samples. In the line of the aspiration flow we can found in order the inlet tube, a gate valve, the collection chamber, a second gate valve, a net of Swagelok tubes to connect the chamber to two sets of six micro vacuum pumps, controlled by an electro-valve (Figure 2.4).

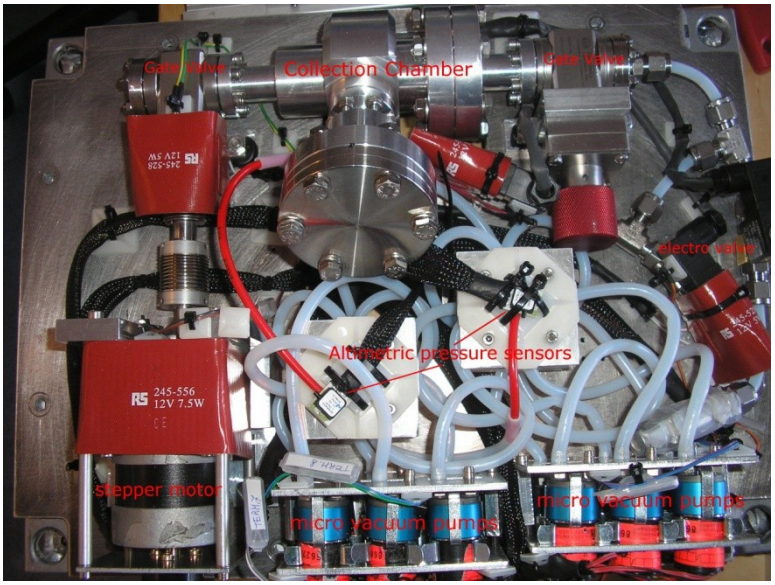

Figure 2.4 Upper floor of DUSTER2008 instrument. The inlet tube is not shown in this picture, it is visible in Figure 2.5.

The inlet tube is sealed by a flange hold in place by the pressure gradient between the inner inlet and the external environment. In this way the inlet is preserved uncontaminated until the operative altitude, when the flange automatically will open. At that altitude the inner pressure equal the outside pressure. The gate valve between the inlet and the collecting chamber is driven by a stepper motor controlled by the main electronics. This valve is opened during the operative time and is sealed when the instrument is on standby or during landing. The second gate valve (between the chamber and the pumps) is not connected to a motor; it is opened at the starting time and it is closed by hand during recovery operations, to ensure the seal of the collecting chamber until the retrieval in laboratory.

The two sets of micro pump are redundant, i.e., to have the required flow rate only one set is sufficient, while the second is used in case of emergency (fortunately it wasn't necessary during the flight).

In order to control when the instrument reach the operating altitude, two atmospheric pressure sensors are mounted on DUSTER2008. They measure in an absolute pressure range of *0 - 121 kPa* with an error of *0.03%* in the operating temperature range.

To monitor the temperature of the mechanical parts eight thermometers (LM135) are displaced in the structure. In order to allow the good working of mechanical parts, a limit is set at *25 °C*, value. If the temperature drop below *25 °C* the software switch on the heaters positioned on the gate valve, the motor and pump benches.

The software allows the complete management of the instrument, and it can operate in slave or autonomous mode. In the first case the instrument is commanded from ground using telecommands. In the second case the software handle the instrument operation following data from instrument sensors. In both cases DUSTER2008 received telecommands and sent data to the ground base using the telemetry provided by ASI balloon platform, based on an IRIDIUM modem.

In this configuration the instrument performance are: 1) capability of working on a stratospheric balloon flight in compliance with environmental conditions such as *-80°C* and *3-10 mbar*; 2) collection of stratospheric aerosol particles by sampling at least *20 m^3* of gas; 3) sample storage and retrieval with monitoring of contamination; 4) capability to collect particles in the size range of *0.1 – 150 µm* at an altitude of *30 – 40 km*.

At the switch on DUSTER is in a 'Safe Status', that imply the gate valve closed to seal the collecting chamber and the pumping system switched off. When the pressure sensor reach the operative value the instrument turn in 'Autonomous Mode' and starts to sample, unless something critical happens to the mechanical parts. In this case the systems turn back the instrument in 'Safe Status' to protect the collecting chamber.

The software monitors at regular interval the sensors (pressure, temperature and other housekeeping data), if the pressure goes down the operative value the software stop to sample air and turn the instrument in 'Safe Status'.

In 'Slave Mode' the instrument is controlled by telecommand from the experimenter, but the system is continuously monitoring the sensors. If something critical occur the software switch the instrument in 'Safe Mode' (Della Corte et al 2010).

2.4 Sample holders (Blank and Collector)

The collecting chamber is the core of the instrument, it has two communicating modules, one directly expose to the incoming air flux, wherein the Collector (the actual sample holder) is located, and a second module in which the Blank (an identical sample holder) is located, but is not directly exposed to the air flux (Figure 2.5). The stratospheric particles stick onto the Collector.

The Blank is a continuous monitor of the ambient environment before the flight and during stratospheric collection.

The sample holder is studied to allow the analysis with Field Emission Scanning Electron Microscope (FE-SEM), Energy Dispersive X-rays analysis (EDX) and transmission analyses techniques without sample manipulation. It collects particles by direct deposition with no need of sticking materials, and it is kept in controlled contamination conditions until DUSTER reached the collection altitude.

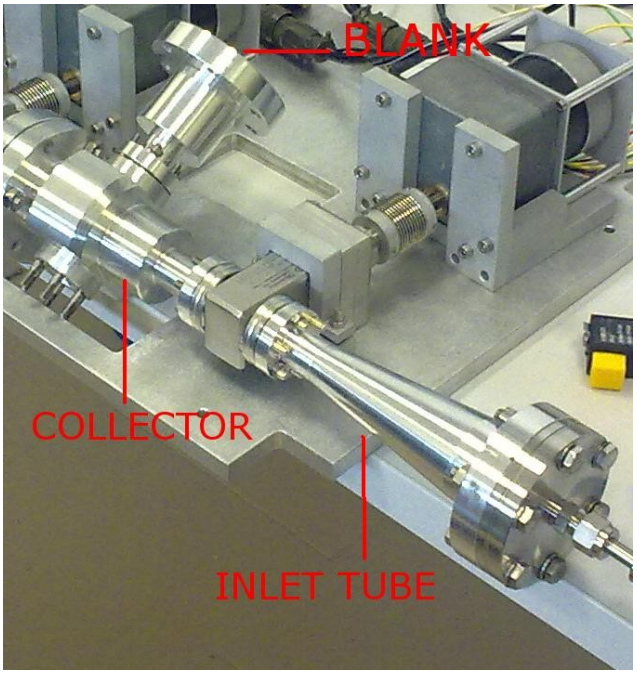

Figure 2.5 Collection chamber, in the figure are shown the position of collector and blank inside the chamber .

2.4.1 Structure

The sample holders are composed of a round smooth surface made of gold-plated stainless steel, pierced with 14 holes to accommodate TEM (Transmission Electron Microscope) grids (300 mesh type), made of gold and coated with holey carbon thin film. All this structure is linked together by 14 stainless steel pins and a stainless steel base that connects all the elements by three screws (Figure 2.6).

The sample holder measures are:

- diameter of gold round surface *23 mm*
- total diameter of the sample holder *24.5 mm*

- total height of the sample holder *16 mm*
- diameter of the holes *2.46 mm*
- diameter of the TEM grids *3.05 mm*

This configuration was chosen to allow FE-SEM analyses and transmission analyses. The first one needs a smooth surface, and for this reason half of the gold disk is not pierced. The analyses in transmission mode need to have the samples free from background elements, for this reason half of the disk surface is covered by dismountable TEM grids.

Figure 2.6 DUSTER2008 sample holder.

2.4.2 Assembling

Before to assemble the sample holders all the components and the tools used to mount them, have to be cleaned with isopropyl alcohol in an ultrasonic cleaning machine for at least 30 minutes. Only the TEM grids have not to be clean because they are already free from contamination and the isopropyl alcohol damages the holey carbon thin film. For the same reason all the components and the tool washed with the isopropyl alcohol has to be dried before to assemble the sample holders.

The assembling takes place under a laminar bench flow located in a cleaned laboratory. The operations have to be done with single use gloves, hair cap, white coat, and filter mask. The tools used to assemble them are a micro-tweezers, to grab safely the TEM grids, and a screwdriver suitable for M5 type screws.

The main components of the sample holders are shown on Figure 2.7.

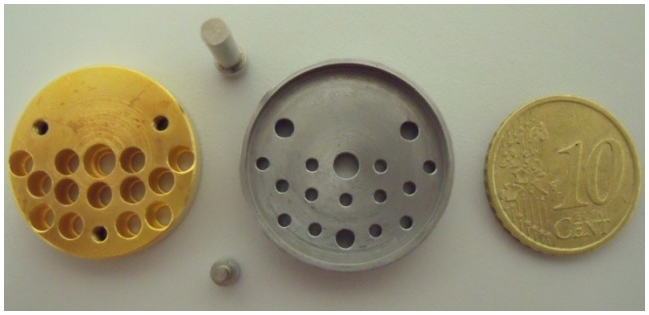

Figure 2.7 Main components of sample holder. From left to right: gold pierced surface, central pin (up), little pin (down), and stainless steel pierced plate.

Assembling procedure

Hold the gold surface with two fingers being careful to not touch the collection surface. The surface has to be down and the side with the canals to accommodate TEM grids has to be in front of the experimenter (Figure 2.8). The gold surface has not to touch anything.

With the micro-tweezers take the TEM grids one by one being careful to hold it by the round gold perimeter and not to damage the holey carbon thin film. Then accommodate them one for each of the *14* canals (Figure 2.8).

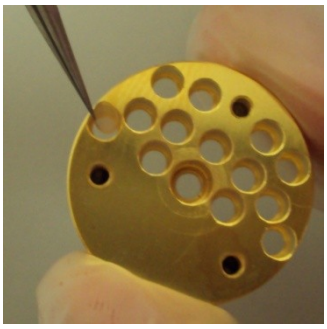

Figure 2.8 Accommodation of TEM grid in the pierced gold surface.

With the tweezers take the pins from the thin side and accommodate them in the canals ensuring they hold the TEM grids. There are *13* identical pins and one bigger than the others. The big one goes to the central hole to be used as fixing point into the DUSTER collection chamber (Figure 2.9).

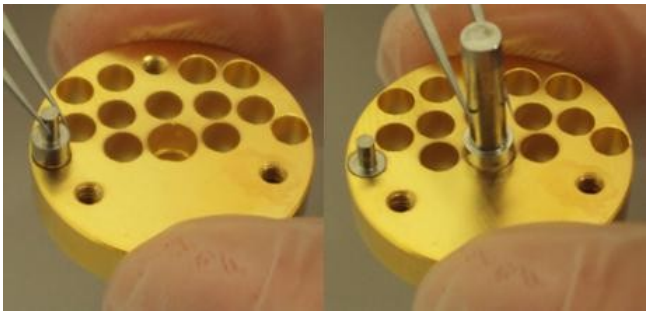

Figure 2.9 Accommodation of the pins in the pierced gold surface to hold the TEM grids.

Align the stainless steel pierced plate with the pins and drive them into the holes to hold the two sample holder parts. Finally fix all with three screws (Figure 2.10).

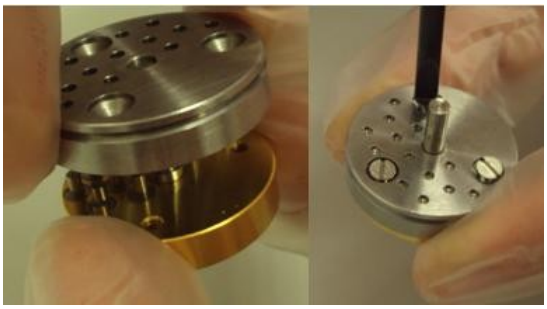

Figure 2.10 Fixing of the stainless steel pierced plate.

Conclusions

DUSTER2008 collected particles in the size range *0.5 -150 μm* at the mean altitude of *37Km*. The commands in slave and autonomous mode worked good and the contamination control showed a collection surface sufficiently clean. For this reasons we can say that the principal aims of the project are reached.

As we will see in the chapter dedicated to the sample holders curation (Chapter 4), the TEM grids are not easily dismountable as expected, this is the only requirement that is not totally respected.

The difference between DUSTER and the previous experiments that aim to study the stratosphere environment, is the altitude, collection and the contamination control.

In conclusion, as described in Chapter 1, before DUSTER project many experiments had the aim to study stratosphere composition by collection or in remote sensing; but any of it could offer simultaneously an operating altitude around *40 km*, collection and retrieval of samples for laboratory analyses and a good contamination control.

3 Analytical techniques used for collected particles identification, manipulation and characterization

In this chapter are described the techniques used to identify, manipulate and analyse the particles collected during the June 2008 campaign (see Table 3.1).

Technique	Application
FE-SEM (Field Emission –Scanning Electron Microscope)	Identification Morphological classification
EDX (Energy Dispersive X-rays analysis)	Elemental analysis
SEM-FIB (Scanning Electron Microscope – Focused Ion Beam)	Relocation of some particles to allow transmission analyses
FT-IR (Fourier Transform – Infrared Spectroscopy)	Molecular composition Molecules bond Mineral structures

Table 3.1 Techniques used to identify, manipulate and analyze DUSTER collected particles

3.1 FE-SEM (Field Emission Scanning Electron Microscope)

The instrument used is a ZEISS SUPRA FESEM equipped with an electron optic system configured to have a good resolution also at low voltage applications.

It consists of a beam booster and a combined electrostatic-electromagnetic lens duplet. The electrons created in the gun are accelerated to the set acceleration voltage on their passage to the anode. The beam booster is installed directly behind the anode (Figure 3.1) to ensure that the energy of the electrons, in the entire beam path, is always 8kV higher than the set acceleration voltage. On this way the sensitivity of the electron beam to magnetic stray fields is considerably reduced. Before the electron beam exits, the electrostatics lens creates an opposing field that reduces the potential of the electrons by 8kV. This allow to the electron to reach the sample surface at the set acceleration voltage. Into the beam path is integrated a multiple-hole aperture with 6 different apertures (*7.5, 10, 20, 30, 60, 120 µm*) in which the beam current can be set through.

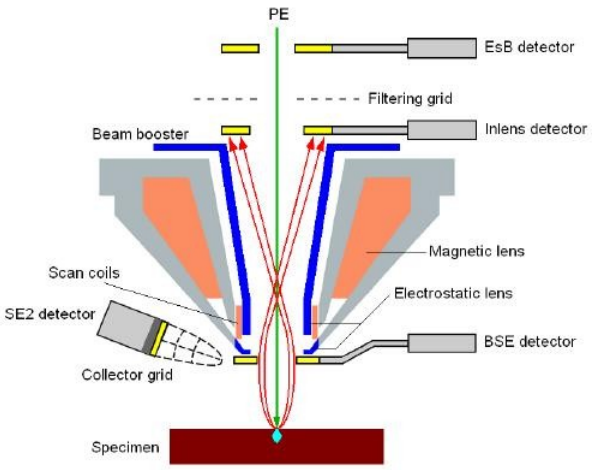

Figure 3.1 FESEM internal structure. In the picture is show the inner of the specimen chamber. The location for the sample, the four detectors (from top to down: EsB, Inlens, SE2 and BSE), the mechanical parts and the path of the preliminary electron beam (green and red lines).

The gun area and the specimen chamber are under vacuum. The gun area is pumped by an Ion Getter Pump (IGP) in ultra high vacuum (*> 9 x 10^{-9} mbar*), the specimen chamber is pumped by a Turbo-Molecular Pump (TMP) in high vacuum (*10^{-6} – 10^{-7} mbar*). The specimen chamber has to be vented with Argon before opening to introduce the samples. For this reason the Column Separation Valve (CSV) separate the gun's column and the specimen chamber during vent operation (Figure 3.2).

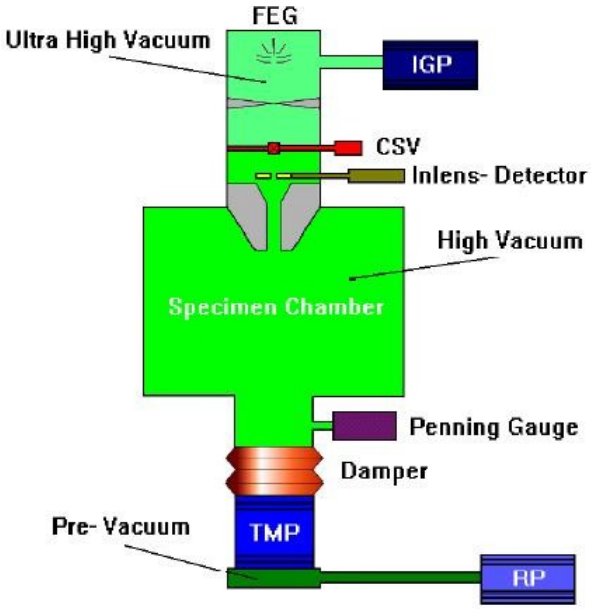

Figure 3.2 FESEM high vacuum system. Compose of three pumps (IGP, TMP and RP) to allow the vacuum inside the specimen chamber, and two gate between the pump system and the chamber (CSV and a damper). In the picture is shown also the penning gauge to measure the vacuum in the chamber.

When the Primary Electron (PE) beam hits the sample the interaction produces different types of signals (Figure 3.3), the most used are the Secondary Electrons (SE) and Back-Scattered Electrons (BSE). SE are generated by inelastic scattering of the PE on the atomic core or on the electrons of the atomic shell of the sample material. They are low energy (*<50 eV*) electrons and, depending on the mode of origin, they are divided in different groups (Figure 3.3):

- SE1: generated directly in the spot centre
- SE2: generated after multiple scattering and leave the surface at a greater distance from the spot centre
- SE3: are generated by BSE at a greater distance from the spot centre and do not contribute to the image information.

All the electrons with energy *> 50 eV* are BSE, they are generated by elastic scattering in a much deeper range and carry depth information.

Inside the specimen chamber there are four different detectors (Inlesn, SE2, BSE, and Energy and angle selective BSE (EsB)) each of it is specific for some different kinds of electrons. In the following the detector are described one by one except for the EsB detector that will not be used for DUSTER collected particles.

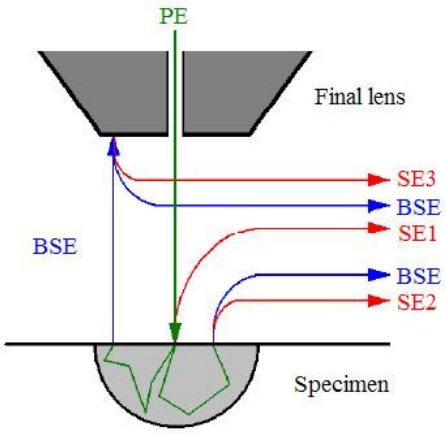

Figure 3.3 Secondary and Back Scattered electrons deriving from the interaction of Primary Electron with the specimen.

In-lens Detector

To map the surface of the sample the electron type SE1 and SE2 should be detected, because they are generated in the proximity of the spot centre and in the upper range of the interaction bulb, therefore contain direct information of the sample surface. These electrons can be detected by the In-lens detector, which is placed above the objective lens and detects directly in the beam path (Figure 3.1).

The efficiency of the detector is determined by the electric field and the electrostatic lens. The Working Distance (WD) is one of the most important factors to determine the signal/noise ratio and the efficiency of the detector. To have a good image has to be set a reasonable WD (< 10 mm) and acceleration voltage between 100 V - 20 kV.

The In-lens detector is often used at low voltages, especially to see all the structure of the sample. The same image at *2 kV* and *15 kV* shows different characteristics of the same sample (Figure 3.4). The image at low voltage shows clearly a structured surface because of a good contrast, instead the image at high voltage seems to be flat and transparent.

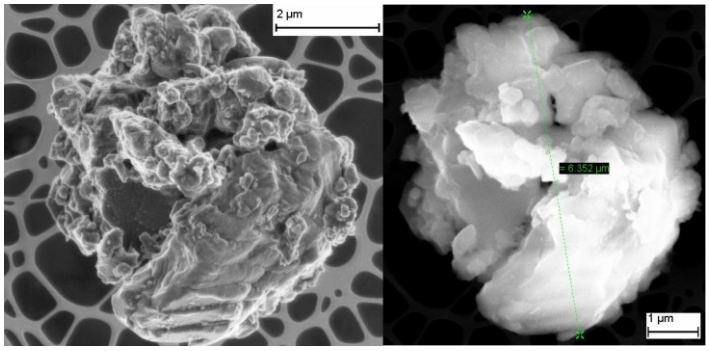

Figure 3.4 Image of a particle collected by DUSTER. On the left the picture is taken with Inlens detector and 2kV, on the right the same detector but at 15 kV.

Further reason for the use of very low acceleration voltage is the minimization of the charges and irradiation effects on the sample surface. If the electron hits a non-conducting surface, it cannot discharge and local charges are generated. This affects the electron beam and may significantly deteriorate imaging quality.

SE2 Detector

This detector is mounted in the specimen chamber (Figure 3.1). It looks at the samples laterally and allows detecting secondary and backscattered electrons. Unlike the In-lens detector the SE2 can be used in the complete high voltage range (1 – 30 kV), in fact if the energy of the primary electrons is low the efficiency of this detector decreases, because the WD has to be small (> 4 mm) and shadow effects occur. If the sample is positioned too close to the final lens, most electrons will be deflected by the electronic field of the electrostatic lens or moved to the final lens.

BSE detector

It is positioned below the final lens and views the sample from above (Figure 3.1). This position offers a very large solid angle to detect BSE electrons. It allow to shows material differences in the samples by displaying the contrast based on backscattering coefficient: the brighter the area displayed the higher the atomic number.

The WD controls the efficiency of the detector: if the WD is too small (less than 8 mm), only few electrons will hit the detector; if it is too long (more than 10 mm), many electrons will miss the detector (Figure 3.5).

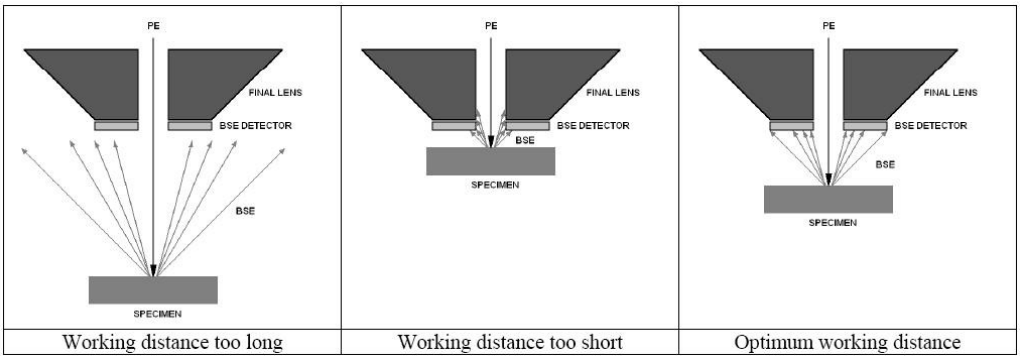

Figure 3.5 Efficiency of BSE detector at different working distances.

3.2 EDX (Energy Dispersive X-rays)

Energy Dispersive X-rays (EDX) analysis was performed by an Oxford INCA Energy 350 system linked to the FESEM with a Si(Li) INCA X-sight "PREMIUM" detector. The energies of the X-rays, emitted by the sample after the interaction with the FESEM electron beam, are measured to determine the chemical elements present in the samples.

It can be used at different accelerating voltages, usually *10, 15, 20 kV,* depending on the elements to be detected and on the sample conductivity/preparation. The analyzed surface could be a single spot, a bulk or a map of the entire sample. The geometry of the analyzed area is a choice of the experimenter, but the minimum size is 1 μm^3 that is the extension of the spot.

To calibrate the FESEM/EDX system a pure Cobalt (Co) sample is used for accelerating voltage *≥ 10 kV* while for accelerating voltage *< 10 kV* Silicon (Si) is used.

The out-put of the EDX analyses are:

- *list of detected chemical elements*;
- *weight %*, wt% = Apparent Concentration / Intensity correction, after correction for inner-elements effect;
- *type of the X-ray lines* used for quantification of the elements (i.e.: K or L line);
- *element apparent concentration*, i.e. before any matrix correction;
- *intensity correction.* A first estimate of the sample composition is obtained from the normalized sum of the apparent concentrations. Inter-element effects are calculated according to the correction procedure currently selected. The iterative process continues until the results converge. The intensity correction show the ratio of the combined correction for the sample to the combined correction for the standard used for that element. Ideally, correction factors should be within the range *0.8 to 1.2;*
- *weight % sigma*. i.e. the statistical error for the calculated wt%;
- *atomic %* **=** wt % / atomic weight. The sum of atomic % for all elements in the sample is normalized to 100%.

3.3 SEM-FIB (Scanning Electron Microscope-Focused Ion Beam)

The FIB instrument (Figure 3.6) was used to relocate some particles, by courtesy of LIME (Interdepartmental Laboratory of Electron Microscopy) in Rome.

Basically the FIB is an accessorize of the SEM microscope compose of a needle and a welder. The SEM is useful to see the sample from different angle and to do the work as clean as possible.

Figure 3.6 SEM-FIB instrument located in LIME laboratory (Rome).

During the relocation procedure the particle is approached by the needle (made of Tungsten) and welled (with Lead) to it, in this way the particle can be moved on the new support (TEM-FIB grid in Copper) and welled on this new grid. Finally the particle is unwelded from the needle by a ion beam of Gallium.

In Figure 3.7 is report an example of particle relocation with FIB instrument.

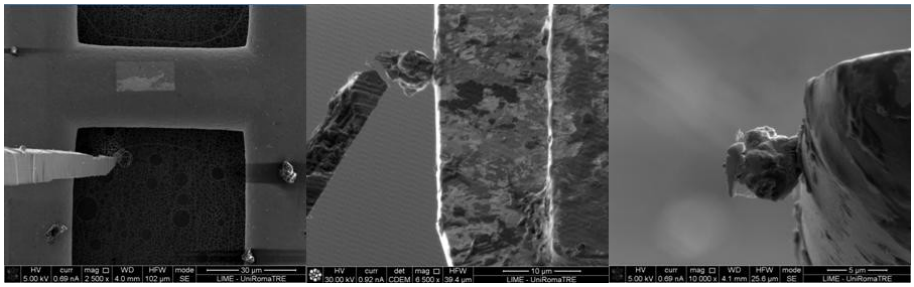

Figure 3.7 In this figure is shown the procedure to relocate particles with FIB.

The instrument is a FEI Helios Nanolab 600, and the specifics are:

- Dual Electron Beam Scanning Microscope (FEG) and ionic (FIB)
- SEM resolution: 0.7nm a 15kV, 1.4nm a 1kV
- FIB resolution: 5nm a 30kV
- Sample holder stage: 5 motor axis, X and Y piezo (150 x 150) mm
- Available gases: Pt (deposition), SCE (Surface-Conduction Electron emitted), IEE (Enhanced Etching)
- Detectors: ETD (Everhart Thornely Detector), CDEM (ion and electrons), TLD (Through the Lens Detector), IR camera.
- Micromanipulator: Omniprobe (3 axis)

3.4 Fourier Transform Infra-Red (FT-IR) spectroscopy

An FT-IR spectrometer works by irradiating a sample with an infrared light source, from 9000 cm^{-1} to around 200 cm^{-1}. Infrared radiation is absorbed by molecules in the sample and converted into energy of molecular vibration. When the radiant energy matches the energy of a specific molecular vibration, absorption occurs. In order to be IR active, a vibration must cause a change in the dipole moment of the molecule. The intensity of light transmitted through the sample is measured at each wavenumber (the inverse of the light wavelength) allowing the amount of light absorbed by the sample to be determined as the difference between the intensity of light before and after the sample: the IR spectrum.

Molecules bond lengths and angles represent the average positions about which atoms vibrate and there are two types of molecular vibrations: stretching and bending.

Stretching of chemical bound is a periodic vibration that could be symmetric (if the atoms bring near or move away contemporary) or asymmetric (if the atoms bring near or move away not contemporary). Bending of bound angle, could be symmetric or asymmetric and could be on the same plane of the bound angle or not. It is called scissoring (symmetric bending in the plane), rocking (asymmetric bending in the plane), wagging (asymmetric bending outside the plane), or twisting (symmetric bending in the plane).

The FT-IR microscope is based on a combination of a Michelson's interferometer and a Fourier transform process. The infra-red light is guided through the Michelson interferometer to the sample (Figure 3.8). The interferometer is composed of three mirrors; one is an half-silvered

mirror that splits the light onto the other two, a fixed and a mobile mirror. The mobile mirror allows having a different path light that form constructive and destructive interferences with the light reflected by the fixed mirror. This raw data is processed by a Fourier transform function that gives the sample's infrared spectrum.

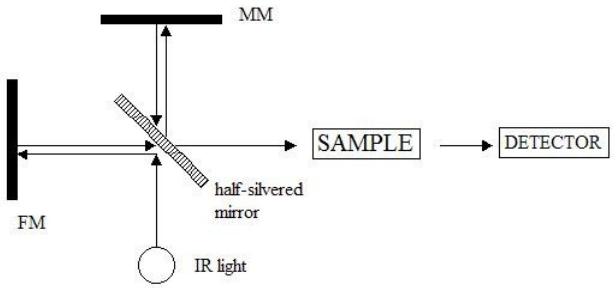

Figure 3.8 Schematized FT-IR instrument

4 Sample holders pre- and post-flight characterization, laboratory procedures, including sources of contaminations.

In this chapter I will address:

- how characterize the sample holder before and after the flight in order to have a clean reference before the launch and to identify the particles collected during the DUSTER2008 flight;
- curation of sample holders in laboratory and procedures to move samples between laboratories without contamination of the samples;
- problems that were noticed after recovery with regard to concerns about FESEM-EDX characterization and the possibility to dismount TEM grids from the sample holder;
- solutions to these problems for the collected particles and possible solutions for future flight campaigns;
- sources of contamination.

4.1 Characterization

As explained in Chapter 2, the sample holders surface and each of its components were cleaned before assembling of collector and blank. The two sample holders are assembled with care to not contaminate their surface. The particles of interest for the DUSTER experiment are greater than 0.1 µm and smaller than 10 µm, and in the same range there are many particles coming from the environment that may accidentally contaminate the collection surface. To reduce contamination from the environment all handling procedures were conducted in a clean room. To be sure to have a very clean surface the sample holders were characterized with FESEM imaging after assembling.

The aim of characterization is to have a map of collection surface (the gold surface of the sample holder and the TEM grids) to compare with a map of the same surface after the collection flight. This is useful to see how many and where are the collected particles, and to check that pre existent particles are still where they were before flight, in order to avoid confusion between contaminant and collected particles. To have a good characterization and allow comparison with post-flight analyses, I had to choose an orientation of the sample holders (Figure 4.1). I chose to look at the sample holders with the gold smooth surface up and the holes down and to assign a number/name to each TEM grids, as reported in Figure 4.1.

Figure 4.1 Sample holder surface with assigned identification number/name of the TEM grids.

The 'central grid' is more exposed to the flux respect to the other grids, because it is in the center of the sample holder and is directly run over by the air flux. Thus, it has the largest collection efficiency. This probability decreases with the distance from the central grid, being the grids number 2, 3 and 7 the ones with larger collection efficiency respect with the grids in the border of the sample holder.

The TEM grids are simple to orient when looking at them with FESEM magnifications, because in the center they have a little square with different shape for each corner (Figure 4.2). Thanks to this feature it was possible to chose an orientation for each grid before the flight and take a picture of it to have a reference to relocate each grid after flight. Each grid is numbered/named and oriented, in this way it is easy to identify each collected particles through the position of its mesh, that is the square grid area with holey carbon thin film. This is given in turn by a reference system centered in the central square (Figure 4.2).

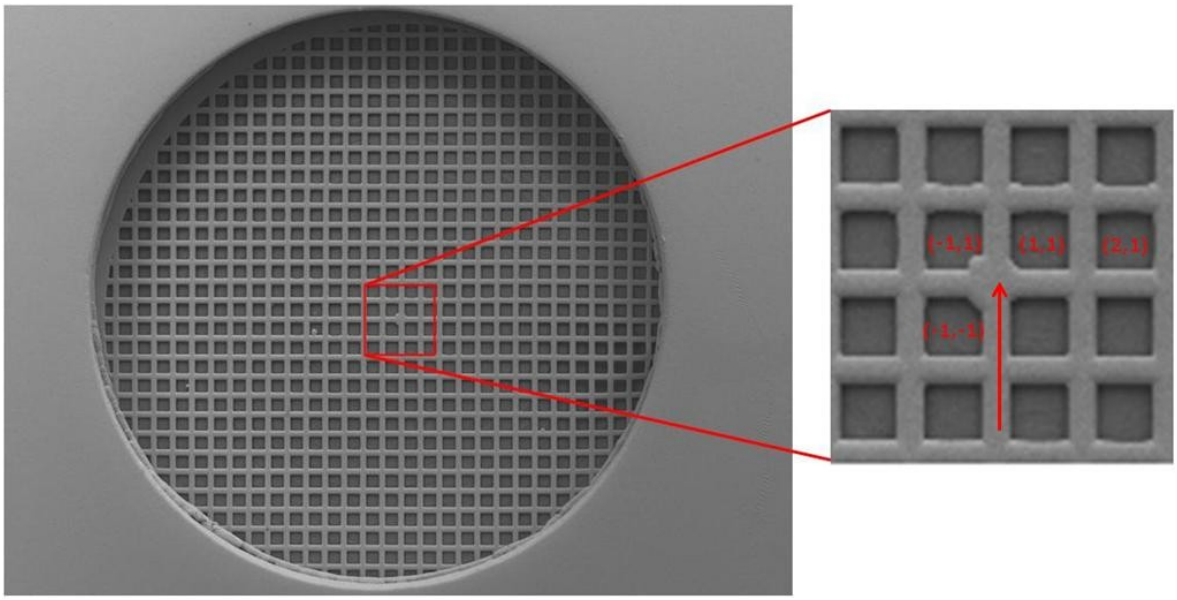

Figure 4.2 Orientation of 'central grid' (left) magnification of the central square (right) with an example of the reference's system coordinates (the red arrow shows the center of the TEM grid).

The next step was to characterize the sample holders (both Collector and Blank). Using a FESEM instrument, I performed a scan of all the grids. The scans have to be done for each grid individually. In order to have a good scanning resolution for the grids, which had the highest probability to collect particles, the grids were scanned at different magnification depending on their relative positions to the central grid.

Grids 2, 3, 7 and the 'central grid' were scanned at 3250 magnifications that implies an area of *(92 x 69)* μm^2 for each image, a resolution of *0.09 µm* for each pixel, a total of ~1000 images per grid, and a dimension of 768 KB for each image file. The others 10 grids were scanned at 1625 magnifications that cover a scanning area of *(184 x 138)* μm^2 for image, a resolution of *0.18 µm* for pixel, and a total of ~ 300 images per grid.

I tried to do the same scanning for the whole gold smooth surface, but it was possible only for a strip above the first line of grids at 2000 magnifications. The reason why the gold smooth surface is not perfectly characterized is that it has no clear reference markings. This make almost impossible to know what are the areas scanned and consequently the particles identification. This

problem did not allow to identify the particles collected on the gold smooth surface, making a cut-off on information about the number of particles collected.

The same operations were repeated for the two sample holders at DUSTER2008 recovery to allow the identification of new particles by comparing pre- and post-flight images of the same areas at the same magnifications. This characterization procedure produced a total of 31994 images file for a volume data of 24 GB.

Scanning procedure

The scanning procedure is not completely automatic. The operations that imply the selection of the scanning area and the focusing of the image were done by hand.

The experimenter has to choose an area to scan that can be either a square or a rectangle. This area is selected by hand using the 'stage scan' tool of the FESEM. In the case of TEM grids, the area is a rectangle that inscribes a circle (the TEM grid shape); for the gold smooth surface it is an area of *(3.5 x 2.5) mm^2*. Next step is focusing the image at the magnification required for scanning (3250, 1625 or 2000 times).

The remaining steps are automated. The 'stage scan' tool divides the selected area in stage steps proportional to the selected magnification. The scanning direction is from left to right and line-by-line. Using the 'macro editor tool', a short program was written to perform the following operations: freeze the image, save the image, unfreeze the image, shift the stage of one step, wait 5 seconds to stabilize the image, and repeat the previous operations.

All the scanning procedure spent ~8 h for scan at 3250 magnification, ~6 h at 1650 magnification and ~5 h at 2000 magnification.

4.1.1 Problems during characterization of sample holders

The scanning characterization performed with the procedure described above allows recognizing the particles collected from spurious contamination, but the identification was not as simple as expected because of some problems due to human errors and inaccuracy of the instrument's tools.

The problems common to all the scanning areas, and due to the instrument tools, are:

- the inability to choose exactly the same areas for pre- and post-flight scans;
- gaps in scan due to irregular shift of the stage scan.

As explained in the 'scanning procedure', the area to be scanned is selected by hand. For this reason the pictures stored in the pre-flight files do not cover the same areas as in the post-flight files. In Figure 4.3 an example of identification of a collected particle is shown, looking at the pre- and post- flight images; in the two images it is clear that the area where the particle is located is in a different position in the two pictures.

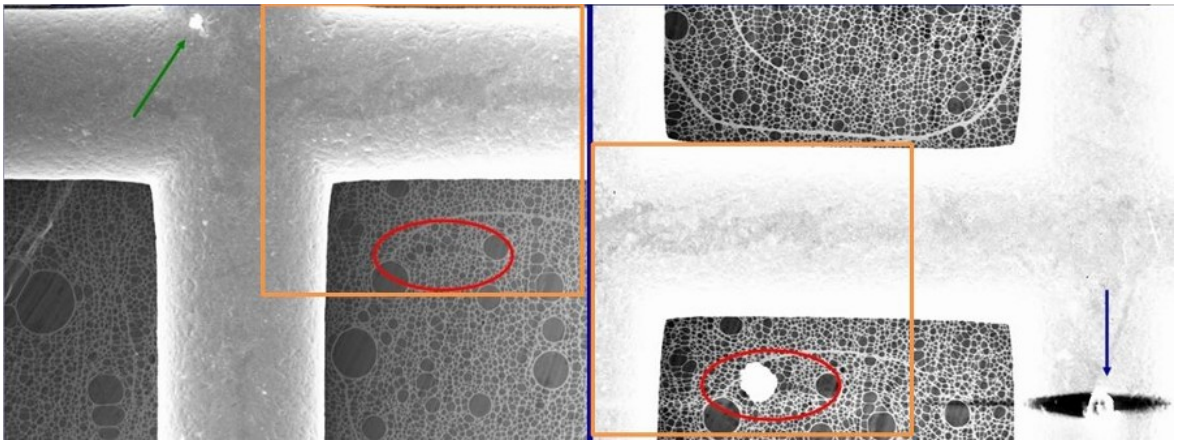

Figure 4.3 Example of identification of a particle by comparing pre- (left) and post-flight (right) images. In this pictures is evident the problem due to the different areas (the area highlighted by the orange square is the common area in the two images). The green arrow in pre-flight image, underline the presence of a particle pre-flight (it was still there post-flight). The blue arrow in post-flight image shows a collected particle (it is charge due to the FESEM beam), but the corresponding area of pre-flight is in the next picture respect to the one shows in this example. Finally the collected particle recognize from this two pictures is highlighted by a red circle.

Another problem is due to the 'stage scan' tool and it is really a problem for the characterization of the whole sample holder surface. The stage scan is the tool responsible for shifting of the stage to where they were positioned the sample holders during the scanning operations. The macro gives the command to the stage scan to move the stage for some microns in a given direction, but this movement has a random error of few microns, that is roughly in the range 0.1 to 2 µm. This error in the scanning images produces a gap of missing information from one picture to the following one and from the line above and the line below.

Both problems combined resulted in ambiguous cases of decisions whether a given particles was a contaminant or collected stratospheric particle. For example, if in post-flight picture is visible a new particle, but in pre-flight the area where the particle is located correspond to a gap without information, we cannot know if this particle is collected or if it is pre-existent contamination. **In cases of ambiguity I decided to reject the particle as collected dust and this decision is a source of underestimation of the number of particles collected**.

Going through the human errors, the top of the pins that fixed the TEM grids had to be flat, but the manufacturer built them with a convex surface. Thus, the pins press down not only on the gold rim but also pressing directly to the grids and the holey carbon thin film supporting the collected particles. This implies damage of the carbon film in some areas. Also some of the grids are not positioned flat, but are quite deformed. This is not visible for human eye, but is important to focus the FESEM. Often the grids are focused only in some areas (usually in proximity of the centre); also the brightness change in different places of the same grid. This makes it difficult, or sometimes impossible, to detect any particles.

The grids numbers 5 and 6 have not been scanned pre-flight. As a result for these two grids we cannot know what are collected stratospheric particles and what are possible grains from manufacturing of the individual DUSTER components, manufacturing and laboratory handling of the collection substrates despite all reasonable precautions taken, including the use of a clean room.

In the end the consequences of the problems discussed above are:

- the number of grids for which we have information are 12 out of 14;
- the size distribution of the particles recognized as collected will have a cut-off at ~0.5 μm due to the scanning resolution. The cut-off for nanometer particles is also caused by the holey carbon film structure. Such small particles can go straight through the holes and deposit on the pin surface.
- an underestimation of number of collected particles.

4.2 Curation

Taking care of the sample holder is not a work that has end after the post-flight characterization. It requires a continuous attention from the experimenter, in order to preserve the collected particles from spurious contamination.

For this reason the sample holders are stored in laboratory in a special seal box far from any contamination due to human and laboratory tools. Each time the sample holders have to be moved from the box they are handled following a strict procedure that the experimenter has to respect. The most common procedures are:

(1) how to accommodate and extract the sample holders from FESEM-EDX instrument;

(2) how to transport the sample holders from a laboratory to another and how to move them;

(3) preserve the relocated samples.

There is a laboratory procedure that has to be followed once for each flight campaign: it is the opening of collection chamber to extract the sample holders after recovery. The DUSTER2008 collection chamber was opened on 15th October 2008. First, the external part of the chamber was cleaned with isopropyl alcohol using optic wipes. It took place in a clean room by an individual wearing single-use gloves, hair cap, white coat, and filter mask. It was checked that the two gate valves were closed (the valve between the chamber and the pumps were closed in Thule at ground pressure, as required by the recovery procedure). As expected, the pressure inside the collection chamber was found to be close to the ground-level value. In order to keep clean the chamber ambient the internal and external pressures were equalled connecting a Swagelok filter to allow clean air entrance in the sample chamber.

After those checks the collection chamber was opened using hex keys cleaned with isopropyl alcohol. The sample holders were placed in a clean box where the positions of Blank and Collector were labelled. This box is used as storage when the sample holders are not inserted in one of our analyses instruments. To monitor the box contamination, a monitor identical to the sample holders, but without TEM grids, is placed inside.

The same day, after collection chamber opening, the sample holders were placed in the FE-SEM to proceed with the post-flight scanning procedure.

4.2.1 Description of the procedures to handle the sample holders

The procedures I am going to describe typically take not place in a clean room, so it is sufficient to wear single-use gloves and using cleaned tools.

How to accommodate and extract the sample holders from FESEM-EDX instrument.

Before placing the sample holders in the FESEM chamber, it has to be cleaned with optic wipes and isopropyl alcohol. Both the collector and blank sample holders are placed on the sample plate inside the FESEM chamber, and fixed in position with the hex key. The two sample holders are identical. Therefore it has to be record the position of both, in order to recognize them when the chamber will be opened. Close the chamber and pump to reach vacuum conditions. Then close the box where collector and blank were stored and save it into the sealed box.

After analyses to extract the sample holders follow the procedure to open the FESEM chamber: switch off EHT; vent the chamber with Argon; when the right pressure is reached, switch off Argon flux and open the FESEM chamber.

Remove the collector and blank sample holders and place them inside the box taking care to put them in the right place shows by the label written on the box's cover. Store them in the sealed box.

How to transport the sample holders from one laboratory to another.

To do this there is no unique procedure, because it depends on the laboratory and the location of the facility. It is mandatory that handling the sample holders is done with single-use gloves and with the appropriate clean tools; they have to be enclosed inside special clean bags.

The sample holders have to be moved always together in the same box with the monitoring box. The box has to be sealed with parafilm, and the box has to be put inside a clean bag. The sample holders and the tools have to be stored in a special suitcase to avoid that the sample holders jump out from theirs accommodation.

How to move and preserve the relocated samples.

The samples moved from the DUSTER2008 sample holders are now fixed to a FIB-TEM grid (Figure 4.4). These grids are easier to transport than sample holder, because they are held inside a box that holds each grid between two thin transparent membranes. In this way the samples are shielded from external contamination and kept held in place.

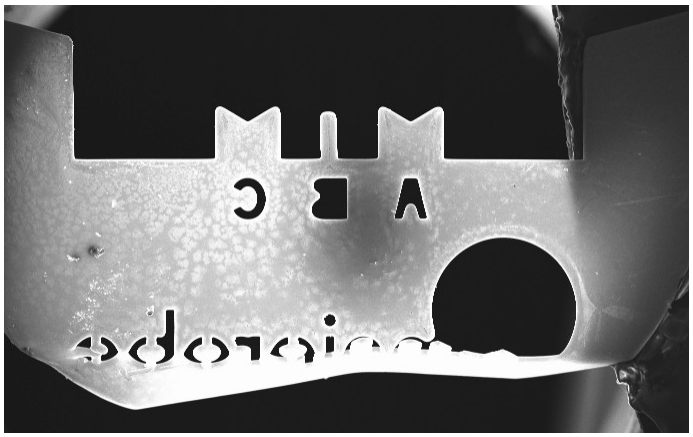

Figure 4.4 FIB-TEM grid

In particular cases and when required by another laboratory the grids should be placed in stubs for TEM grids (Figure 4.5) and placed in custom-designed boxes. In each case, as above, it is recommended to manipulate them using clean tools and single-use gloves.

Figure 4.5 Stub for TEM grids

4.2.2 TEM grids disassembly

In the design of the sample holders, the idea was to have a surface for analyses in transmission mode. For this reason, TEM grids were used in a configuration that had to allow easy disassembling. In the original idea the grids after cataloguing and characterization have to be separated from the gold smooth surface and stored individually to be sent to different laboratories.

Actually that approach was not possible. As mentioned in the previous section, the pins had to be flat, but they were made rounded. This inaccuracy caused the rims of TEM grids to be damaged and part of the holey carbon thin film to stick to the pin (Figure 4.6).

In these conditions, dismounting the grids will be very dangerous for two reasons:

- the rims of the grids are all crumpled and is difficult to hold them with the micro tweezers without damages on the entire grid;
- being the holey carbon film attached to the pin in some areas, it is extremely likely that by slipping off the pin, it drags off the holey carbon film from the grid that could remain attached to the pin itself. The consequence is that the particles collected on holey carbon film remain attached to the pin and are lost for further analyses.

Therefore, we decided to relocate the particles between 4 and 20 μm using the FIB technique. We decided on this particular range because it allowed us to perform FT-IR and Raman analyses with the laboratory instrumentation available for this study. This specific issue was addressed for the DUSTER2009 campaign (see Chapter 6).

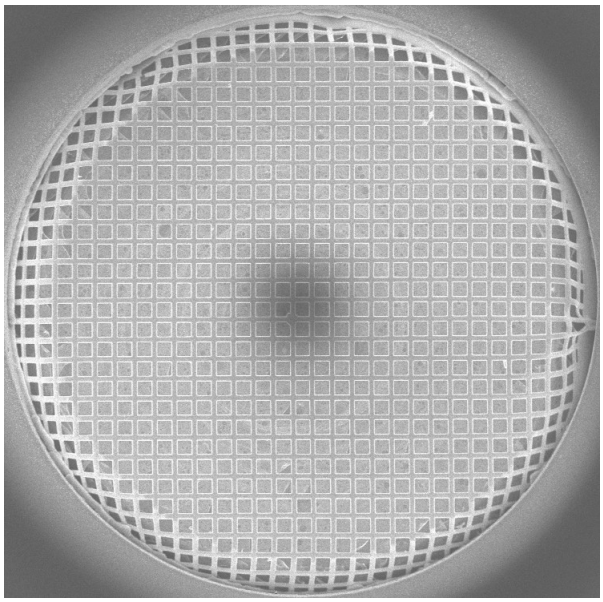

Figure 4.6 In this image is clear the pin below the TEM grid who press on it damaging some meshes and the rim of the grid (up and right rim).

4.3 Sources of contamination

Even if the experimenter takes care to follow at his best all the procedures to avoid spurious contamination the structure of the sample holder itself and the FIB instrument used to relocate

the particles are sources of contamination for the chemical analyses. In the end also the flight train may be a source of contamination.

4.3.1 Sources of contamination from the sample holder

As explained in Chapter 3, the EDX spot has a minimum volume of 1 μm^3, for this reason often the analyses (bulk or spot) of the particles (especially for particle < 3 µm) may involve the substrate. For example, the analyses of particles collected on the gold grid shown the contribution of gold; in this case all the gold detected in the EDX analyses has removed and the particle's analysis is normalized at 100%.

In the case of particles collected on carbon thin film above the pins, the EDX analyses will have a contribution of the pins beneath the TEM grids. The pins are made in stainless steel; in Table 4.1 are reported the EDX analyses of the pin that flown during DUSTER2008 campaign and two analyses on a spare pin cleaned and stored in laboratory. Plotting these three analyses (Figure 4.7) is clear that the pins have not undergone modifications during the flight.

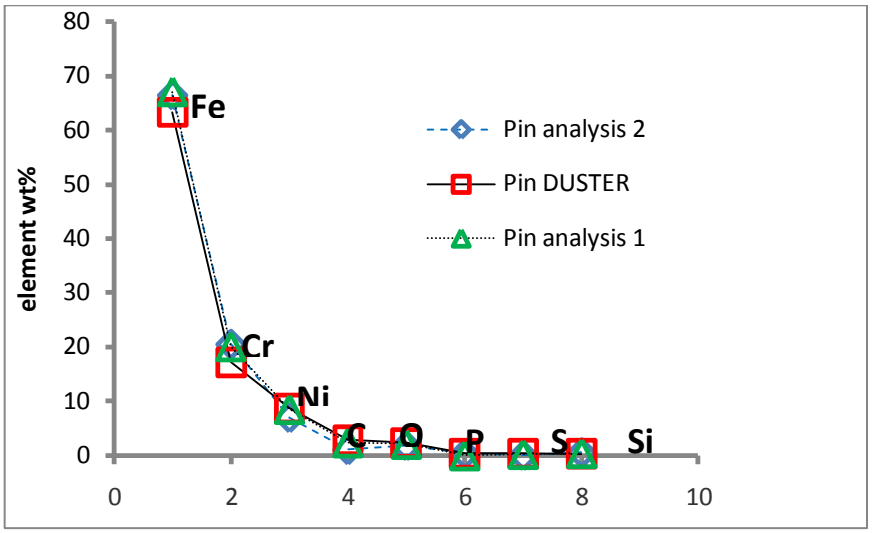

Figure 4.7 Plot of elements wt% EDX analyses of two different pins: one that flown during DUSTER 2008 campaign; and a spare Pin stored in laboratory.

Element wt% of Pin beneath the TEM grids			
	Pin mounted on DUSTER2008 sample holder (10 keV)	Pin (analysis 1) stored in laboratory (15 keV)	Pin (analysis 2) stored in laboratory (15 keV)
C	2.8 ± 0.2	2.4 ± 0.25	1.05 ± 0.1
O	2.3 ± 0.2	2.1 ± 0.2	1.8 ± 0.2
Si	0.3 ± 0.1	0.4 ± 0.1	0.5 ± 0.1
P	0.3 ± 0.1	-	0.3 ± 0.1
S	0.3 ± 0.1	0.25 ± 0.1	-
Cr	17.2 ± 2.15	20.1 ± 0.25	20.5 ± 0.3
Fe	63.3 ± 1.4	67.1 ± 0.5	66.5 ± 0.5
Ni	8.65 ± 0.7	8.55 ± 0.3	7.0 ± 0.3

Table 4.1 Element wt% EDX analyses of two different pins: one that flown during DUSTER 2008 campaign; and a spare Pin stored in laboratory.

The pins are manufactured objects and the element ratios have to be constant. The Cr/Ni ratio given by the factory to recognize the stainless steel used is 1.98 and it match with the EDX analyses (see Table 4.2).

Ratios of the stainless steel pin elements	
Cr/Ni	1.98 ± 0.29
Fe/Cr	3.69 ± 0.47
Fe/Ni	7.32 ± 0.60
Fe/C	22 ± 2
Fe/O	28 ± 3
Fe/Si	235 ± 78
Fe/P	186 ± 60
Fe/S	198 ± 68

Table 4.2 Ratios of the stainless steel pin (the one that is on DUSTER collector) elements.

Being the most abundant elements Fe, Cr and Ni, I decided to solve the problem of contamination by pin elements with the following procedure:

- if the analyses shown contemporary Fe, Cr and Ni it means that the grain analyses have the contribution of the pin;
- compare the Fe-ratios of the pin (Table 4.2) with the Fe-ratios of the particle and take off the elements for which the ratios mach;
- the grain analyses were renormalized to 100%.

Gold contamination

Another source of contamination came from the gold smooth surface of the sample holder (Figure 4.1); it is an electrodepositing of gold and it is subjected to structural deterioration as can be see looking at the surface at high magnification. In this case splinters of gold can detached from the surface and move on the sample holder surface. Particles with this characteristic (Figures 4.8, 4.9, 4.10) were found on the TEM grids; in this cases the comparison of the scanning images pre- and post-flight let think that they were collected in stratosphere, but the analyses (Table 4.3) shown that they are almost all gold with traces of carbon and oxygen that can be due to the presence of holey carbon film. Particle D08C_004 also contained a small amount of Sn which is a laboratory contaminant (see below). So because of the deterioration of the gold smooth surface and because the gold is too heavy to be updrafted from Earth surface to the upper stratosphere at the DUSTER collection altitude the particles D08C_004, D08C_010 and D08C_018 are considered to contaminate the sample holder.

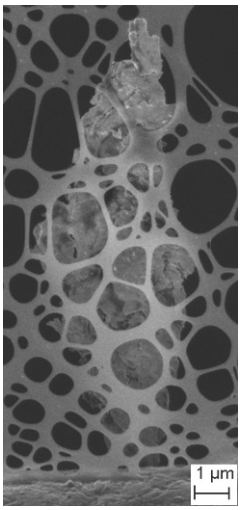

Figure 4.8 Particle D08C_004

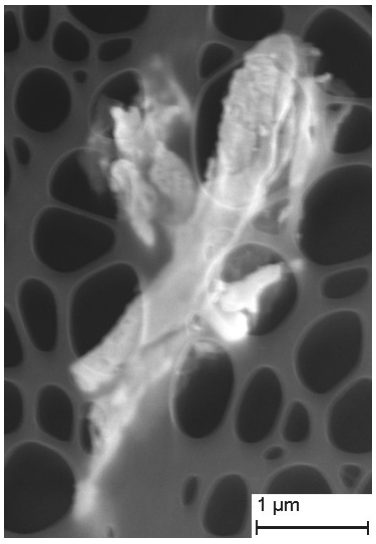

Figure 4.9 Particle D08C_010

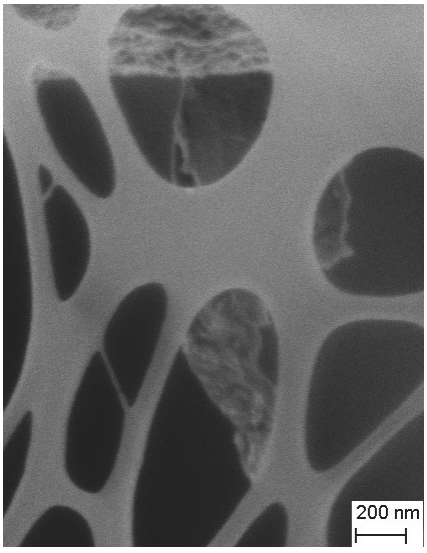

Figure 4.10 Particle D08C_018

Element wt% normalized at 100%					
	D08C_004(#1)	D08C_004(#2)	D08C_010(#1)	D08C_010(#2)	D08C_018
C	4.5	5.8	4.7	10.8	7.9
O	1.4	1.5	0.7	1.2	2.4
Cr					1.7
Fe					5.7
Cu				0.5	
Sn	1.3				
Au	92.8	92.7	94.6	87.5	82.3

Table 4.3 EDX analyses of particles D08C_004, D08C_010, D08C_018. The elements are normalized to 100%

Tin particles

On the sample holder were detected three particles Sn-rich (Figure 4.11-12-13, Table 4.4), they all three were consider laboratory contaminants, for the following reasons:

- in this particles is also present a considerable amount of gold (in particle D08C_016 more than tin);
- as can be seen in Table 4.3 one Au-rich particle (D08C_004) has tin in traces;
- the Sn-rich particles are in the same grid and in the same square of the Au-rich particles and all them are near the grid rim (exposed to the contamination from the sample holder surface);
- looking at the (Ca,Si) plot (Figure 4.14) of all the particles recognized as collected (see Chapter5) the Sn- rich particles are in the same cluster of the Au-rich particles;
- there are no evidence of pure tin with the size and morphology of DUSTER particles in the stratosphere, and this probably because it is an heavy element.

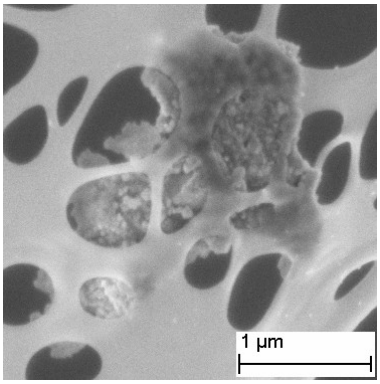

Figure 4.11 Particle D08C_013

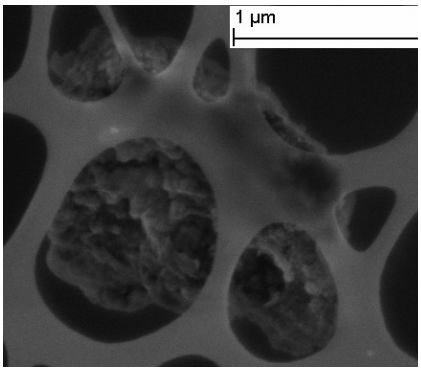

Figure 4.12 Particle D08C_016

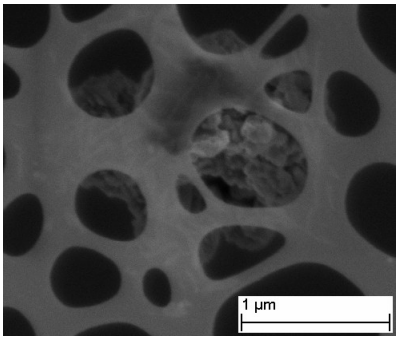

Figure 4.13 Particle D08C_021

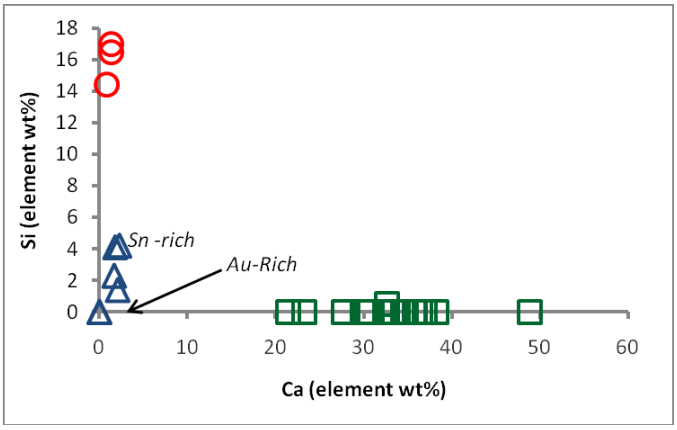

Figure 4.14 Plot (Ca, Si) of all the particle recognize as not present before flight using comparison of scanning images (for particles represent with red circles and green square see Chapter5).

There are some detected particles that for different reasons have not analyses information (see Chapter 5). This is the case of D08C_003 (Figure 4.15), that for its morphological similarity with the Gold and Tin particles is considered a laboratory contamination. This particle has not analyses because it was lost during FIB relocation.

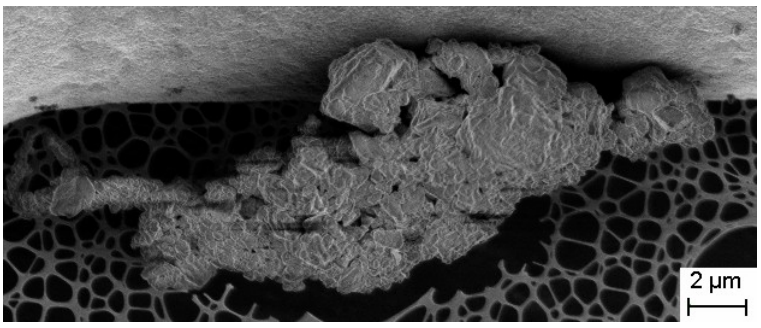

Figure 4.15 Partile D08C_003

Element wt% contamination corrected				
	D08C_013 (#1)	D08C_013 (#2)	D08C_016	D08C_020
C	26.6	26.4	32.5	21.8
O	23.0	23.3	24.2	17.2
Na		0.6	1.0	
Al			0.6	0.6
Si	1.2	1.9	3.3	3.6
Ca	1.7	1.4	1.4	2.0
Fe				18.5
Cu			3.5	
Zn	2.1			
Sn	27.1	29.0	14.3	22.3
Au	18.3	17.4	19.2	14.0

Table 4.4 EDX analyses of particles D08C_013, D08C_016, D08C_020. The elements are normalized to 100% after Fe, Cr, Ni correction

4.3.2 Source of contamination by FIB

As mentioned in Chapter 3, the particles relocated with FIB instrument are fixed in a copper grid, the needle used to relocate them is made of tungsten and the sealing and unsealing is made with platinum and gallium respectively. So the particles relocated with FIB could be contaminated with Cu, Pt, Ga, and W. Also in this case the problem of contamination is solved subtracting the contaminant elements and normalizing the remnants elements to 100%.

In the Table 4.5 is shown an example of particle relocated with FIB. The particle in the DUSTER collector looks like a single particle, but in reality it was composed of two particles. The first thing notable is that D08C_008b has a composition similar to the EDX bulk analyses of almost all the particle (D08C_008) performed when the particle was still on the DUSTER collector. However, D08C_008a is different. A subsequent Raman analysis of D08C_008a and D08C_008b shown that in the particles and in the copper grid where they are sealed there is the amorphous carbon feature (see Chapter 5). All the evidences above let suppose that the FIB instrument is a also a source of contamination for sub-micron size amorphous carbon particles too.

Element wt% of the same particle before and after relocation with FIB instrument			
	D08C_008	D08C_008a	D08C_008b
C	24.8	66.4	22.3
O	39.2	24.0	37.8
Na	0.4	1.2	
Mg		0.2	
Al		1.5	4.4
Si		1.2	
S		1.0	
Cl		1.7	
K		1.1	
Ca	34.5	1.7	35.5
Fe	1.1		

Table 4.5 Example of particle (D08C_008) relocated with FIB instrument. After relocation the particle divided into two different parts (D08C_008a and D08C_008b). The analyses reported in the table are EDX analyses contamination corrected and normalized to 100%. The D08C_008a in Raman analyses has a-C, the particle D08C_008b has a-C and calcite. The EDX spectrum of D08C_008b is more similar to the D08C_008 than the D08C_008a.

4.3.3 Sources of contamination from the flight train

In the flight train of the DUSTER collector has above it, in a range of almost 20 m: a balloon, a parachute, 4 solar panels and a telemetry package. All these objects can be potential sources of contamination being exposed to the external environment for all the time from the preparation of the launch to the end of collection. It is not possible to exclude contamination from the flight train, but we can be confident that there is a low probability of contamination from these sources for the following reasons:

1. the particles in the nanometer/micrometer range remain attached to the objects were they are deposit thanks to the Van der Waals forces;

2. the particles deposit on the balloon surface are not ejected because of the difference of pressure that blow up the balloon because the decreasing of pressure with altitude was constant and not sudden (Figure 4.16);

3. the inlet tube remain closed until the altitude of ~25 km when the pressure inside the inlet equal the external pressure and the flange that seal the inlet falls down;

4. the valve that open the collecting chamber is opened at ~35 km, and the pressure inside the chamber is higher than outside, so the first air flux is directed outside the chamber. If there is something deposit in the inlet is not aspired but pushed out.

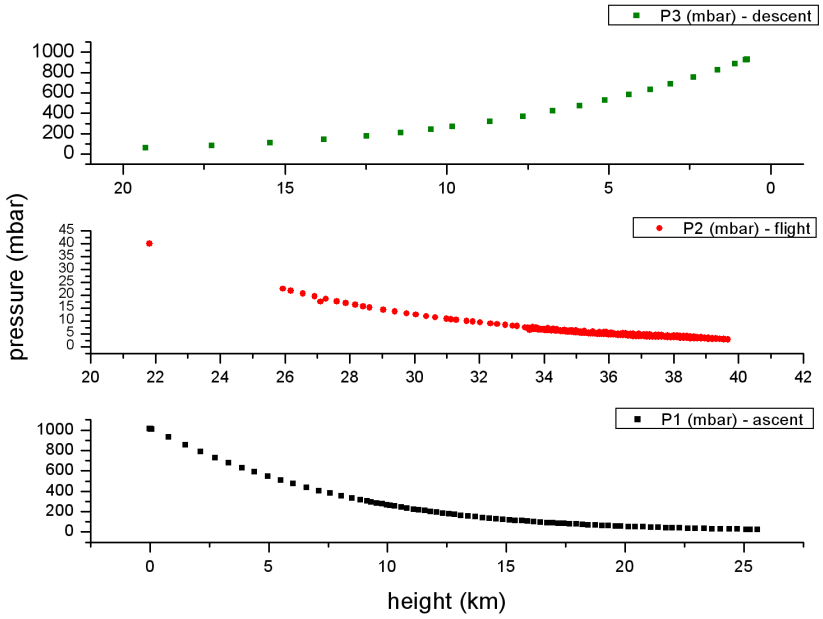

Figure 4.16 Plot of changing of pressure with altitude. From down to up the ascendant phase (during which the balloon blow up), the floating phase (during which the balloon has almost a constant volume) and the descendent time (the instrument is free from the balloon).

Conclusions

Even when the procedures to preserve clean the sample holders were correctly followed, on the collection surface were found contamination almost all due to the sample holder itself. The contamination problem is solved for DUSTER2008 campaign by not considering all the particles that are sources of ambiguity and removing the chemical elements due to substrate. The problem of contamination due to the sample holder structure and materials is definitively solved changing the structure for the DUSTER 2009 campaign (see Chapter 6).

Also the problems due to the scanning procedures were solved for DUSTER 2009 campaign, but in DUSTER 2008 collection the lost of information fixed a cut-off in size and number of particles that could be identified as collected. For example all the particles less than 0.5 µm are too little to be detected from the resolution of our scanning.

In the end trying to relocate the particles with FIB instrument it is clear that this kind of technology is not useful for particles <20 µm; the range is established by the particles collected and relocated with FIB, we have not information on what happened for particles > 20 µm. For particles less than 5 µm the FIB technique causes the loss of part of the particle's mass and the presence of contamination due to the tools used to relocate samples. For particles less than 5 µm the particle's mass lost after relocation is almost 50% and the remnant is totally embedded in contamination elements. For this reasons I can conclude that FIB technology is not useful to handle the particles in the size range less than 20 µm for the DUSTER experiment.

5 Sample collected during the June 2008 campaign: analyses results

In this chapter are shown the results of DUSTER 2008 flight:

- the particles are classified by size, morphological class and composition;
- it is reported a catalogue of raw data of chemical analyses (FESEM-EDX, FT-IR and Raman spectroscopy);
- are discussed the origins of contaminants element and how to remove it;
- finally there is a discussion of data reduction and the origins of collected particles.

5.1 Particle statistics and size distribution

DUSTER flew from Svalbard to Greenland (Figure 2.3) and collected particles at an average altitude of 37 km during a 55h period during June 2008.

The scanning procedure performed by FESEM on the collector led to the identification of 32 particles as present only post-flight. Among the 32 identified particles, 7 are classified as laboratory contamination (cf. Chapter 4) and 25 as collected stratospheric particles. In this chapter only the 25 stratospheric particles will be considered.

As discussed on the previous chapter, not all the collecting areas were examined. The procedure of comparison between pre- and post-flight FESEM scanning to recognize the collected particles was limited to 12 grids instead of 14. Grids 5 and 6 were not scanned pre-flight. Particles > 100 μm when placed in the FESEM electron beam using at EHT (Extra High Tension) = 10 kV (the voltage used to scan the grids) are at risk of charging causing them to jump away; in order to not lose the spheres (100 – 150 μm size) the grids wherein they are located were not scanned during post-flight analysis. For this reason the comparison for grids 4 and 9 (where the spheres are collected) was done looking at the grids in real time with FE-SEM and using pre-flight images to check the particles identified.

Each TEM grid has roughly 500 mesh (metal squares that compose the grid), it means a total of 5000 mesh for 10 grids. Because of the pin structure (see Chapter4) before the flight there was 148/5000 mesh damage, that after flight became 1074/5000 probably due to thermal shock.

Finally the Collector's area investigated to search for particles collected in stratosphere is less than 50 % of the whole collector and consequently the number of collected particles might be higher. The distribution of particles is shown in (Table 5.1), the majority is in the 'central grid' and neighboring grids, but this is not statistically relevant because those are the grids with the high resolution scanning (see Chapter 4).

'central grid'	12 particles
Grids 1 and 2 (1 particle each grid)	2 particle
grid 7	3 particles
grids 4, '9, 10', 11, 12 and 13 (one each grid)	6 particles
grids 8	2 particles

Table 5.1 Numbers of stratospheric particles collected in the investigated grids.

The size of each collected particle was measured (μm) by a FESEM tool. For particles that are not perfect spheres were measured the minimum (*a*) and maximum (*b*) dimension and calculated the equivalent size using the quadratic mean (Table 5.2) of the two measures:

$$Size = \sqrt{\frac{a^2 + b^2}{2}}$$

The aspect ratio *a/b* gives an estimate of the particle's degree of roundness (Figure 5.2), if it is 1 the particle is a disk or a sphere, if it is about 0 it is similar to a hourglass or a needle. Examining the collected particle size distribution it is evident that more than 90% of them are in the size range (0.5 – 7) μm (Figure 5.1), according to the instrument requirements and that except for the particles > 100 μm (they are spherical) the particles identified as collected are in the range of ellipsoidal shape (Figure 5.3).

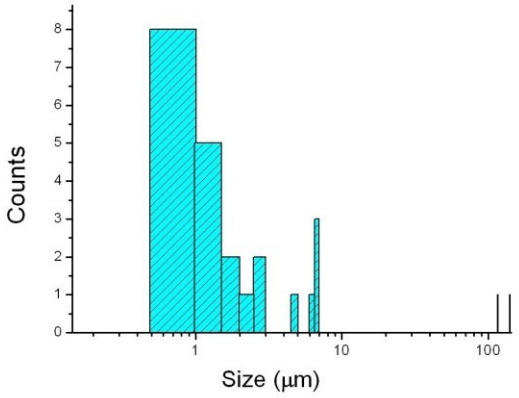

Figure 5.1 Size distribution of the 25 stratospheric particles collected

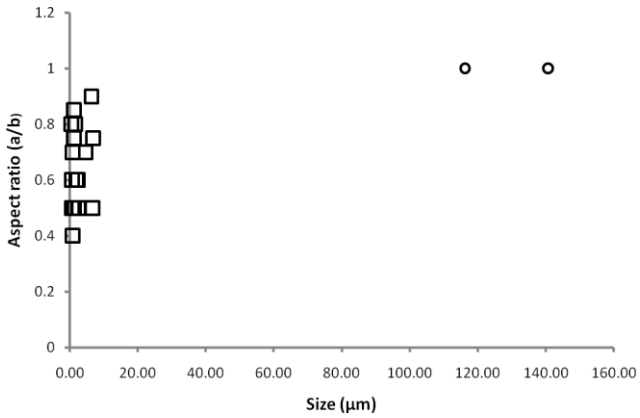

Figure 5.2 Plot size vs aspect ratio of the 25 stratospheric particles collected. The two circles represent the spheres.

Particle	*a*	*b*	*a/b*	equivalent size
D08C_001	140.70	140.70	1	140.70
D08C_002	116.30	116.30	1	116.30
D08C_005	4.40	8.18	0.5	6.60
D08C_006	5.84	7.75	0.75	6.85
D08C_007	6.10	6.64	0.9	6.40
D08C_008	3.88	8.50	0.5	6.60
D08C_009	3.86	5.41	0.7	4.70
D08C_011	1.60	3.40	0.5	2.65
D08C_012	1.65	3.10	0.5	2.50
D08C_014	1.85	2.96	0.6	2.40
D08C_015	1.41	2.35	0.6	1.95
D08C_017	0.50	1.85	0.2	1.35
D08C_019	1.00	1.31	0.75	1.20
D08C_021	1.42	1.47	0.8	1.60
D08C_022	0.60	1.29	0.5	1.00
D08C_023	0.86	1.66	0.5	1.30
D08C_024	1.15	1.35	0.85	1.25
D08C_025	0.66	1.00	0.7	0.85
D08C_026	0.47	0.90	0.5	0.70
D08C_027	0.49	0.86	0.6	0.70
D08C_028	0.44	1.07	0.4	0.80
D08C_029	0.54	0.87	0.6	0.70
D08C_030	0.47	0.84	0.6	0.70
D08C_031	0.45	0.56	0.8	0.50
D08C_032	0.42	0.52	0.8	0.45

Table 5.2 In this table are reported the minimum (*a*) and maximum (*b*) elongation, the level of roundness (*a/b*) and the equivalent size (sqrt[(a^2+b^2)/2]) of the 25 stratospheric particles collected.

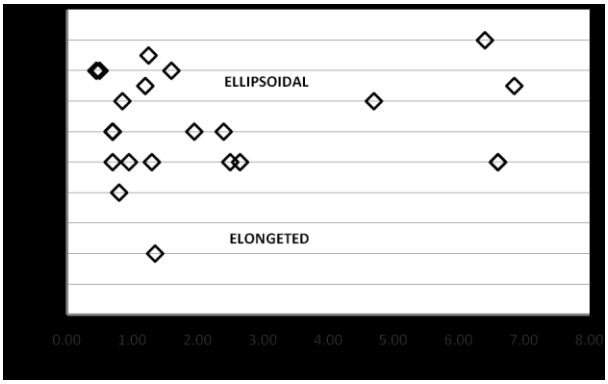

Figure 5.3 Plot Size vs Aspect ratio of the stratospheric particles collected in the size range (0.5 - 7) µm

5.2 Morphology

The morphological classification consist of observing particles with the FESEM, setting the EHT of the Inlens detector (see Chapter 3) at 2kV to avoid sample charging effects, thus to enhance the details of the particle's surface. The particles were classified taking inspiration from the classification described in Mackinnon et al. (1982) for stratospheric particles collected by NASA program.

The morphological classes recognized for DUSTER's particles are: spheres (Figure 5.4), aggregates and fragments (Figure 5.6). The aggregates can be of spherical grains (Figure 5.7) or non spherical grains (Figure 5.5). The term fragment has not to be confused with the fragmentation process, the morphological class called 'fragment' is referred to particles that are neither spheres nor aggregates. Following this classification, DUSTER collected 2 spherical particles and the remnants are well distributed between fragments and aggregates (Figure 5.8).

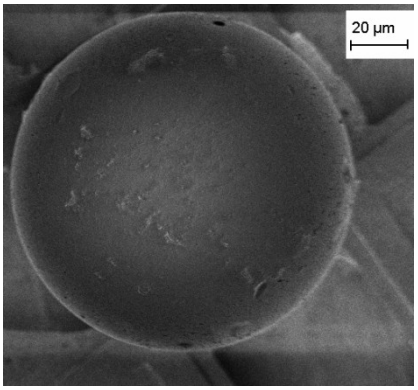

Figure 5.4 Spherical particle D08C_002.

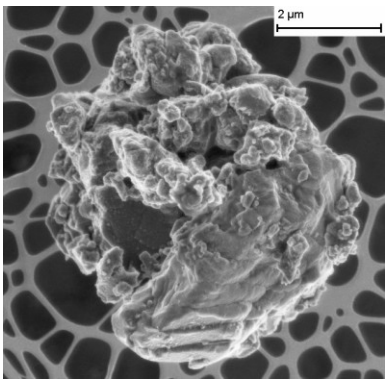

Figure 5.5 Aggregate of non spherical grains, particle D08C_007.

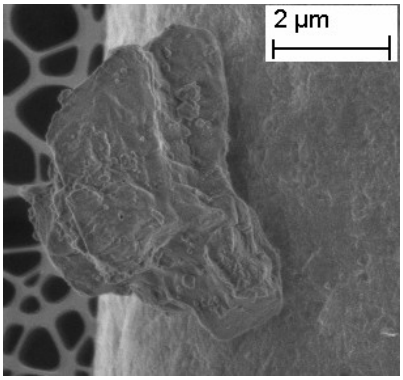

Figure 5.6 Fragment, particle D08C_009.

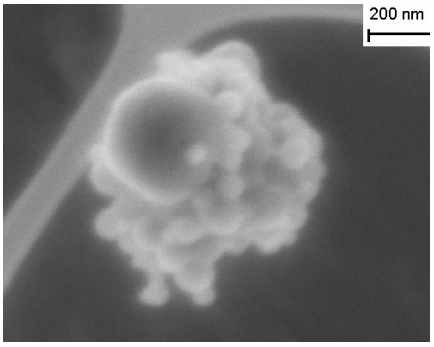

Figure 5.7 Aggregate of spherical grains, particle D08C_031.

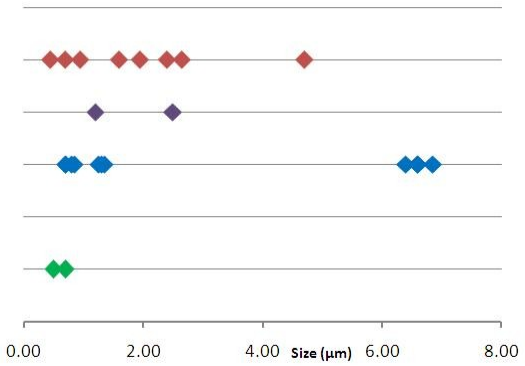

Figure 5.8 In the plot are represented the morphological groups in function of size. The red diamonds are the fragments, the light blue diamonds are the aggregates of non spherical grains, the purple diamonds are the particles defined as fragment/aggregates, and the green diamonds are the aggregate of spherical grains.

5.3 Catalogue of raw data

Here following I will present the particle's catalogue with the relative results obtained with the different analytical techniques applied.

For each of the 25 particles collected is shown:

- FE-SEM image (where they are necessary to highlight particular morphological features, there are more images);
- EDX analyses (without contamination removal);
- size (µm);
- morphological class;

- composition;
- position on the sample holder.

For some of the 25 particles we do not have information about composition. They are moved in a particular section at the end of the catalogue, called ‘Particles Unknown’.

D08C_001

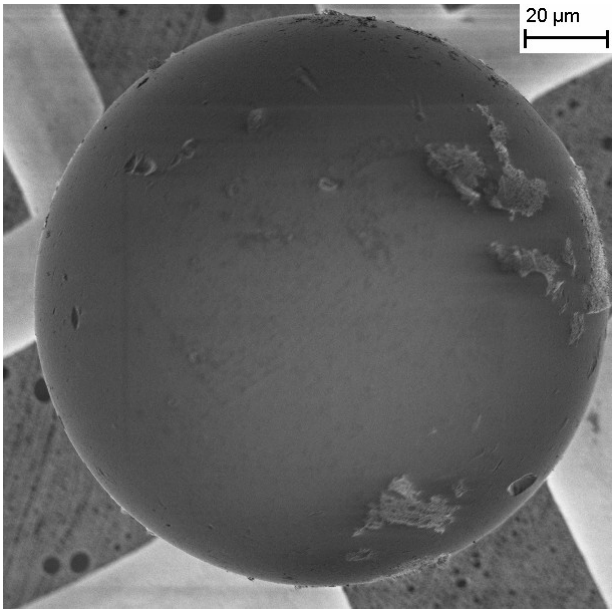

Size: 140.70 µm

Position: grid 9

Morphological class: Sphere

Composition: O, Si, Na, C, Ca, Mg, Fe, Al

Analyses Performed:

- FESEM-EDX

Figure 5.9 FESEM image at 2 kV of particle D08C_001

The surface is mainly smooth but there are pits, projections and fractures.

Looking at the mosaic of pictures taken by FE-SEM going into high magnification (Figure 5.10) are visible structures that seems to come up from the surface or be under surface. There are also (unidentified) fragments that seems to be extraneous to the sphere attached on the surface. Pieces of holey carbon film, detached from the TEM grid, are visible on the sphere's surface.

Looking at the sphere with an optical microscope are visible bubbles inside (Figure 5.11) it show also that the sphere is transparent.

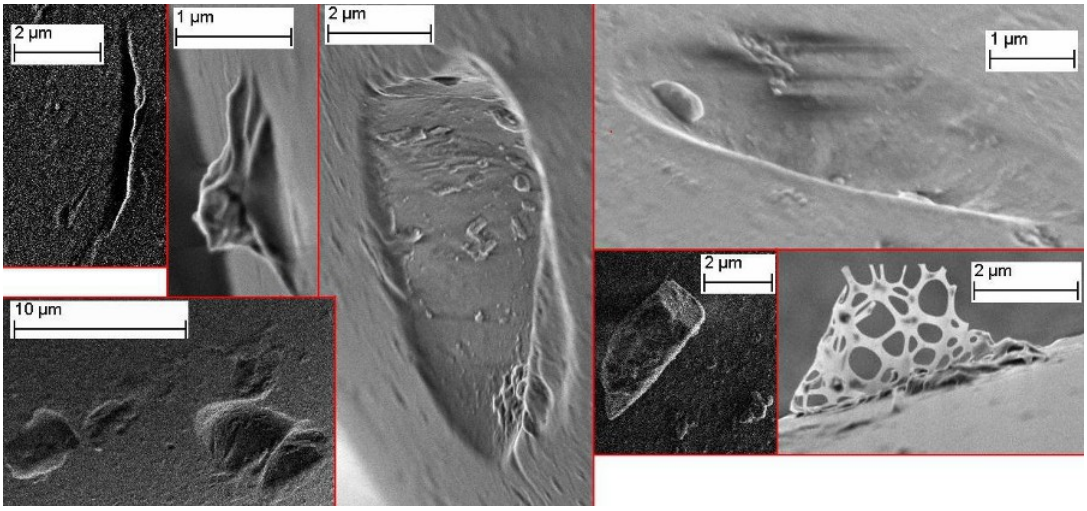

Figure 5.10 Mosaic of particulars of particle D08C_001 performed with FESEM at 2 kV.

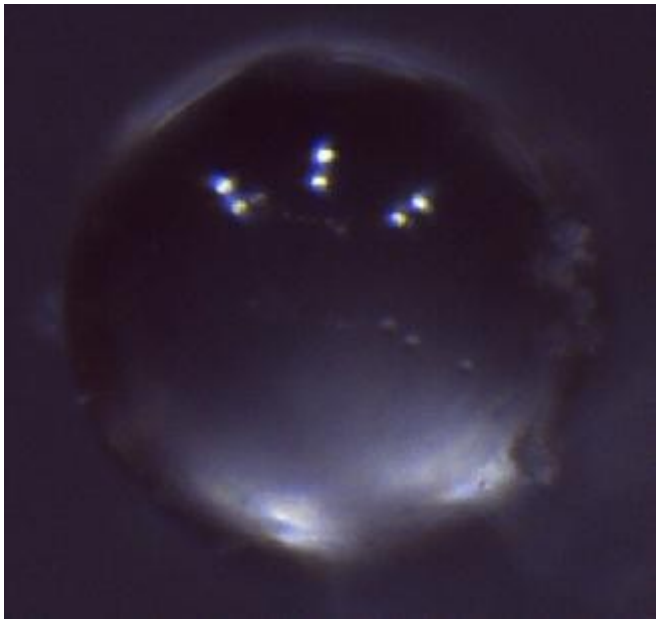

Figure 5.11 Picture of the particle D08C_001 on a substrate of KBr. The white spots are reflection of the light of the microscope on the particle. Is also visible near the center little bubbles of different size. On the external part can be see residual of carbon film.

EDX (15kV) bulk analysis		
Elements	Weight %	Sigma
O	62.92	0.50
Na	9.24	0.17
Mg	2.03	0.09
Al	0.16	0.06
Si	22.97	0.19
Ca	2.55	0.10
Fe	0.47	0.12
Au	5.43	0.34
TOT	105.77	

Table 5.3 EDX analysis of the area shown in Figure 5.12

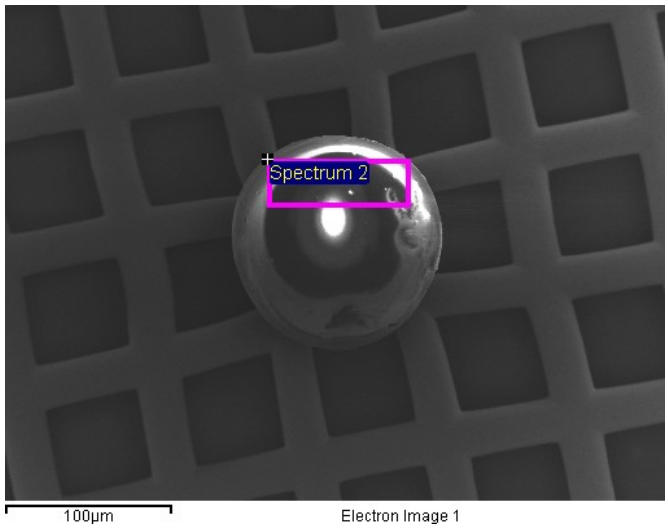

Figure 5.12 Area of the particle in which is performed the EDX

EDX (15kV) spot analysis		
Elements	Weight %	Sigma
C	6.62	0.45
O	63.60	0.51
Na	6.27	0.15
Mg	1.59	0.08
Al	0.20	0.06
Si	18.35	0.17
Ca	1.57	0.08
Au	4.73	0.32
TOT	102.93	

Table 5.4 EDX analysis of the area shown in Figure 5.13

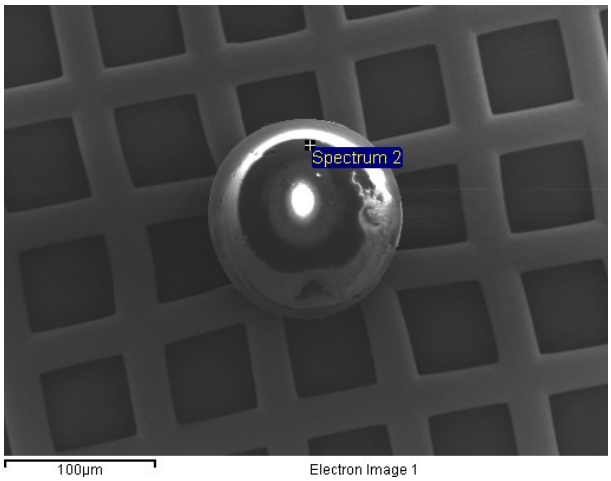

Figure 5.13 Area of the particle in which is performed the EDX

D08C_002

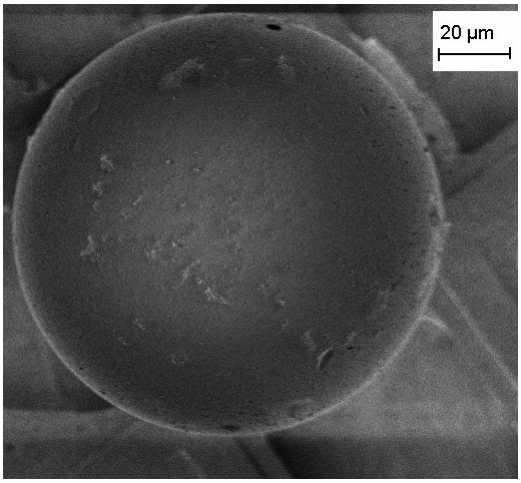

Size: 116.30 µm

Position: grid 4

Morphological class: Sphere

Composition: O, Si, C, Na, Ca, Mg, Al

Analyses Performed:

- FESEM-EDX

Figure 5.14 FESEM image at 2 kV of particle D08C_002

As in the previous case (D08C_001) the sphere is not so smooth as it appears looking at the Figure 5.14. Going into high magnifications also in this case are visible pits, fractures and fragments attached on the surface (Figure 5.15).

During relocation this particle was lost, but in Figure 5.16 there is a picture of the particle on the DUSTER sample holder performed with the optical microscope and it is transparent and with bubble inside. The bubbles show a size gradient from the smaller (near the center) to the largest (near the surface).

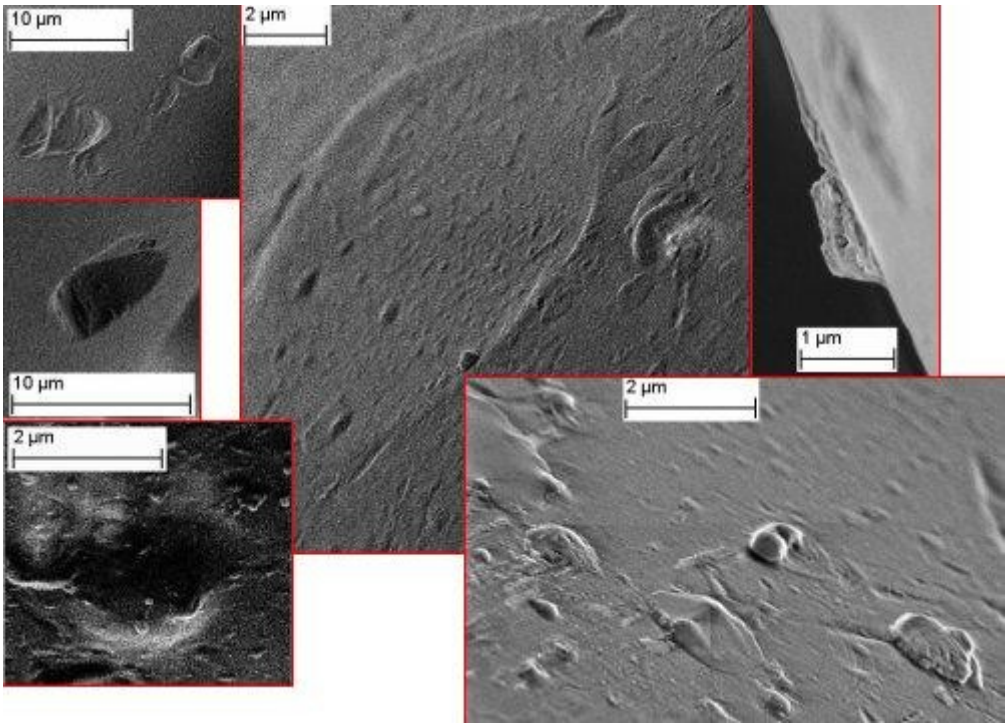

Figure 5.15 Mosaic of particulars of particle D08C_002 performed with FESEM at 2 kV.

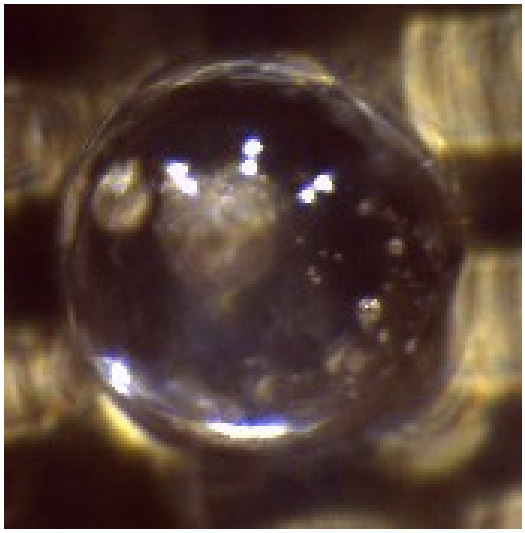

Figure 5.16 Picture of the particle D08C_002 on the DUSTER sample holder. The white spots are reflection of the light of the microscope on the particle. Is also visible on left side a big bubble and on right side bubbles of different size. In this picture is also evident that the particle is transparent.

EDX (15 kV) bulk analysis		
Elements	Weight %	Sigma
C	7.65	0.45
O	53.50	0.50
Na	7.28	0.15
Mg	1.68	0.08
Al	0.16	0.06
Si	19.39	0.18
Ca	2.10	0.09
Au	3.55	0.28
TOT	95.31	

Table 5.5 EDX analysis of the area shown in Figure 5.17

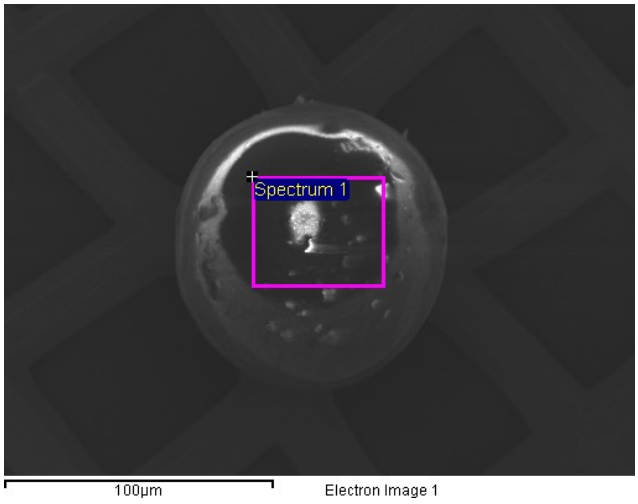

Figure 5.17 Area of the particle in which is performed the EDX

D08C_006

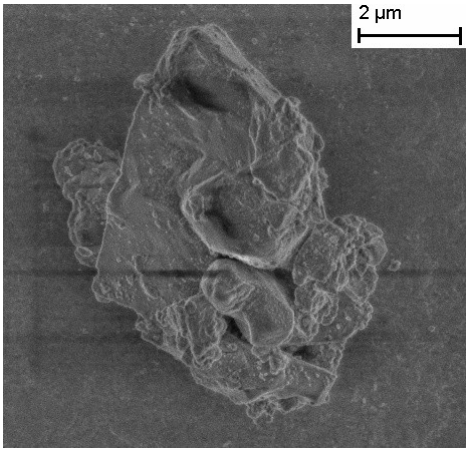

Figure 5.18 FESEM image at 2 kV of particle D08C_006

Size: 6.85 µm

Position: central grid

Morphological class: Aggregate of non spherical grains

Composition: O, Ca, C

Analyses Performed:

- FESEM-EDX
- Relocated using FIB instrument
- Raman

EDX (10 kV) spot analysis		
Element	Weight %	Sigma
C	14.13	0.12
O	52.73	0.52
Ca	35.78	0.44
Au	4.71	0.48
TOT	107.35	

Table 5.6 EDX analysis of the area shown in Figure 5.19

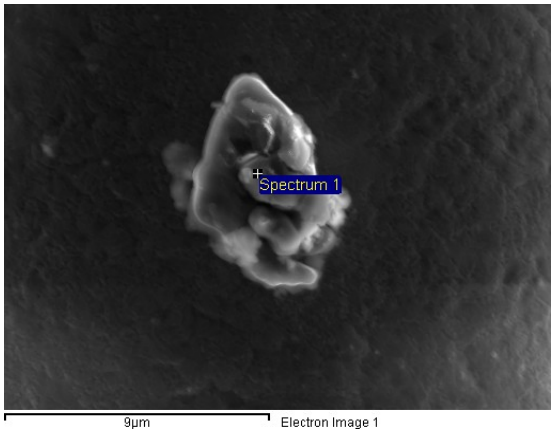

Figure 5.19 Area of the particle in which is performed the EDX

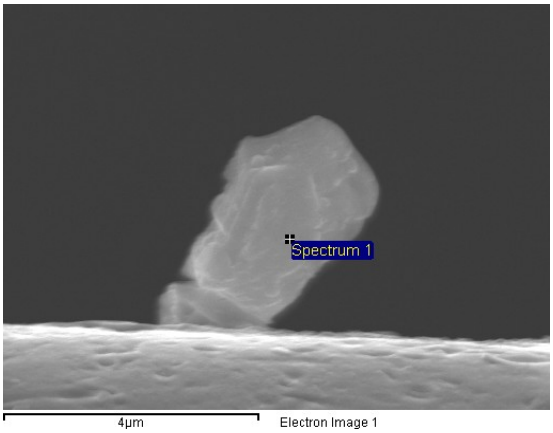

Figure 5.20 Area of the particle in which is performed the EDX

EDX (15 kV) spot analysis		
Element	Weight %	Sigma
C	13.79	0.15
O	14.14	0.43
F	1.24	0.29
Al	2.03	0.11
Ca	29.76	0.30
Cu	24.05	0.47
Pt	8.57	0.38
TOT	93.58	

Table 5.7 EDX analysis of the area shown in Figure 5.20

D08C_007

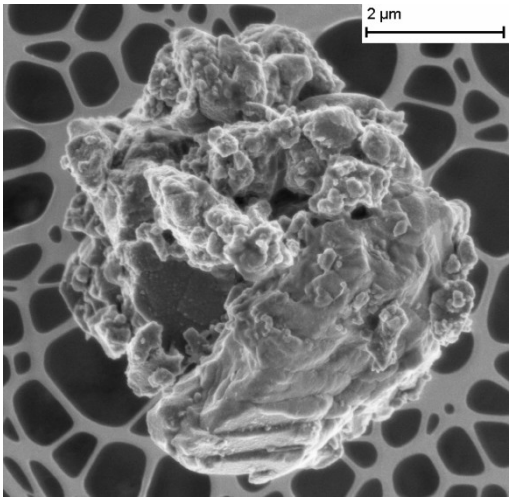

Figure 5.21 FESEM image at 2 kV of particle D08C_007

Size: 6.40 µm

Position: central grid

Morphological class: Aggregate of non spherical grains

Composition: Ca, O, C, F, Fe, Si

Analyses Performed:

- FESEM- DX
- Relocated using FIB instrument
- FT-IR
- Raman

EDX (10 kV) bulk analysis		
Element	Weight %	Sigma
C	19.44	0.12
O	29.66	0.50
F	11.93	0.54
Ca	31.20	0.46
Si	0.47	0.08
Fe	2.93	1.66
Au	2.72	0.39
TOT	98.35	

Table 5.8 EDX analysis of the area shown in Figure 5.22

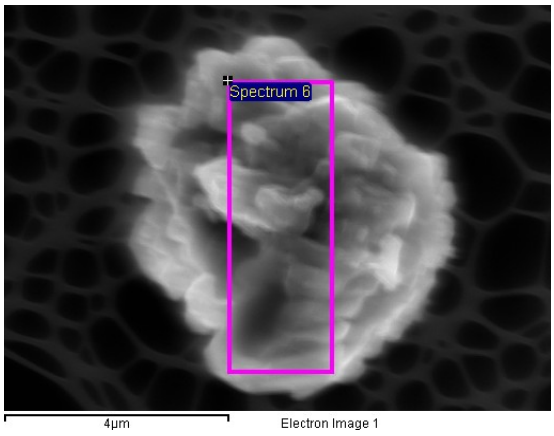

Figure 5.22 Area of the particle in which is performed the EDX

D08C_008

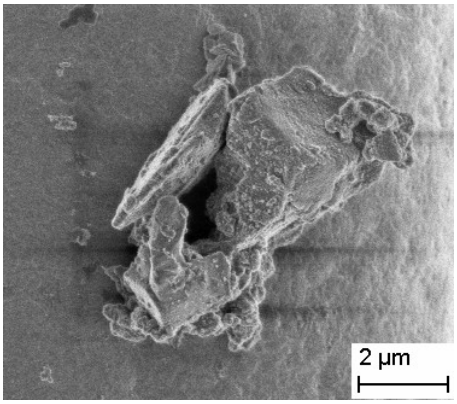

Figure 5.23 FESEM image at 2 kV of particle

D08C_008

Size: 6.60 µm

Position: central grid

Morphological class: Aggregate of non spherical grains

Composition: O, Ca, C, Fe, Na

Analyses Performed:

- FESEM-EDX
- Relocated using FIB instrument
- FT-IR
- Raman

EDX (15 kV) bulk analysis		
Element	Weight %	Sigma
C	16.30	0.12
O	25.75	0.39
Na	0.24	0.06
Ca	22.62	0.23
Fe	0.71	0.16
Au	48.52	0.57
TOT	114.14	

Table 5.9 EDX analysis of the area shown in Figure 5.24

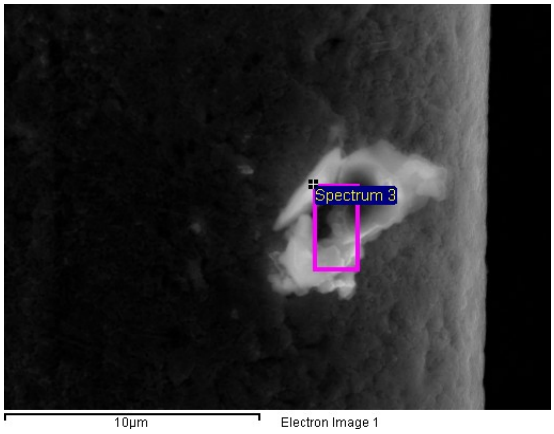

Figure 5.24 Area of the particle in which is performed the EDX

On DUSTER collector it seems to be a single particle compose of a fragment and some little grains attached on it. During FIB relocation was clear that actually it is an optical effect. There are two particles very close one to each other.

They were renamed D08C_008(a) (the biggest fragment) and D08C_008(b) (the smallest fragment). The EDX reports above is in a bulk region that takes in account both the fragments. In order to have an EDX for each single fragment, after relocation it was performed a new EDX analysis for each of the two particles.

D08C_008(b)

EDX (15 kV) bulk analysis		
Element	Weight %	Sigma
C	17.12	0.14
O	29.04	0.47
Al	3.38	0.11
Ca	27.28	0.25
Cu	16.91	0.36
Pt	7.92	0.31
TOT	101.65	

Table 5.10 EDX analysis of the area shown in Figure 5.25

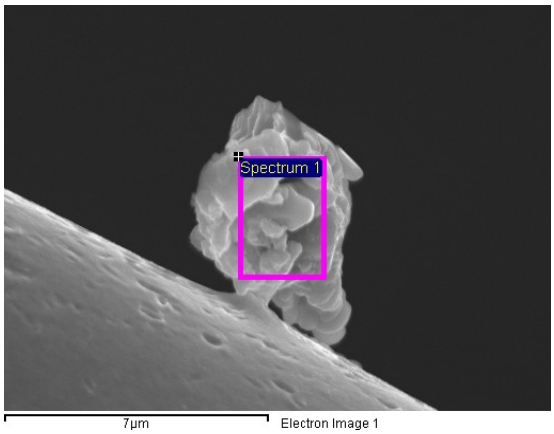

Figure 5.25 Area of the particle in which is performed the EDX

D08C_008(a)

EDX (15 kV) bulk analysis		
Element	Weight %	Sigma
C	62.23	0.66
O	22.55	0.43
Na	1.11	0.09
Mg	0.19	0.06
Al	1.37	0.08
Si	1.12	0.06
S	0.96	0.09
Cl	1.6	0.07
K	1.02	0.08
Ca	1.75	0.10
Cu	2.78	0.26
TOT	96.68	

Table 5.11 EDX analysis of the area shown in Figure 5.26

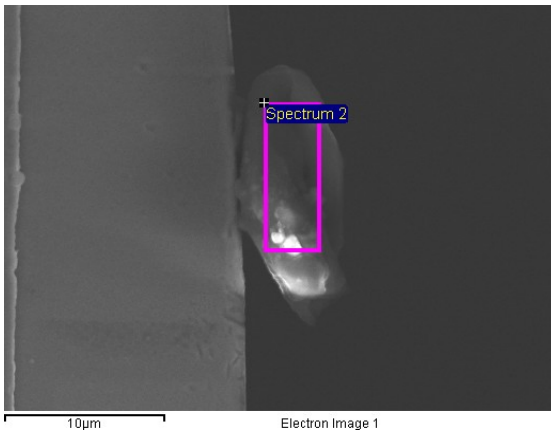

Figure 5.26 Area of the particle in which is performed the EDX

D08C_009

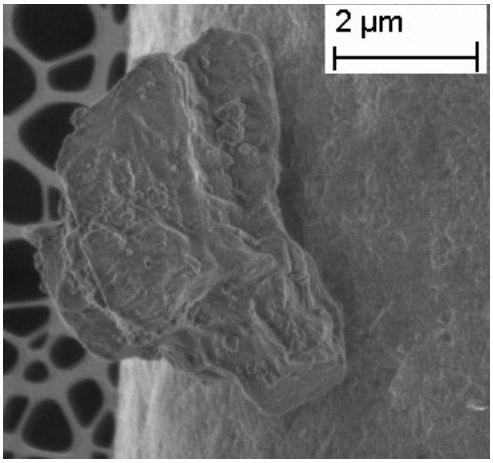

Figure 5.27 Image at 2 kV of particle D08C_009

Size: 4.70 µm

Position: central grid

Morphological class: Fragment

Composition: O, Ca, C, F

Analyses Performed:

- FESEM-EDX
- Relocated using FIB instrument
- FT-IR

EDX (10 kV) bulk analysis		
Element	Weight %	Sigma
C	15.35	0.11
O	47.12	0.55
F	2.33	0.36
Ca	26.95	0.44
Au	9.2	0.53
TOT	100.95	

Table 5.12 EDX analysis of the area shown in Figure 5.28

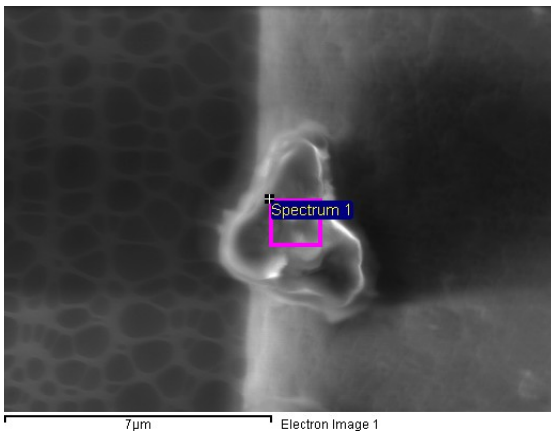

Figure 5.28 Area of the particle in which is performed the EDX

EDX (15 kV) bulk analysis		
Element	Weight %	Sigma
C	16.74	0.11
O	32.73	0.42
F	1.88	0.28
Mg	0.23	0.06
Al	1.53	0.07
Ca	23.16	0.20
Cu	9.09	0.27
W	0.57	0.15
Pt	6.55	0.26
TOT	92.48	

Table 5.12 EDX analysis of the area shown in Figure 5.29

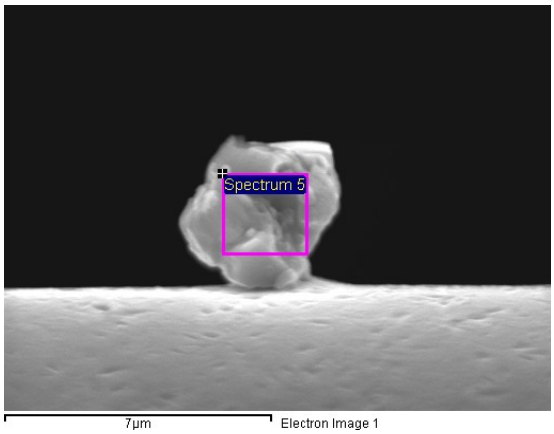

Figure 5.29 Area of the particle in which is performed the EDX

D08C_011

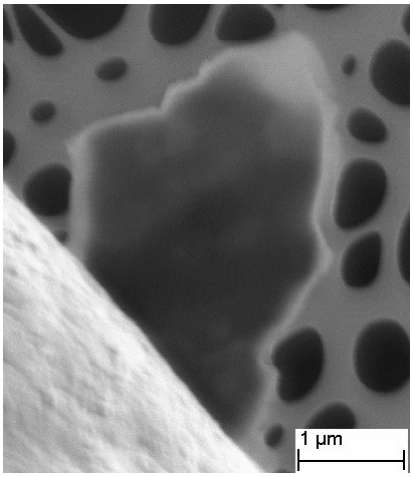

Size: 2.65 µm

Position: grid 1

Morphological class: Fragment

Composition: O, C, Si, Al, K, P, Na

Analyses Performed:

- FESEM-EDX

Figure 5.30 Image at 2 kV of particle D08C_011

EDX (10 kV) bulk analysis		
Element	Weight %	Sigma
C	4.41	0.51
O	10.94	0.28
Na	0.42	0.12
Al	2.55	0.11
Si	2.92	0.12
P	0.48	0.12
K	0.98	0.12
Cr	11.87	3.05
Fe	43.86	1.31
Ni	5.95	0.59
TOT	84.38	

Table 5.13 EDX analysis of the area shown in Figure 5.31

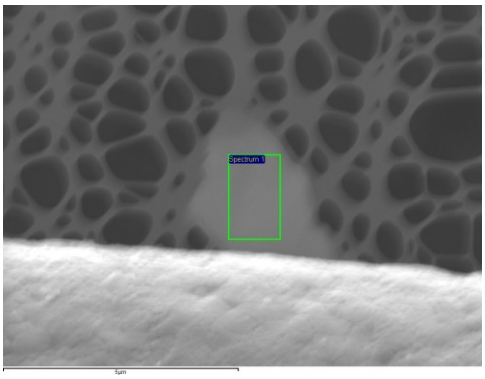

Figure 5.31 Area of the particle in which is performed the EDX

EDX (10 kV) spot analysis		
Element	Weight %	Sigma
C	4.74	0.50
O	10.64	0.27
Na	0.47	0.12
Al	2.21	0.11
Si	2.96	0.12
P	0.52	0.12
K	0.26	0.12
Cr	12.53	3.01
Fe	45.95	1.34
Ni	6.08	0.61
TOT	83.36	

Table 5.14 EDX analysis of the area shown in Figure 5.32

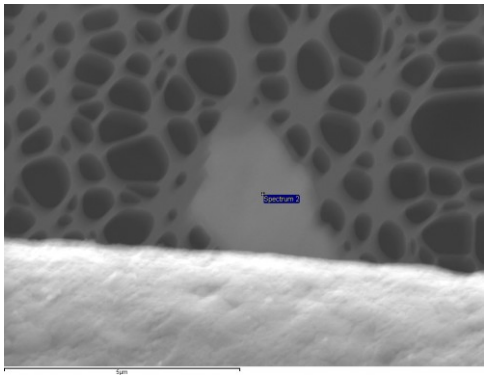

Figure 5.32 Area of the particle in which is performed the EDX

D08C_012

Size: 2.50 µm

Position: central grid

Morphological class: Fragment/Aggregate

Composition: O, Ca, C, F, Mg

Analyses Performed:

- FESEM-EDX

Figure 5.33 Image at 2 kV of particle D08C_012

EDX (10 kV) spot analysis		
Element	Weight %	Sigma
C	13.76	0.31
O	32.14	0.50
F	1.17	0.25
Mg	0.25	0.07
Ca	27.67	0.42
Au	27.84	0.79
TOT	102.83	

Table 5.15 EDX analysis of the area shown in Figure 5.34

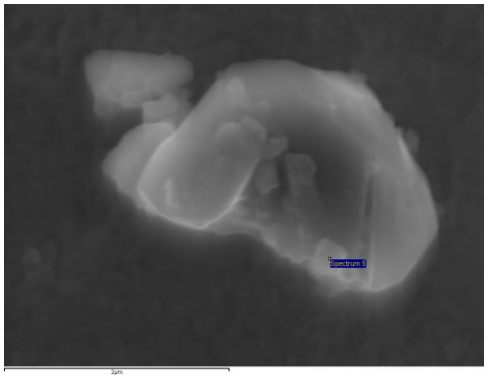

Figure 5.34 Area of the particle in which is performed the EDX

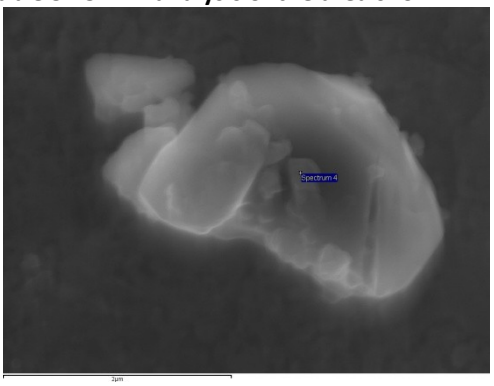

Figure 5.35 Area in which is performed the EDX

EDX (10 kV) spot analysis		
Element	Weight %	Sigma
C	18.88	0.34
O	54.29	0.64
Mg	0.29	0.08
Ca	35.41	0.47
Au	10.04	0.59
TOT	118.91	

Table 5.16 EDX analysis of the area shown in Figure 5.35

EDX (10 kV) bulk analysis		
Element	Weight %	Sigma
C	15.46	0.33
O	44.91	0.58
Ca	30.34	0.44
Au	23.13	0.74
TOT	113.84	

Table 5.17 EDX analysis of the area shown in Figure 5.36

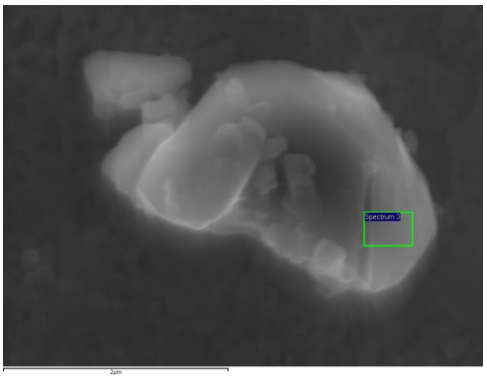

Figure 5.36 Area of the particle in which is performed the EDX

D08C_015

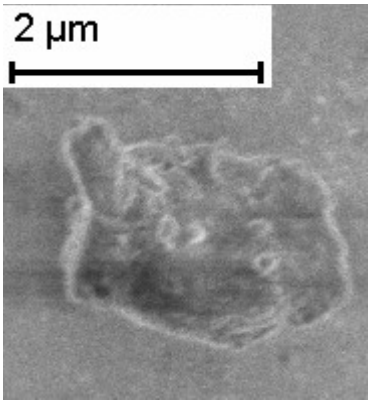

Figure 5.37 Image at 2 kV of particle D08C_015

Size: 1.95 µm

Position: central grid

Morphological class: Fragment

Composition: O, Ca, C, F, Mg

Analyses Performed:

- FESEM-EDX

EDX (10 kV) bulk analysis		
Element	Weight %	Sigma
C	16.94	0.40
O	29.90	0.47
F	1.46	0.31
Ca	14.69	0.34
Au	71.67	1.12
TOT	134.66	

Table 5.18 EDX analysis of the area shown in Figure 5.38

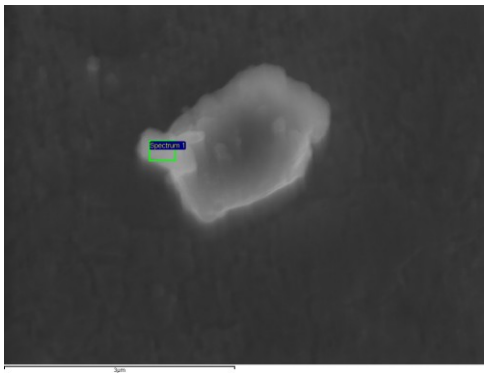

Figure 5.38 Area of the particle in which is performed the EDX

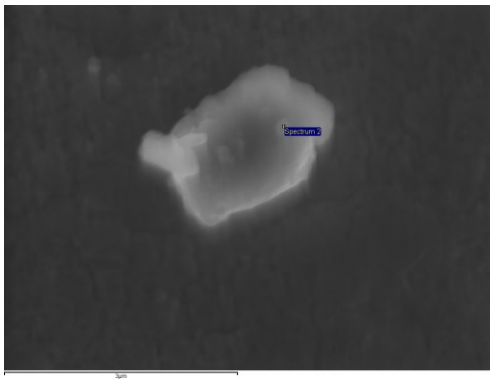

Figure 5.39 Area of the particle in which is performed the EDX

EDX (10 kV) spot analysis		
Element	Weight %	Sigma
C	16.80	0.36
O	44.01	0.57
Mg	0.28	0.09
Ca	29.62	0.43
Au	38.99	0.92
TOT	129.70	

Table 5.19 analysis of the area shown in Figure 5.39

D08C_019

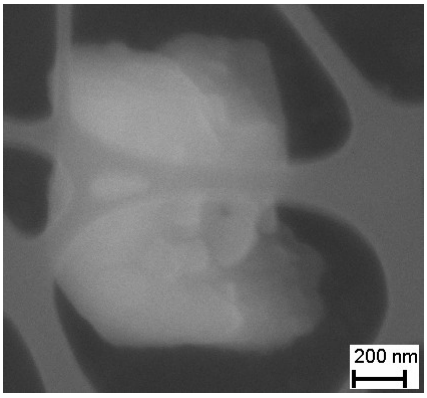

Figure 5.40 Image at 2 kV of particle D08C_019

Size: 1.20 µm

Position: central grid

Morphological class: Fragment/Aggregate

Composition: O, Ca, C, P, Na

Analyses Performed:

- FESEM-EDX

EDX (10 kV) spot analysis		
Element	Weight %	Sigma
C	14.97	0.33
O	32.12	0.51
Ca	26.27	0.39
Cr	13.29	5.38
Ni	2.09	0.45
Fe	27.00	1.35
TOT	115.74	

Table5.20 EDX analysis of the area shown in Figure 5.41

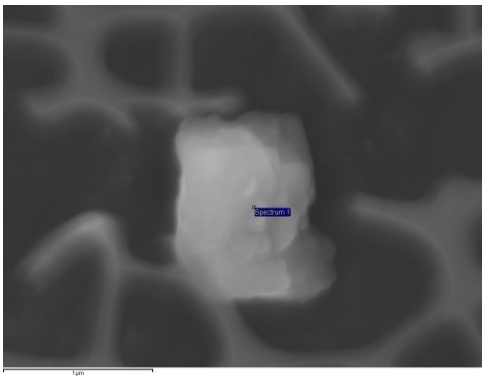

Figure 5.41 Area of the particle in which is performed the EDX

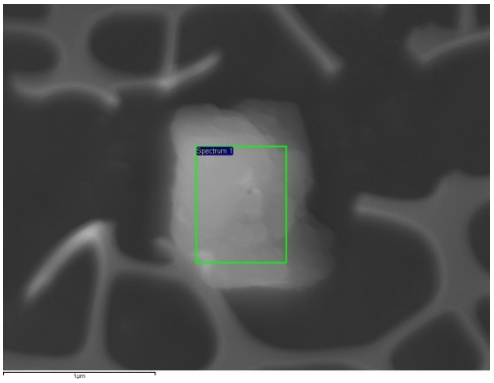

Figure 5.42 Area of the particle in which is performed the EDX

EDX (10 kV) bulk analysis		
Element	Weight %	Sigma
C	15.16	0.34
O	29.00	0.48
Na	0.39	0.11
P	0.47	0.13
Ca	24.05	0.38
Cr	15.20	5.01
Ni	2.38	0.47
Fe	31.74	1.39
Au	1.61	0.50
TOT	120.00	

Table 5.21 EDX analysis of the area shown in Figure 5.42

D08C_021

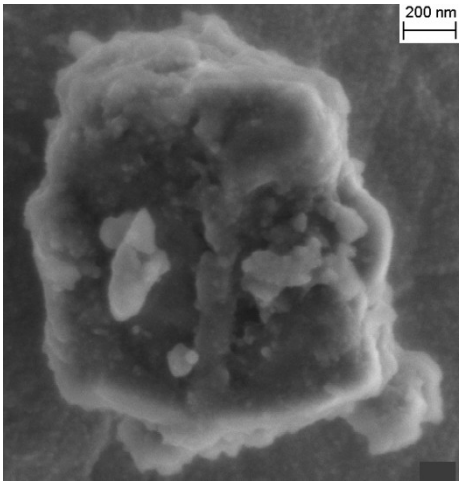

Size: 1.60 µm

Position: central grid

Morphological class: Fragment

Composition: O, Ca, C, F

Analyses Performed:

- FESEM-EDX

Figure 5.43 Image at 2 kV of particle D08C_021

EDX (10 kV) bulk analysis		
Element	Weight %	Sigma
C	12.75	0.30
O	38.48	0.55
F	1.07	0.31
Ca	29.97	0.43
Au	18.98	0.70
TOT	101.25	

Table 5.22 EDX analysis of the area shown in Figure 5.44

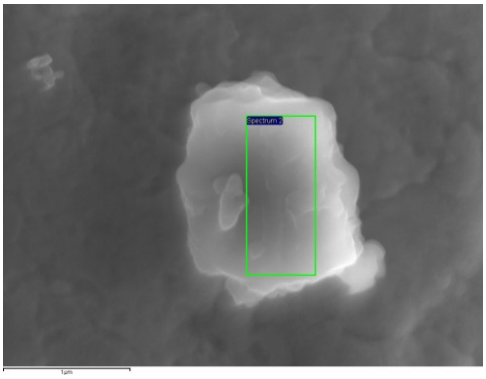

Figure 5.44 Area of the particle in which is performed the EDX

D08C_022

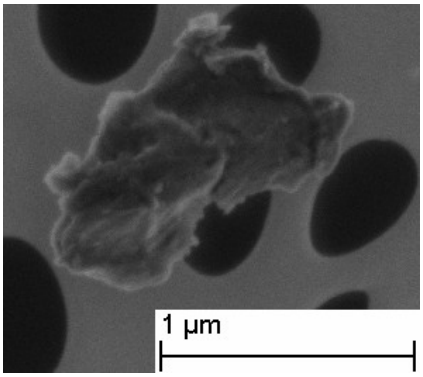

Figure 5.45 Image at 2 kV of particle D08C_022

Size: 0.95 µm

Position: grid 7

Morphological class: Fragment

Composition: C, O

Analyses Performed:

- FESEM-EDX

EDX (10 kV) spot analysis		
Element	Weight %	Sigma
C	5.30	0.29
O	4.78	0.24
Si	0.52	0.09
Cr	13.94	2.56
Fe	58.73	1.44
Ni	14.53	0.74
Au	4.49	0.52
TOT	102.29	

Table 5.23 EDX analysis of the area shown in Figure 5.46

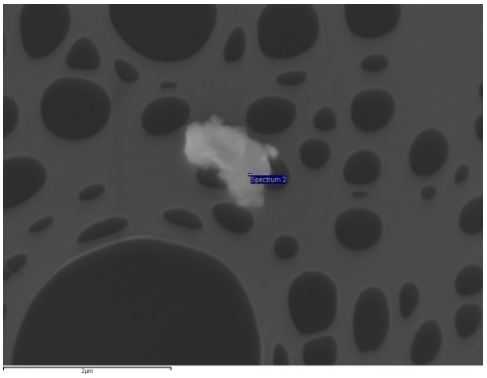

Figure 5.46 Area of the particle in which is performed the EDX

D08C_023

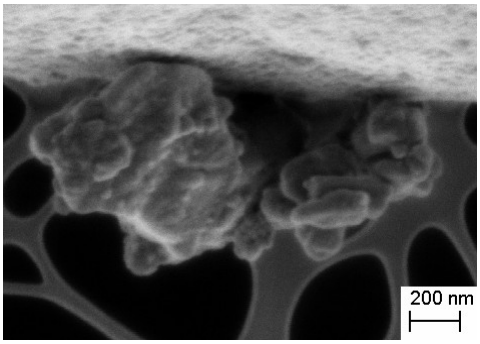

Figure 5.47 Image at 2 kV of particle D08C_023

Size: 1.30 µm

Position: central grid

Morphological class: Aggregate of non-spherical grains

Composition: C, O, Ca, Na

Analyses Performed:

- FESEM-EDX

EDX (10 kV) bulk analysis		
Element	Weight %	Sigma
C	7.31	0.33
O	4.28	0.27
Na	0.70	0.14
Si	0.38	0.10
Ca	1.02	0.16
Cr	21.56	2.80
Fe	74.67	1.64
Ni	10.97	0.79
Zr	1.43	0.38
TOT	122.32	

Table 5.24 EDX analysis of the area shown in Figure 5.48

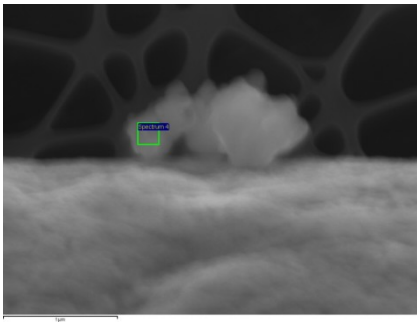

Figure 5.49 Area in which is performed the EDX

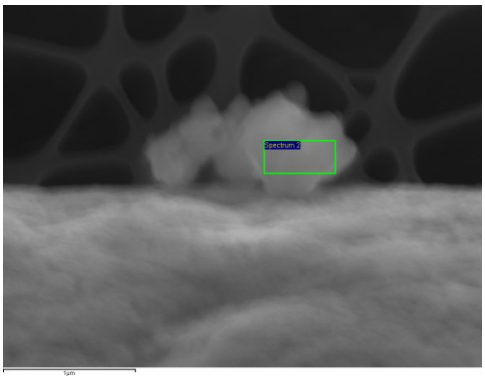

Figure 5.48 Area of the particle in which is performed the EDX

EDX (10 kV) bulk analysis		
Element	Weight %	Sigma
C	7.75	0.31
O	3.75	0.25
Na	0.79	0.14
Si	0.29	0.10
P	0.58	0.13
Cr	16.49	2.58
Fe	70.81	1.54
Ni	11.98	0.76
TOT	112.44	

Table 5.25 EDX analysis of the area shown in Figure 5.49

D08C_025

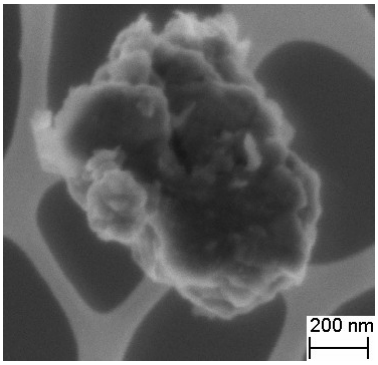

Figure 5.50 Image at 2 kV of particle D08C_025

Size: 0.85 µm

Position: grid 7

Morphological class: Aggregate of non-spherical grains

Composition: C, O

Analyses Performed:

- FESEM-EDX

EDX (10 kV) bulk analysis		
Element	Weight %	Sigma
C	21.27	0.43
O	8.64	0.30
Si	0.35	0.08
Cr	17.45	3.10
Fe	61.09	1.55
Ni	9.68	0.69
Au	5.24	0.50
TOT	123.72	

Table 5.26 EDX analysis of the area shown in Figure 5.51

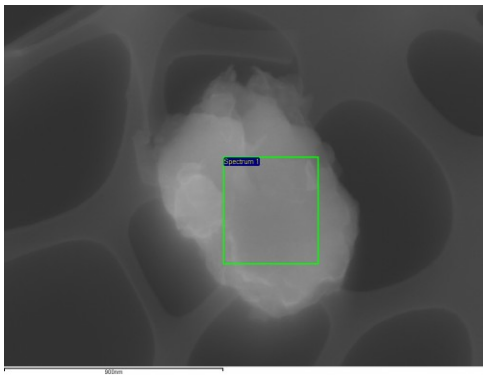

Figure 5.51 Area of the particle in which is performed the EDX

D08C_026

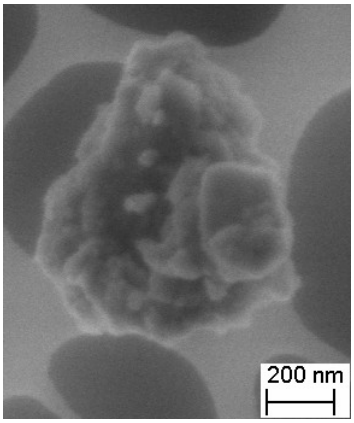

Figure 5.52 Image at 2 kV of particle D08C_026

Size: 0.70 µm

Position: grid 8

Morphological class: Aggregate of non-spherical grains

Composition: C, O, Na

Analyses Performed:

- FESEM-EDX

EDX (10 kV) bulk analysis		
Element	Weight %	Sigma
C	5.12	0.27
O	3.97	0.24
Na	0.46	0.14
Si	0.27	0.09
P	0.69	0.13
Cr	16.08	2.49
Fe	63.26	1.47
Ni	8.58	0.73
TOT	98.43	

Table 5.27 EDX analysis of the area shown in Figure 5.53

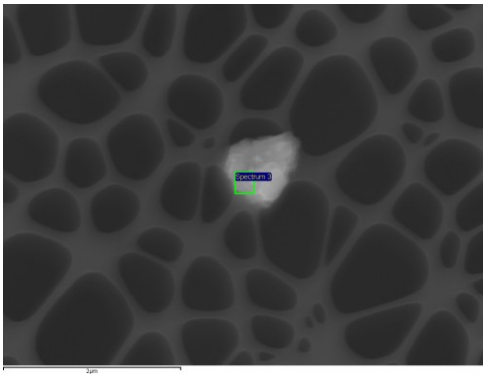

Figure 5.53 Area of the particle in which is performed the EDX

D08C_027

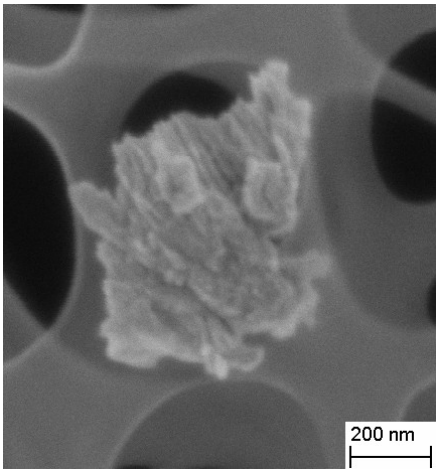

Size: 0.70 µm

Position: grid 7

Morphological class: Aggregate of non-spherical grains

Composition: C, O

Analyses Performed:

- FESEM-EDX

Figure 5.54 Image at 2 kV of particle D08C_027

EDX (15 kV) spot analysis		
Element	Weight %	Sigma
C	8.20	0.37
O	1.75	0.25
Cr	0.96	0.14
Fe	2.70	0.20
Cu	0.49	0.30
Au	78.14	0.72
TOT	92.24	

Table 5.28 EDX analysis of the area shown in Figure 5.55

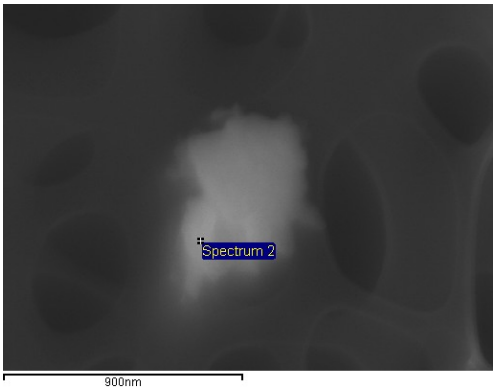

Figure 5.55 Area of the particle in which is performed the EDX

D08C_028

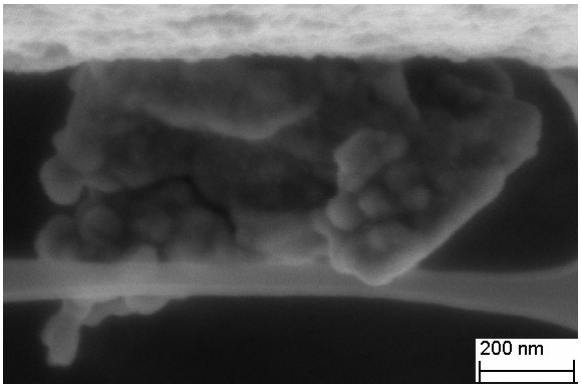

Figure 5.56 Image at 2 kV of particle D08C_028

Size: 0.80 µm

Position: central grid

Morphological class: Aggregate of non-spherical grains

Composition: C, O, Na

Analyses Performed:

- FESEM-EDX

EDX (15 kV) bulk analysis		
Element	Weight %	Sigma
C	15.44	0.42
O	12.23	0.36
Na	0.50	0.13
Si	0.31	0.07
Ca	4.37	0.12
Cr	14.85	0.25
Fe	51.33	0.51
Ni	5.31	0.32
Au	2.75	0.36
TOT	107.09	

Table 5.29 EDX analysis of the area shown in Figure 5.57

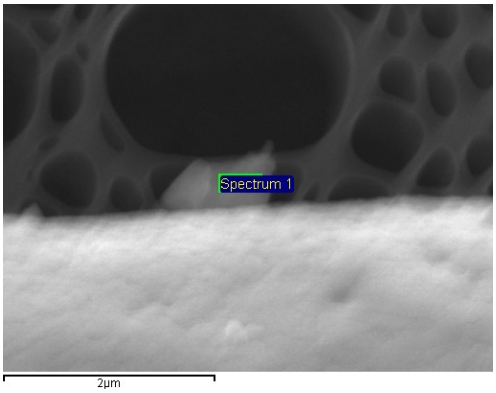

Figure 5.57 Area of the particle in which is performed the EDX

D08C_029

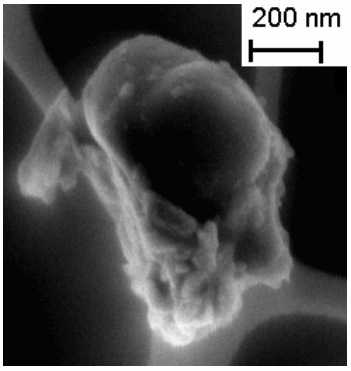

Figure 5.58 Image at 2 kV of particle D08C_029

Size: 0.70 µm

Position: grid 11

Morphological class: Plate aggregate with a spherical grain

Composition: C, O

Analyses Performed:

- FESEM-EDX

EDX (10 kV) spot analysis		
Element	Weight %	Sigma
C	10.16	0.34
O	2.34	0.25
Si	0.32	0.09
Cr	18.25	2.55
Fe	69.74	1.56
Ni	10.70	0.78
TOT	111.51	

Table 5.30 EDX analysis of the area shown in Figure 5.59

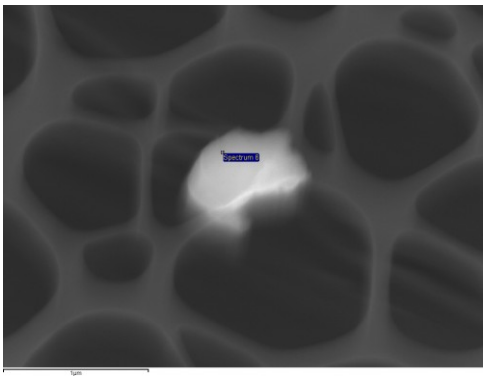

Figure 5.59 Area of the particle in which is performed the EDX

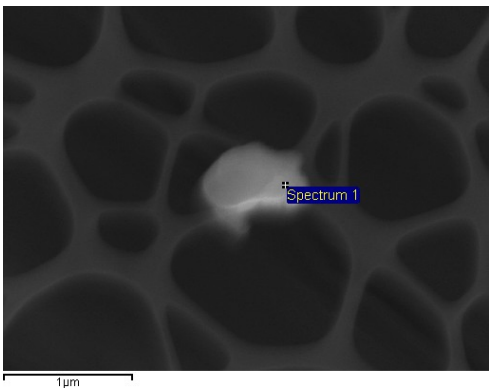

Figure 5.60 Area of the particle in which is performed the EDX

EDX (15 kV) spot analysis		
Element	Weight %	Sigma
C	45.46	0.58
O	5.74	0.37
Si	0.33	0.06
Cr	13.15	0.24
Fe	48.77	0.51
Ni	5.76	0.31
Au	1.84	0.32
TOT	121.05	

Table 5.31 EDX analysis of the area shown in Figure 5.60

D08C_030

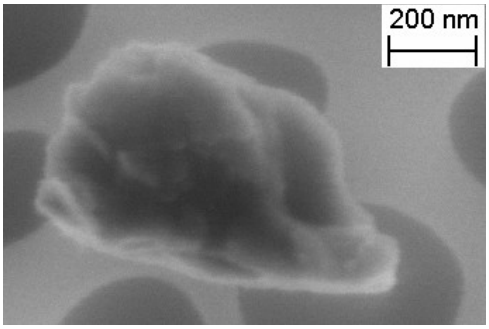

Figure 5.61 Image at 2 kV of particle D08C_030

Size: 0.70 µm

Position: grid 8

Morphological class: Fragment

Composition: C, O, Na

Analyses Performed:

- FESEM-EDX

EDX (10 kV) bulk analysis		
Element	Weight %	Sigma
C	45.52	0.53
O	6.29	0.32
Na	0.45	0.11
Si	0.27	0.08
Cr	12.52	3.07
Fe	39.32	1.31
Ni	4.12	0.50
Au	6.86	0.55
TOT	115.35	

Table 5.32 EDX analysis of the area shown in Figure 5.62

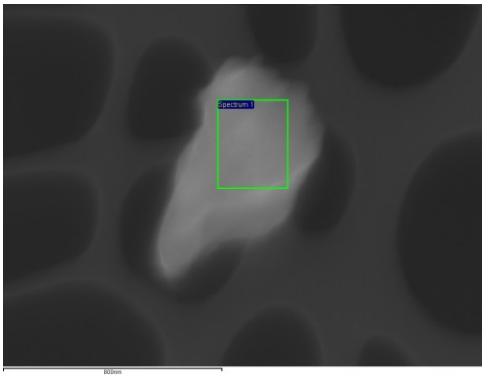

Figure 5.62 Area of the particle in which is performed the EDX

D08C_031

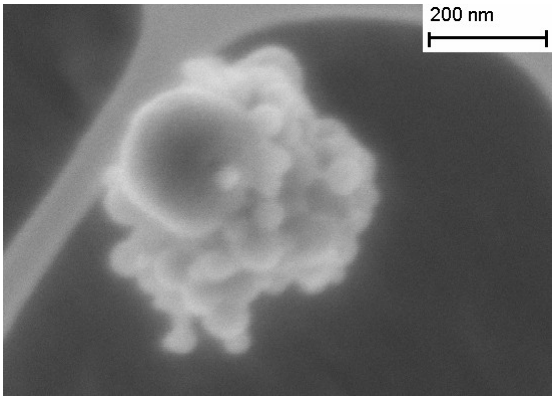

Figure 5.63 Image at 2 kV of particle D08C_031

Size: 0.50 µm

Position: central grid

Morphological class: Aggregate of spherical grains

Composition: C, O

Analyses Performed:

- FESEM-EDX

EDX (10 kV) bulk analysis		
Element	Weight %	Sigma
C	6.35	0.29
O	10.59	0.28
Si	0.25	0.08
Cr	12.63	3.07
Fe	64.33	1.47
Ni	5.43	0.61
Au	4.54	0.48
TOT	104.12	

Table 5.33 EDX analysis of the area shown in Figure 5.64

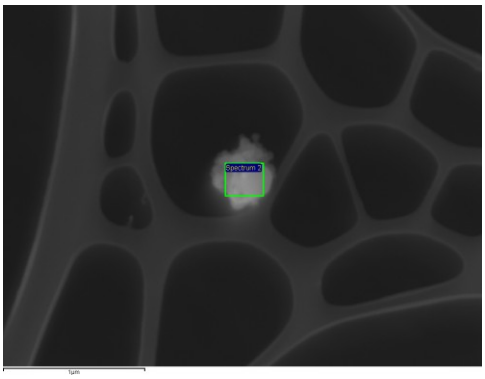

Figure 5.64 Area of the particle in which is performed the EDX

D08C_032

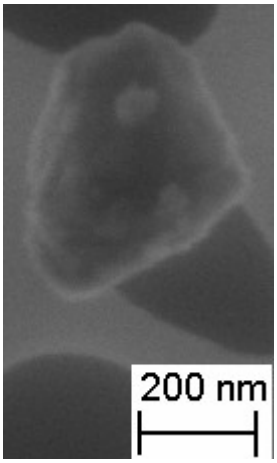

Size: 0.45 µm

Position: grid 2

Morphological class: Fragment

Composition: C, O, Na

Analyses Performed:

- FESEM-EDX

Figure 5.65 Image at 2 kV of particle D08C_032

EDX (10 kV) spot analysis		
Element	Weight %	Sigma
C	9.15	0.30
O	11.18	0.27
Na	0.23	0.10
Si	0.26	0.07
Cr	15.60	2.89
Fe	50.58	1.36
Ni	7.29	0.60
Au	2.70	0.41
TOT	96.99	

Table 5.34 EDX analysis of the area shown in Figure 5.66

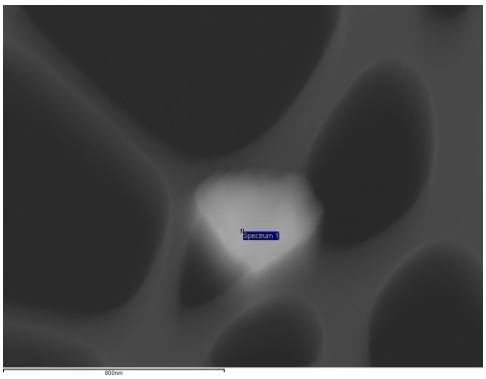

Figure 5.66 Area of the particle in which is performed the EDX

Particles of unknown composition

The particles present in this catalogue are particles for which there are not compositional analyses and they are now lost or relocated. In the case they are relocated they lost to much mass to allow EDX analyses.

D08C_005

Size: 6.60 µm

Position: central grid

Morphological class: Aggregate of non-spherical grains

Analyses Performed:

- FESEM-EDX
- Relocated using FIB instrument

Figure 5.67 Image at 10 kV of particle D08C_005

During EDX analyses the biggest part of the particle disappeared (may be evaporated) by the interaction with the electron beam. It seems to be some kind of membrane that encapsulating many small grains, but noting remained after analysis except for a 3.20 µm aggregate of non spherical grains. This behavior let suppose that the membrane was made of light elements, such as some kind of hydrocarbons.

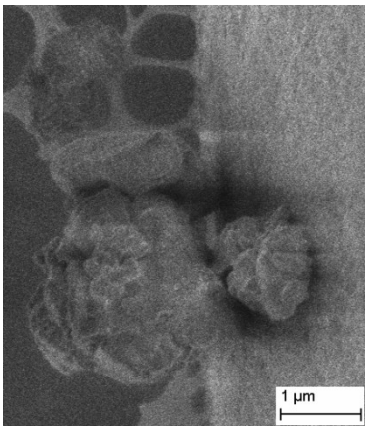

Figure 5.68 Image at 2 kV of particle D08C_005 after EDX analysis

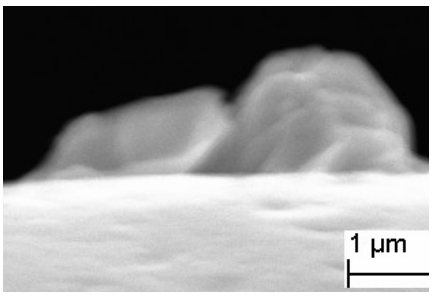

Figure 5.69 Image at 2 kV of particle D08C_005 relocated

To avoid that this residual will evaporate, no analyses ware performed before relocation. But after relocation it seems to be smaller than before and completely embedded in FIB tools elements (Figure 5.69).

D08C_014

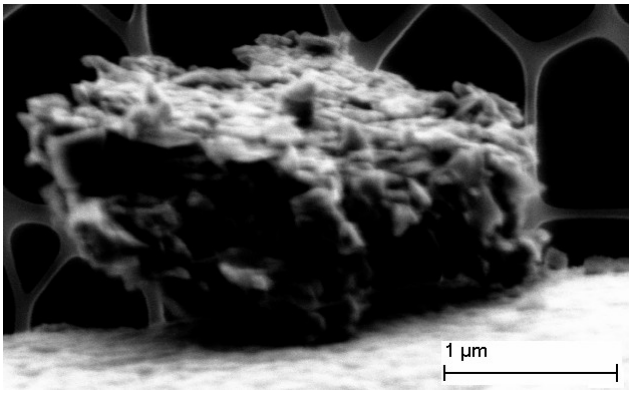

Figure 5.70 Image at 2 kV of particle D08C_014

Size: 2.40 µm

Position: grid 10

Morphological class: Fragment

Analyses Performed:

- FESEM-EDX
- Relocated using FIB instrument
- FT-IR

The EDX analysis was done without a calibration standard. The un-calibrated analysis data show the presence of: O, C, Cr, Fe, Ni and Au.

After relocation it was sent to another laboratory (no data are available as yet).

D08C_017

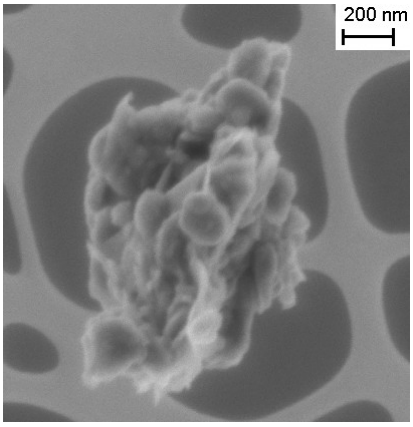

Figure 5.71 Image at 2 kV of particle D08C_017

Size: 1.35 µm

Position: grid 13

Morphological class: Aggregate of mostly non-spherical grains

Analyses Performed:

- FESEM-EDX
- Relocation using FIB instrument

The EDX analysis was done without a calibration standard. The un-calibrated analysis data shows the presence of C, O, Si, Cr, Mn, Fe, Ni, Au.

During relocation the particle was charged and jumped away, we lost it.

D08C_024

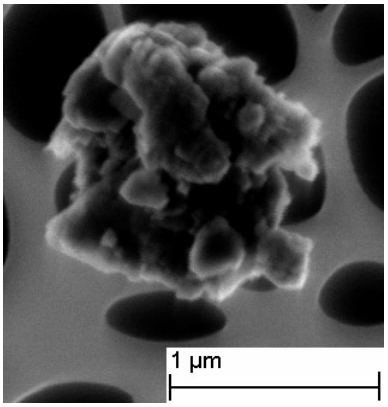

Figure 5.72 Image at 2 kV of particle D08C_024

Size: 1.25 µm

Position: grid 12

Morphological class: Aggregate of non-spherical grains

Analyses Performed:

- FESEM
- EDX
- Relocated using FIB instrument

The EDX analysis was done without a calibration standard. The un-calibrated EDX data show the presence of: C, O, Cr, Fe, Ni and Au.

The particle was relocated (Figure 5.73) before to do a calibrated analysis (no data are available as yet).

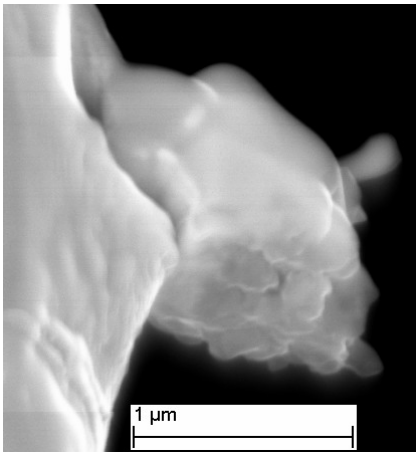

Figure 5.73 Image at 2 kV of particle D08C_024 after relocation

5.4 Data reduction

The data reduction involve the following steps:

1. **remove the contribution of contaminant elements.** As previously discussed in Chapter 4 each particle with a major contribution of gold is removed from the dataset because they are contaminant particles. In the cases where there are Cr, Fe and Ni in the same analysis the grains are removed as contribution of pin substrate. If there are the minor elements of the stainless steel composition (C, O, Si, P and S) they are removed only when these elements occur proportionally with the Fe-ratios in the stainless steel composition (Figure 4.7).

2. **normalization of EDX data.** Looking at the raw data is evident that EDX total is never 100%. It can be more than 100% (probably due to the charge of particle during analyses) or can be less than 100% (due elements undetectable by FESEM-EDX instrument , such as hydrogen);

3. **oxide calculation using EDX data;**

4. **comparison of EDX analyses with FT-IR** (Figure 5.74) **and Raman** (private communication De Angelis S., PhD thesis, in prep.) **where they are available.**

The steps 1 and 2 are reported in the Tables 5.35 - 5.37 and Tables 5.38 - 5.40, that shown the EDX data in element and atomic weight % respectively. The step 3 of data reduction is reported in Table 5.41 - 5.43. Finally in Table 5.44 are compared the three analyses for particles D08C_006, D08C_007, D08C_008 and D08C_014.

A particular case are the particles smaller than 1.5 μm, as explained in Chapter 4 the contribution of the stainless steel pin is difficult to distinguish from the particle composition. For this reason in order to understand which elements can be indigenous of the particle there were compared to the Fe-ratios of the pin and the particles (Table 5.46 and 5.47). It was found that some of the particles < 1.5 μm shown traces of elements different from the stainless steel contribution (Table 5.45).

From the plot of the elements ratios is evident that:

- iron, chromium and nickel are contribution of the pin for all the particles except for D08C_031 that has a visible difference for what concern the nickel component (Figure 5.75 and 5.76);

- carbon and oxygen are present in some amount in the particles too (Figure 5.77). Because carbon and oxygen are present in the substrate too, is not possible to know how much of these elements are in the particles;

- silica is all contamination of the pin except for particle D08C_022 that seems to be far from the pin and its error bar (Figure 5.78).

Element wt % contamination corrected									
	001 (#1)	001 (#2)	002	006	006(FIB)	007	008	009	009(FIB)
C		6.7	8.3	13.8	22.6	20.3	24.8	16.7	21.9
O	62.7	64.8	58.4	51.4	23.2	31.0	39.2	51.4	42.9
F					2.0	12.5		2.5	2.5
Na	9.2	6.4	7.9				0.4		
Mg	2.0	1.6	1.8						0.3
Al	0.2	0.2	0.2		3.3				2.0
Si	22.9	18.7	21.1			0.5			
P									
K									
Ca	2.5	1.6	2.3	34.8	48.9	32.6	34.5	29.4	30.4
Fe	0.5					3.1	1.1		

Table 5.35 Element wt% contamination corrected of DUSTER particles.

Element wt % contamination corrected (continued)									
	011 (#1)	011 (#2)	012 (#1)	012 (#2)	012 (#3)	012 (#4)	012 (#5)	015 (#1)	015 (#2)
C	19.4	21.7	18.4	17.3	17.0	18.5	19.0	26.9	18.5
O	48.2	48.8	42.8	49.9	49.6	53.8	48.7	47.5	48.6
F			1.6				2.1	2.3	
Na	1.9	2.2							
Mg			0.3	0.3			0.3		0.3
Al	11.2	10.1							
Si	12.9	13.6							
P	2.1	2.4							
K	4.3	1.2							
Ca			36.9	32.5	33.4	27.7	29.9	23.3	32.6
Fe									

Table 5.36 Element wt% contamination corrected of DUSTER particles.

Element wt % contamination corrected (continued)					
	015 (#3)	019 (#1)	019 (#2)	021 (#1)	021(#2)
C	18.6	20.4	21.9	19.5	15.5
O	49.5	43.8	42.0	40.9	46.8
F	1.2			1.4	1.3
Na			0.6		
Mg					
Al					
Si					
P			0.7		
K					
Ca	30.7	35.8	34.8	38.2	36.4
Fe					

Table 5.37 Element wt% contamination corrected of DUSTER particles.

Atomic % contamination corrected particle analyses									
	001 (#1)	001 (#2)	002	006	006(FIB)	007	008	009	009(FIB)
C		4.8	6.25	16.1	11.8	15.5	12.8	10.7	12.9
O	71.8	72.7	67.2	62.8	45.9	43.6	64.4	67.9	61.9
F					4.7	16.7		3.2	3.9
Na	7.5	5.4	6.75				0.4		
Mg	1.9	1.6	1.8						0.3
Al	0.2	0.2	0.2		3.0				1.8
Si	17.0	14.4	16.45			0.4			
P									
K									
Ca	1.4	0.9	1.35	21.1	34.6	22.0	21.9	18.2	19.2
Fe	0.2					1.8	0.5		

Table 5.38 Atomic wt% contamination corrected of DUSTER particles.

Atomic % contamination corrected particle analyses(continued)									
	011 (#1)	011 (#2)	012 (#1)	012 (#2)	012 (#3)	012 (#4)	012 (#5)	015 (#1)	015 (#2)
C	12.1	14.1	10.1	10.9	9.6	9.9	10.5	12.5	9.7
O	65.6	65.2	64.1	69.1	70.1	73.4	67.9	68.1	70.0
F			2.3				3.1	4.1	
Na	1.3	1.4							
Mg			0.4	0.3			0.4		0.3
Al	7.9	7.3							
Si	9.0	9.6							
P	1.4	1.6							
K	2.7	0.8							
Ca			23.1	19.7	20.3	16.7	18.1	15.3	20.0
Fe									

Table 5.39 Atomic wt% contamination corrected of DUSTER particles.

Atomic % contamination corrected particle analyses (continued)					
	015 (#3)	019 (#1)	019 (#2)	021 (#1)	021(#2)
C	10.1	9.8	10.2	9.9	8.9
O	69.5	69.4	68.6	63.6	67.0
F	1.8			2.3	1.9
Na			0.5		
Mg					
Al					
Si					
P			0.3		
K					
Ca	18.6	20.8	20.4	24.2	22.2
Fe					

Table 5.40 Atomic wt% contamination corrected of DUSTER particles.

	001 (#1)	001 (#2)	002	006	006(FIB)	007	008	009	009(FIB)
CO_2		28.2	29.4	50.8	50.0	54.0	64.2	58.4	60.3
F(element)					1.2	9.1		2.4	1.8
Na_2O	30.0	19.7	20.6				0.7		
MgO	4.1	3.1	2.9						0.4
Al_2O_3	0.7	0.9	0.6		7.6				5.7
SiO_2	59.3	45.6	43.4			0.8			
P_2O_5									
K_2O									
CaO	4.3	2.5	3.1	49.2	41.2	33.2	34.1	39.2	31.8
Fe_2O_3	1.6					2.9	1.0		

Table 5.41 Oxide wt% of DUSTER particles.

	011 (#1)	011 (#2)	012 (#1)	012 (#2)	012 (#3)	012 (#4)	012 (#5)	015 (#1)	015 (#2)
CO_2	42.9	47.8	55.6	58.0	57.2	63.6	55.8	73.9	59.5
F(element)			1.3				1.9	1.7	
Na_2O	3.0	3.5							
MgO			0.4	0.4			0.5		0.4
Al_2O_3	25.5	23.0							
SiO_2	16.6	17.4							
P_2O_5	5.8	6.6							
K_2O	6.2	1.7							
CaO			42.7	41.6	42.8	36.4	41.8	24.4	40.1
Fe_2O_3									

Table 5.42 Oxide wt% of DUSTER particles (continued).

	015 (#3)	019 (#1)	019 (#2)	021 (#1)	021(#2)
CO_2	60.7	59.9	59.9	56.6	52.1
F(element)	1.1			1.1	1.2
Na_2O			1.6		
MgO					
Al_2O_3					
SiO_2					
P_2O_5			2.3		
K_2O					
CaO	38.2	40.1	36.2	42.3	46.7
Fe_2O_3					

Table 5.43 Oxide wt% of DUSTER particles (continued).

	EDX (major elements)	FT-IR	Raman
D08C_006	C, O, Ca	No data	Calcite, a-C
D08C_007	C, O, F, Ca	C=C (1450 cm^{-1}) C-F (800-1000 cm^{-1})	No data
D08C_008	C, O, Ca	**D08C_008a**: C=O (1700-1900 cm^{-1}) O-H (3200-3500 cm^{-1}) **D08C_008b**: C=C(1450 cm^{-1}) C=O (1700-1900 cm^{-1})	**D08C_008a**: a-C **D08C_008b**: a-C, Calcite
D08C_009	C, O, Ca	C=C (1450 cm^{-1}) C-F (800-1000 cm^{-1})	No data
D08C_014	No data	C=C(1450 cm^{-1}) C=O (1700-1900 cm^{-1}) O-H (3200-3500 cm^{-1})	No data

Table 5.44 Summary results of the particles with EDX, Ft-IR and Raman analyses.

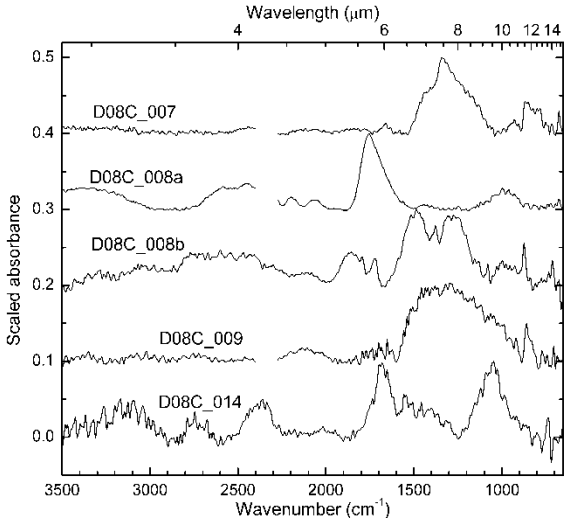

Figure 5.74 FT-IR spectra of the particles D08C_007, D08C_008a, D08C_008b, D08C_009 and D08C_014

Element indigenous of the particles. All particles contain Carbon and Oxygen.						
	023 (#1)	023 (#2)	026	030	032(#1)	032(#2)
Na	*x*	*x*	*X*	*x*		*x*
Al					*x*	
Ca	*x*					

Table 5.45 Particles less than 1.5 µm with indigenous elements different from the pin

Element ratios of particles < 1.5 µm						
	022	023 (#1)	023 (#2)	025	026	028
Cr/Ni	0.96 +/- 0.18	1.96 +/- 0.29	1.37 +/- 0.23	1.80 +/- 0.34	1.87 +/- 0.33	2.79 +/- 0.17
Fe/Cr	4.21 +/- 0.78	3.46 +/- 0.46	4.29 +/- 0.68	3.50 +/- 0.63	3.93 +/- 0.62	3.46 +/- 0.07
Fe/Ni	4.04 +/- 0.23	6.81 +/- 0.51	5.91 +/- 0.40	6.31 +/- 0.48	7.37 +/- 0.65	9.67 +/- 0.59
Fe/C	11 +/- 1	10.0 +/- 0.5	9.0 +/- 0.5	2.9 +/- 0.1	12 +/- 1	3.3 +/- 0.1
Fe/O	12 +/- 1	17 +/- 1	19 +/- 1	7.1 +/- 0.3	16 +/- 1	4.2 +/- 0.1
Fe/Si	113 +/- 20	196 +/- 52	245 +/- 84	174 +/- 40	234 +/- 78	165 +/- 37
Fe/P	-	-	122 +/- 27	-	92 +/- 17	-
Fe/S	-	-	-	-	-	-

Table 5.46 Cr/Ni and Fe-ratios for particles less than 1.5 µm

Element ratios of particles < 1.5 µm (continued)						
	029 (#1)	029 (#2)	030	031	032 (#1)	032 (#2)
Cr/Ni	1.71 +/- 0.23	2.28 +/- 0.13	3.04 +/- 0.83	2.32 +/- 0.62	2.14 +/- 0.43	1.69 +/- 0.39
Fe/Cr	3.82 +/- 0.54	3.71 +/- 0.08	3.14 +/- 0.78	5.09 +/- 1.24	3.24 +/- 0.60	3.84 +/- 0.85
Fe/Ni	6.52 +/- 0.5	8.47 +/- 0.46	9.54 +/- 1.20	11.84 +/-1.35	6.94 +/- 0.60	6.47 +/-0.54
Fe/C	6.7 +/- 0.3	1.07 +/- 0.02	0.86 +/- 0.03	10.0 +/- 0.5	5.5 +/- 0.2	6.22 +/- 0.28
Fe/O	30 +/- 3	8.5 +/- 0.5	6.2 +/- 0.4	6.1 +/- 0.2	4.5 +/- 0.2	4.81 +/- 0.18
Fe/Si	218 +/- 61	148 +/- 27	146 +/- 43	257 +/- 82	194 +/- 53	-
Fe/P	-	-	-	-	-	-
Fe/S	-	-	-	-	-	-

Table 5.47 Cr/Ni and Fe-ratios for particles less than 1.5 µm

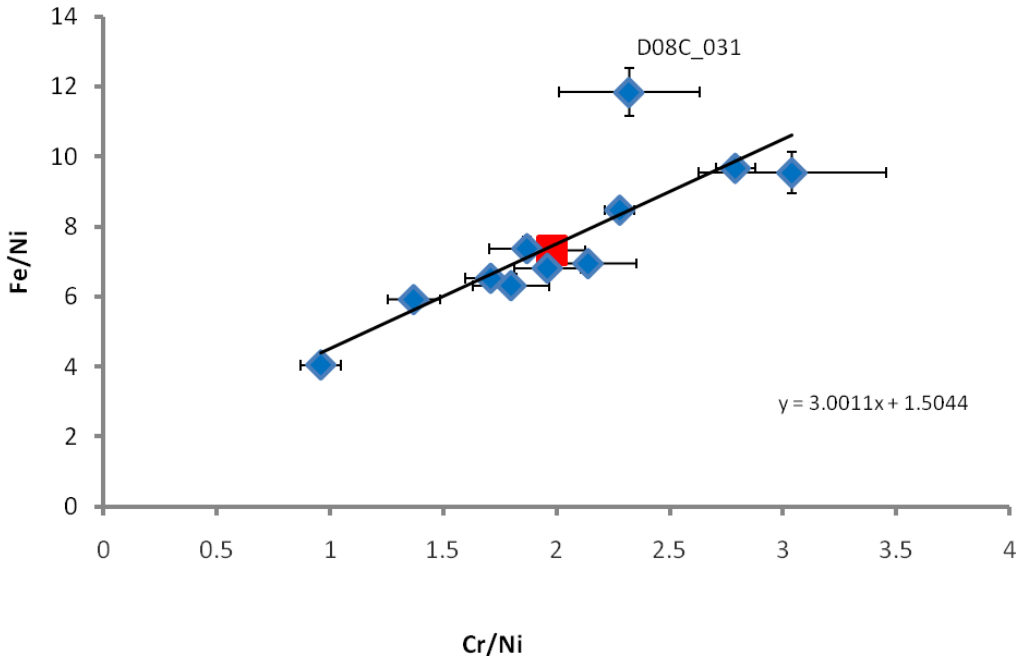

Figure 5.75 Cr/Ni, Fe/Ni plot of DUSTER particles less than 1.5 µm, the red square is the stainless steel pin. This plot shown that Fe, Cr, and Ni detected in the particles are from the stainless steel except for the D08C_031 that seems to has some amount of Fe, Cr or Ni in it.

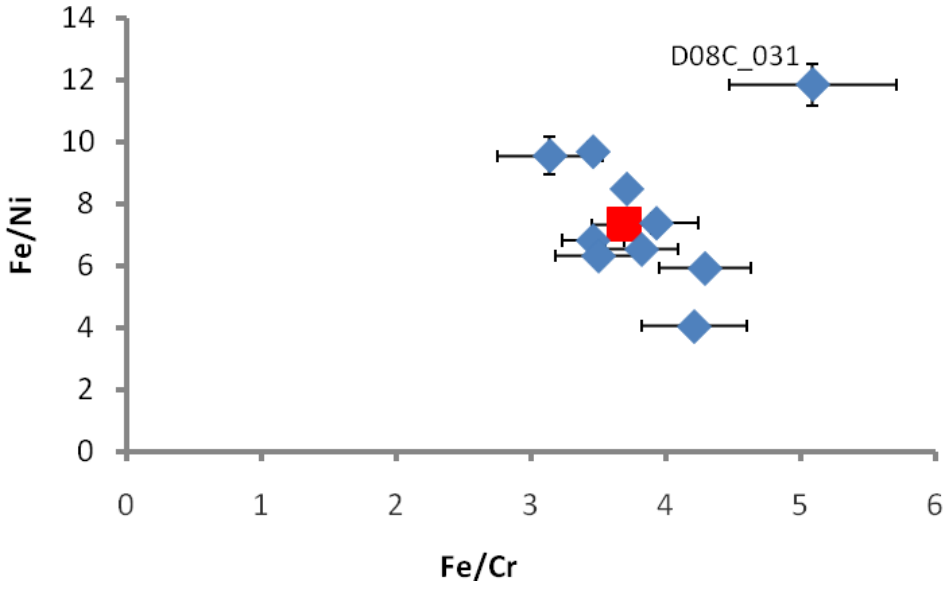

Figure 5.76 Fe/Cr, Fe/Ni plot of DUSTER particles less than 1.5 µm, the red square is the stainless steel pin. This plot shown that Fe, Cr, and Ni detected in the particles are from the stainless steel except for the D08C_031 that seems to has some amount of Fe, Cr or Ni in it.

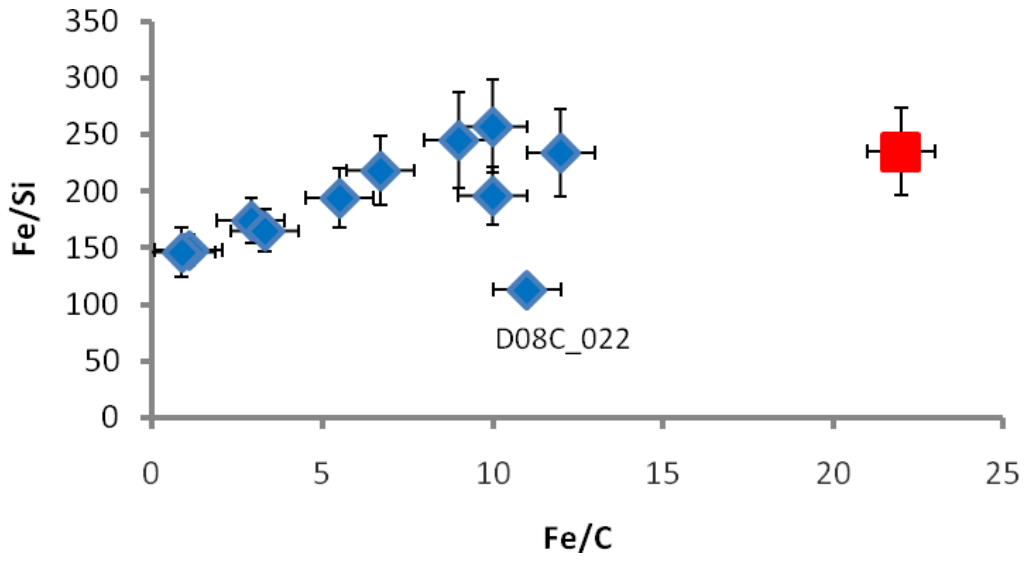

Figure 5.77 Fe/C, Fe/Si plot of DUSTER particles less than 1.5 µm, the red square is the stainless steel pin. This plot shown that there is a carbon component indigenous of the particles, while the Si is a contaminant element except for particle D08C_022 that could has some amount of silica.

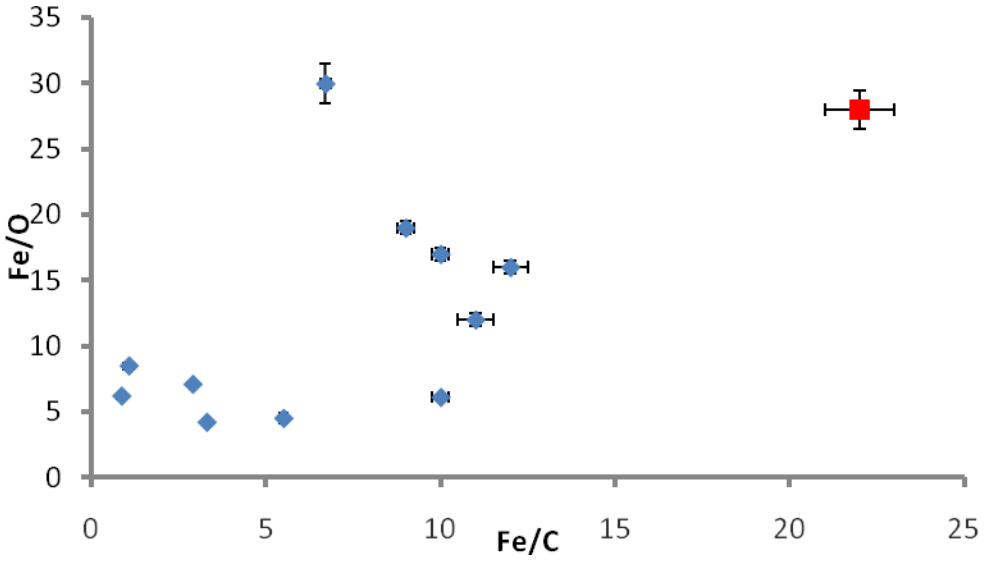

Figure 5.78 Fe/C, Fe/O plot of DUSTER particles less than 1.5 µm, the red square is the stainless steel pin. This plot shown that carbon and oxygen are not all contamination, but some amount of C and O are present in the particles too.

5.5 Discussions

The stratosphere is an atmospheric boundary layer in which particles with terrestrial and extraterrestrial sources could coexist (Table 5.48).

	Particles size (μm) range	Properties
< 30 km	0.5 – 10	Micrometeoritic particles (Bigg et al. 1970, Testa et al. 1990) Icy crystals that embedded particles (Bigg et al. 1971) Volcanic ash particles (Rietmeijer 1993, Testa et al. 1990)
< 30 km	0.4 – 100	Icy crystals of sulphuric acid + ammonium sulphate (Bigg et al.1970) Solid rocket effluent Al_2O_3, volcanic ash and aggregates of IDP (Brownlee et al 1973, Rietmeijer 2000) Tagish Lake materials: olivine rich + CAIs (Calcium Aluminum-rich inclusions); Ca-Mg-Fe-Mn carbonates; Fe-Ni sulphides (Brown et al. 2000)
DUSTER (~ 37 km)	0.5 – 160	SiO_2-rich spheres C,O, Ca-rich particles

Table 5.48 Property of particles present in upper and lower stratosphere, and particles collected by DUSTER instrument.

From the EDX analyses the first thing that jumps out is the evidence that the most common elements between that particles are carbon, oxygen and calcium. Plotting calcium versus silica (Figure 5.79) clearly shows two clusters of particles: the spheres, that are abundant in silica, and particles, that have abundant calcium. There is an exception the particle D08C_011 that has a composition similar to the spheres but is a fragment. The same two groups appear when plotting the data (el wt%) in a ternary diagram of C, O, Si (Figure 5.80).

The persistence of these chemical groupings suggest that DUSTER may have collected particles from two different sources.

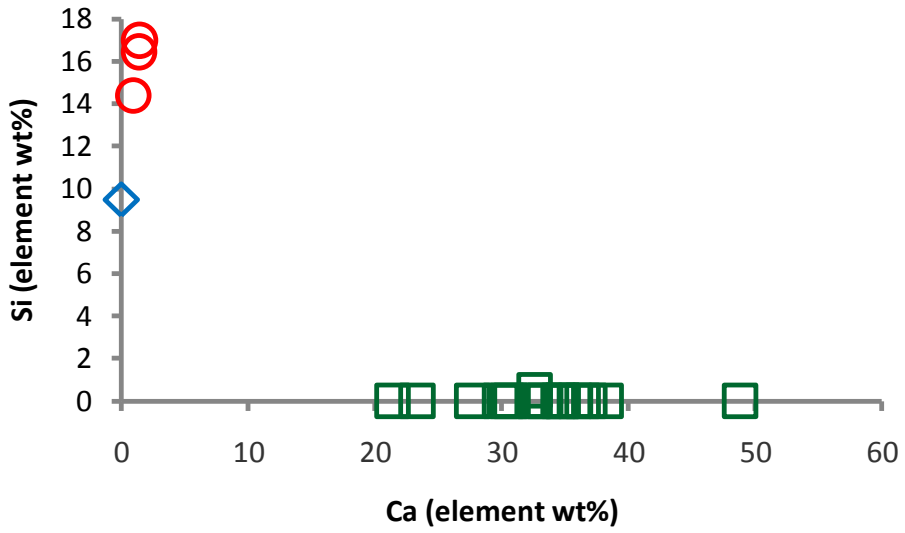

Figure 5.79 Ca, Si plot of the DUSTER particles >1.5 µm, the red circles are the spheres, the blue diamond is the particle D08C_011, the green squares the remnant particles.

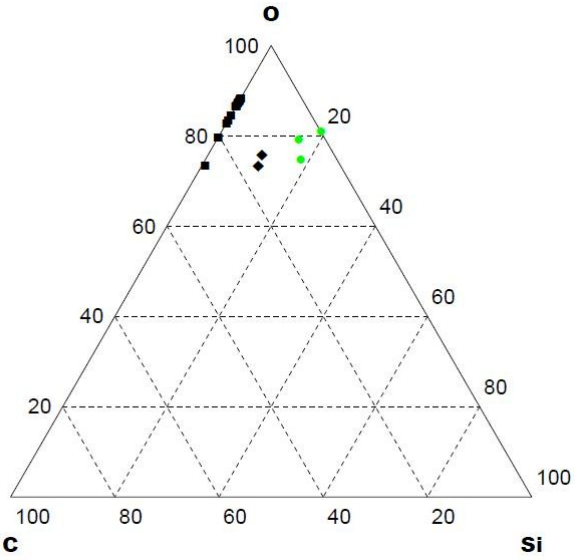

Figure 5.80 Ternary diagram of DUSTER particles >1.5 µm. The green circles are the spheres and fragment, the black diamonds are two analyses of the same particle (D08C_011) and the black squares are the remnant particles.

Origin of spheres

The spheres are a remarkable feature of DUSTER collection, because they are too big to be collected by DUSTER's flow rate. But they were collected, probably because of whirling motion due to the difference of temperature between the instrument and the surrounding environment,

or by pure chance, for example when the spheres are floating in the same trajectory of the inlet tube.

Looking at their morphology I supposed they could be micrometeorites, specifically cosmic spherules (CS). The spherical shape is characteristic of particles that formed as molten droplets during atmospheric entry of meteoroids (Genge et al. 2008). Taylor et al. (2000) reported different kinds of oxides concentration for these glass spherules, a typical composition of a CS of a size close to the DUSTER spherules is reported in Table 5.49.

Sample	SiO_2	TiO_2	Al_2O_3	Cr_2O_3	FeO	MnO	NiO	MgO	CaO	Tot
30-27	52.31	0.12	1.70	0.79	11.24	0.38	0.03	32.21	1.46	100.2

Table 5.49 Oxide weight percent of a cosmic spherule in the size range 106-250µm (Taylor et al. 2000).

Comparing Table 5.49 to data of the spheres collected by DUSTER (Table 5.41) it is possible to see commonalities:

- the SiO_2, Al_2O_3 and CaO compositions are similar;
- MgO in the DUSTER spheres is significantly less than in CS;
- Calculating Fe oxidation for DUSTER spheres as FeO and comparing to the CS data, the DUSTER spheres have significantly less FeO abundance than CS (0.6 compare to 11.24);
- Ti, Cr, Mn, and Ni are not present in the DUSTER spheres. They have the K_α value in the range (4.5 - 7.5) kV so they should be detected from EDX analyses at 10 kV or 15 kV, if they were present;
- Na_2O is not present in CS but is a dominant component in DUSTER spheres.

Because of the strong presence of Sodium is easy to exclude the hypothesis of CS. Sodium is a volatile element that should evaporate with heating during atmospheric entry; it also has a low cosmic abundance (Anders & Grevesse, 1989). Another argument against the hypothesis of micrometeorites is the correlation between Al and Ca that is present in CS (see Figure 5.81); in this correlation the DUSTER spheres are very far from the trend.

In the end they are not micrometeorites.

Another process that could produce spheres is the quenching process, that can occur in different environments: residuals of rockets fuel; volcanic ejects; and power plants that produced sphere as residuals of coal burning. Excluding the residuals of rocket fuel because of the chemical composition that should be pure Al_2O_3, the last two cases will be discussed in the next section 5.4.1.

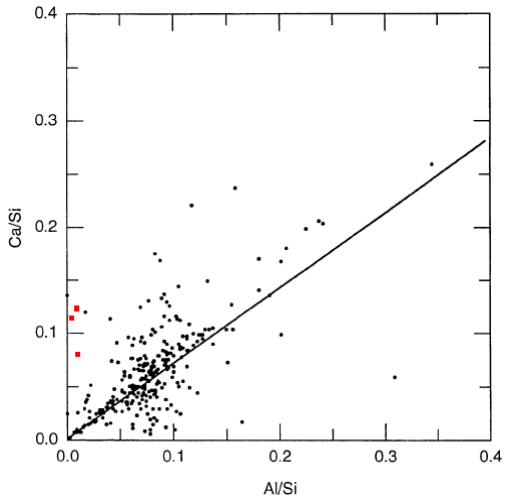

Figure 5.81 Al/Si vs Ca/Si plot. The figure is from Taylor et al. 2000. The red square plotted are the DUSTER spheres values.

Origin of Carbonate particles

For what concern the origin of the Ca-rich particles I considered the possibility that they might be natural contaminants specific to Arctic geological environments that are conducive to the formation of mono-hydrocalcite ($CaCO_3 \cdot H_2O$) or ikaite ($CaCO_3 \cdot 6(H_2O)$). The hydrocalcite is a mineral found in carbonates rich fluid, for example it has been reported as a significant component of the decomposition of ikaite in the towers of the Ikka Fjord in Greenland (Dahl et al., 2006). DUSTER collected in an environment rich of H_2O and $CaCO_3$ that mixed together produced the ikaite. But the EDX analyses of a mineral fragment that is a pseudomorph after Ikaite show a different composition from the DUSTER particles (Table 5.50) and they not match with the data in the (Ca,Si) plot of DUSTER collected particles (Figure 5.82).

The Ikaite Ca/Si ratio is close to the spheres, but this similarity is purely coincidental because they have very different composition (cf. Table 5.35 and Table 5.50) and morphology.

	IKAITE (#1)	IKAITE (#2)	IKAITE (#3)
C	12.0	6.3	9.5
O	49.2	52	50
Na	0.5	0.7	0.4
Mg	2.6	3.1	5
Si	16.1	15.4	17.6
P			0.3
S	3.3	0.5	
Cl			0.2
K	2.3	1.1	1.3
Ca	6.8	10.7	1.7
Ti	0.5		
Fe	6.7	10.2	14

Table 5.50 Ikaite EDX analyses (element wt%) normalized to 100%

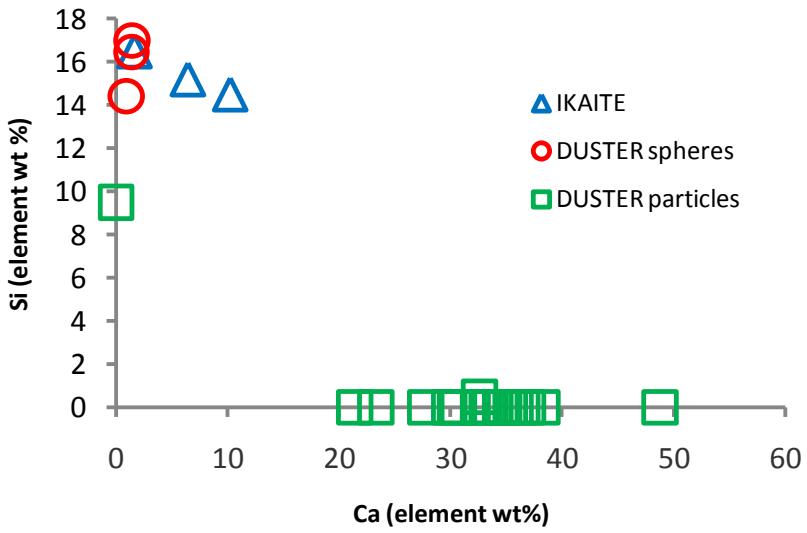

Figure 5.82 (Ca,Si) plot of DUSTER collected particles and IKAITE.

In the class of carbonates particles takes place also a particle that has the characteristic morphology of condensed particles, D08C_031 (Figure 5.63). The condensed particles are the product of the quenching process that transform the vapor phase into solid phase.

The typical morphology of a condensed particle is a chain structure composed of spherical grains (Figure5.83).

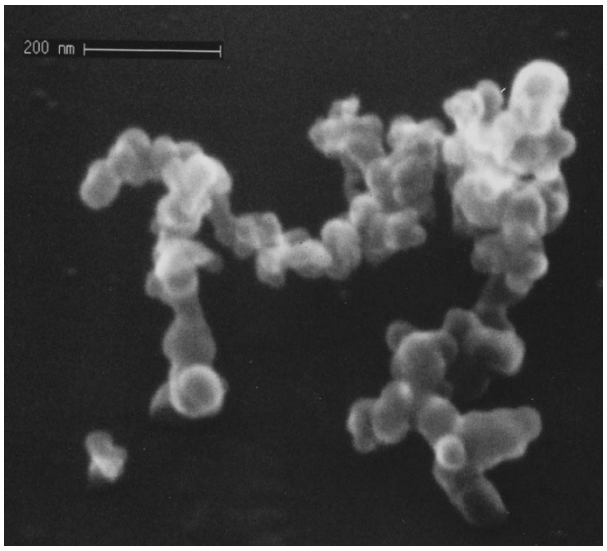

Figure 5.83 FESEM micrograph of carbon+fayalite vapour-condensed sample (Rotundi et al. 2000)

The particle D08C_031 is an aggregate of small spherical grains (diameter of tents of nanometers) and one major sphere (255 nm). The latter could be the result of fusion of more spherical small grains.

Another particle candidate to be a condensate is the D08C_029 (Figure 5.58) that is composed of a major sphere (200 nm) probably formed by vapor condensation lately rolled in a carbon sheet present in the surrounding environment.

The size of particle D08C_029 and D08C_031 match with the size range of vapor condensed particles present in the atmosphere (Figure 5.84).

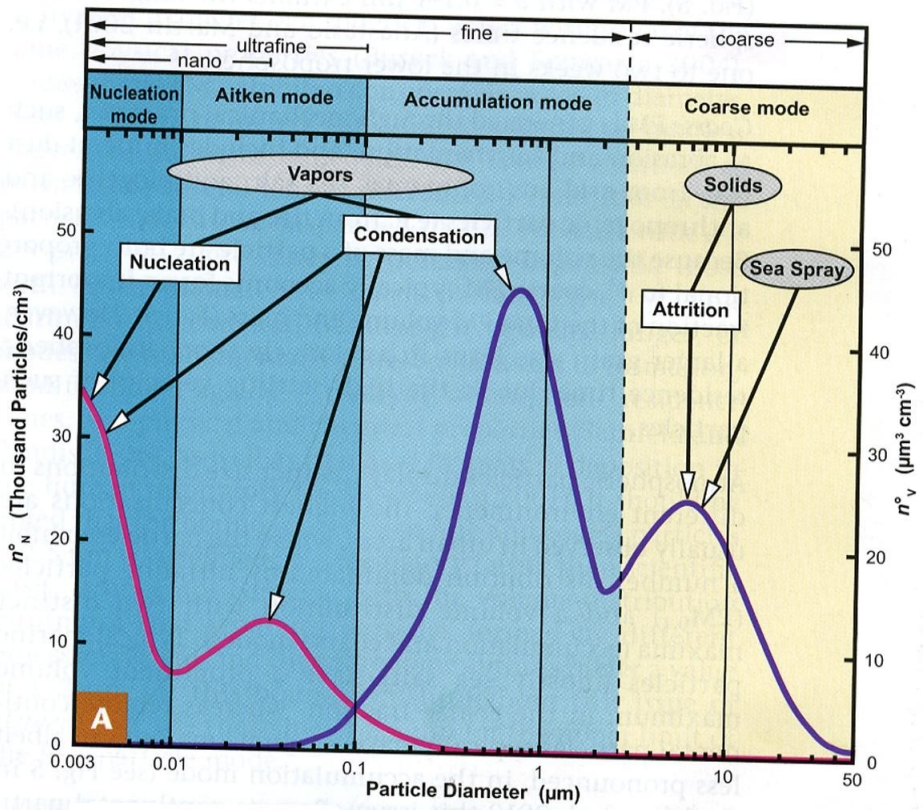

Figure 5.84 Typical size distribution of the number and the volume of atmospheric particles per cubic centimetre of air. In the diagram is also shown the source materials of particles.

Analyzing the spheres and Ca-rich particles in these two clusters of the DUSTER collection separately, we cannot derive a potential single source for the origins of the particles collected by DUSTER. I hypothesize that the particles could be linked to each other and come from by the same source.

This hypothesis is supported by the following morphology features:

- in Figures 5.10 and 5.15 are reported two mosaics of details of the spheres, including fragments of submicron/micron range. The fragments attached on the spheres are very similar to the fragments collected by DUSTER (for example the particle D08C_011, Figure 5.30);
- the particles D08C_008, 012, 015, 021, 025 (in Figure 5.23, 5.33, 5.37, 5.43, 5.50 respectively) are fragment with some nanometer grains attached to it;
- the particles D08C_006, 007, 023, 026 (in Figure 5.18, 5.21, 5.47, 5.52 respectively) are aggregate of different grains;

- a particular case is the particle D08C_029 (in Figure 5.58) it looks like a small sphere embedded in a carbon sheet. It is possible that the nanometer sphere could be a vapor condensed particle.

All these features suggest that the particles were collected in a high dust-density environment composed of different kind of particles and allowing the particle-particle collision and aggregation. As an example we refer to particle D08C_029, that can be the result of a collision of two particle of different origin.

Scenarios of an environment with high dust density could be from terrestrial, volcanic eruptions or a very efficient power plant, or extraterrestrial sources such as a meteor fireball.

TERRESTRIAL SOURCES	EXTRATERRESTRIAL SOURCES
VOLCANIC EJECTION It is a process that products fragment and in some cases spherules. A typical glass produced is the Obsidian (an amorphous silicate, transparent or opaque)	METEOROIDS Process of heating during entry in atmosphere with consequent ablation, evaporation and condensation (there is no gas inside the particle during the cooling process). Could product fragment and spheres.
POWER PLANTS (combustion product) In Svalbard Islands there are coal power plants. A typical combustion product is coal fly ash (spherules of wide size and composition)	FIREBALLS (i.e. Tagish Lake meteorite) There is a process of ablation and fragmentation, could produce fragment and spheres.

Table 5.51 Hypothesis of sources from the terrestrial and from extraterrestrial environment that may introduce dust in stratosphere.

5.5.1 Terrestrial sources

Both terrestrial sources (Table 5.51) produced dust high-density environment. Is known from studies of El Chichòn eruption that the volcanic ash may reach 36 km of altitude and that the particles are reach in Ca-Al-Silicate (Rietmeijer 1993). During the period of DUSTER collection (June 2008) there were no major eruptions except for the first eruption of Chaitén (Chile) reported on the Global Volcanism Program (Smithsonian National Museum of Natural History). The eruption began the morning of 2 May 2008 with an ash plum of about 13.7 - 16.8 km and reached an estimate altitude greater than 21 km. On 6 May, ONEMI (Oficina Nacional de Emergencia - Ministerio del Interior) reported that the eruption became more forceful (Figure 5.85) and generated a wider and darker gray ash plume rising to an estimated altitude of 30 km.

Being the volcano in the south hemisphere is not probably that DUSTER collected the dust ejected by Chaitén.

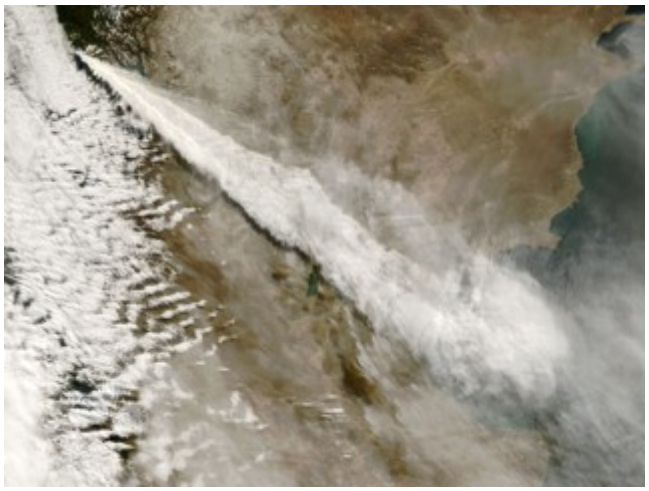

Figure 5.85 The Moderate Resolution Imaging Spectroradiometer (MODIS) on NASA's Terra satellite captured this image of a long, cloud-like plume extending about 700 km SE from Chaitén on 3 May. The plume rises high over the Andes mountains, drifts across Argentina, and thins over the Atlantic Ocean. (NASA Earth Observatory and the MODIS Rapid Response System)

The other terrestrial source that allows a high dust density is the coal combustion product (CCP) of the power plant, it produces mainly coal fly ashes. The coal is a sedimentary rock made of organic and inorganic materials, which contain many elements. During combustion because of the high temperature this elements are release in gaseous or solid phase. The coal fly ash spheres can be hollow or massive.

The typical coal fly ash composition depend on burned materials, as shown on Jablonska et al. (2001) study, about coal fly ash from Ba-enriched coal burning on Silesian Industrial Region. An example of oxide composition is SiO_2, Al_2O, Fe_2O_3, MgO and CaO, with traces of TiO_2, MnO, Na_2O, K_2O, P_2O_5, CO_2 and SO_3 (Vassilev S.V. and Vassileva C.G., 1997). The traces elements are influenced by the original composition of coal, the combustion conditions, the size and mineralogy of the coal fly ash (Brownfield M.E. et al., 2002). For example in low temperature ashes Na_2O is 14%, but it is lost in high temperature ashes (Vassilev S.V. and Vassileva C.G., 1997).

In the Table 5.52 are reported the composition of coal fly ash of nearly pure SiO_2 compared with the composition of DUSTER spheres. In the Figure 5.86 are plotted on the ternary diagram of Gieré et al (2003) the spheres and the fragment D08C_011 and they match with the coal fly ashes.

If the CCP of a power plant could be the source of the particles collected, the fragment attached on the spheres could have the same nature of the fragment collected on the sample holder, and the aggregates could be the product of the interaction between all the particles present in this high dust density environment.

	D08C_001 (#1)	D08C_001 (#2)	D08C_002	Coal Fly Ash (nearly pure SiO_2)	
				min	max
CO_2		28.2	29.4		
Na_2O	30.3	19.7	20.6	0.02	1.16
MgO	4.1	3.1	2.9	0.05	4.03
Al_2O_3	0.7	0.9	0.6	1.63	60.5
SiO_2	59.8	45.6	43.4	6.60	97.7
P_2O_5				0.11	0.63
K_2O				0.05	4.13
CaO	4.3	2.5	3.1	0.06	23.1
TiO_2				0.01	9.51
Cr_2O_3				0.01	0.06
MnO				0.01	0.03
Fe_2O_3	1.6			0.28	22.8
NiO				<0.01	0.01
CuO				0.01	0.02
ZnO				0.02	0.06
UO_2				0.01	0.04

Table 5.52 Comparison between DUSTER spheres and a typical coal fly ash nearly pure SiO_2

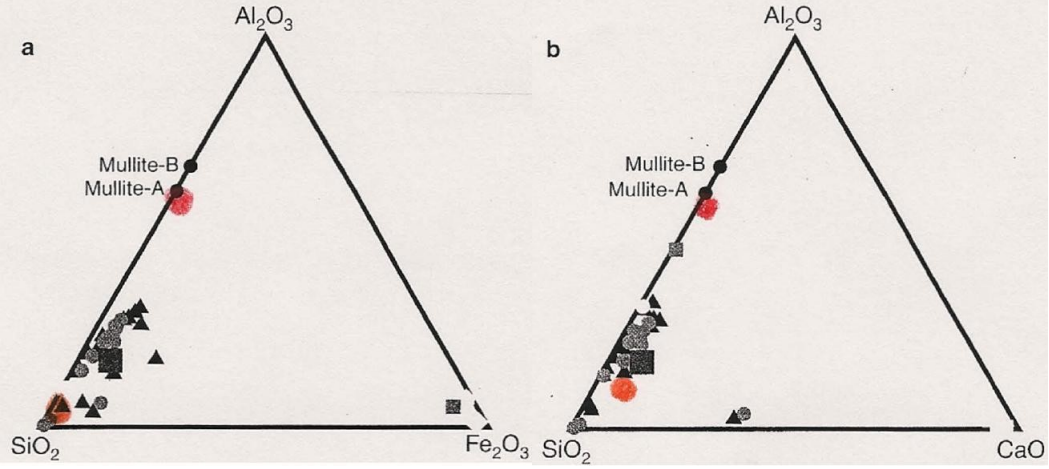

Figure 5.86 Ternary diagrams showing the average composition of the different kinds of coal fly ash. Symbols: large, filled square=bulk ash composition; filled circle=non-magnetic glass; filled triangle=magnetic glass; open diamond=hematite; open circle=almandine(?); filled square=jarosite (?); open square=Ca-rich crystalline phases. Mullite-A=$Al_6Si_2O_{13}$, Millite-B=$Al_2(Al_{2+2x}Si_{2-2x})O_{10-x}$ (Giaré et al. 2003). The red point is the particle D08C_011, the orange point are the DUSTER spheres.

5.5.2 Extraterrestrial sources

The extraterrestrial sources described in Table 5.51 are meteoroids and fireball (or bolides) , but only the second produced a high density dust environment.

In the DUSTER particles collection there are:

- particles (Figure 5.58 and 5.63) that remind cosmic particles collected by NASA aircraft program (Figures 5.87);
- particles rich in calcium (Figure 5.79) and in particular in calcite (Table 5.44);
- also the particles less than 1.5 μm are rich in oxygen and carbon and suggest carbonates (Figure 5.78).

In Figure 5.88 there is an example of a spherical particle of cosmic origin collected by the NASA JSC Cosmic Dust Program. In the Figure 5.89 are reported some particles collected in the lower stratosphere by the same NASA program for the purpose of collecting stratospheric dust that could be hypothesized to be form from the Tagish Lake dust cloud associated with this fireball event (Cosmic Dust Catalog Vol. 17 JSC). They are shown for comparison with DUSTER particles with respect to composition and morphology.

On 18 January 2000 at 16:43 (UT) the Tagish Lake meteoroid entered into the Earth atmosphere with a mass of almost 2 x 10^5 kg. It fragmented between 50 – 30 km of altitude releasing several hundreds of fragment for a total of 1500 kg m^{-3}. The composition of the recovered samples are an intermediate between CM and CI meteorites (see Chapter 1) and it is consider the most primitive

solar system materials yet studied. It was surprisingly rich in carbonate minerals that vary in composition from calcite, to siderite and magnetite (Brown et al. 2000).

Because of the similarity between DUSTER particles and the IDP collected by NASA program, an extraterrestrial source cannot be excluded.

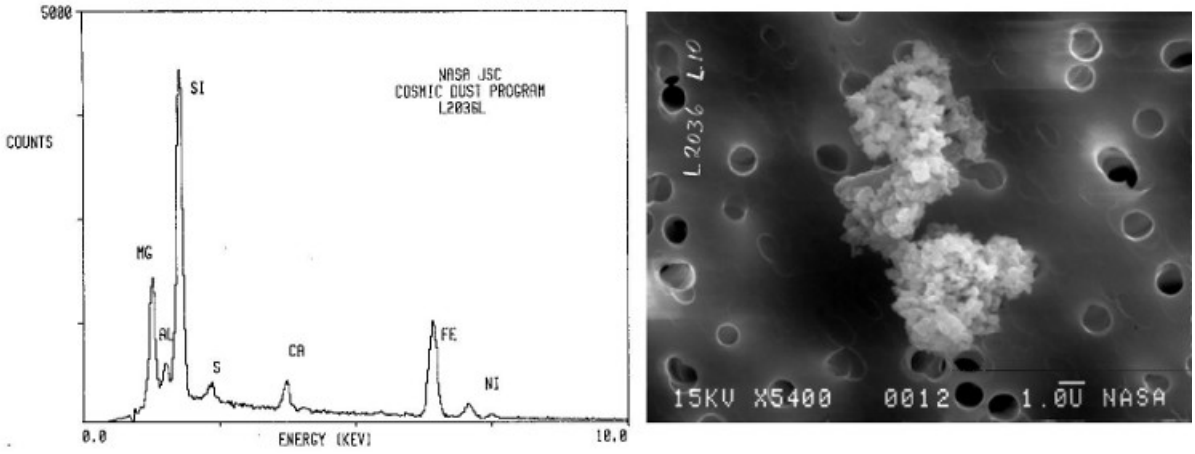

Figure 5.87 IDP collected by NASA IDP program (Catalogue vol.15) classified as Cosmic (?)

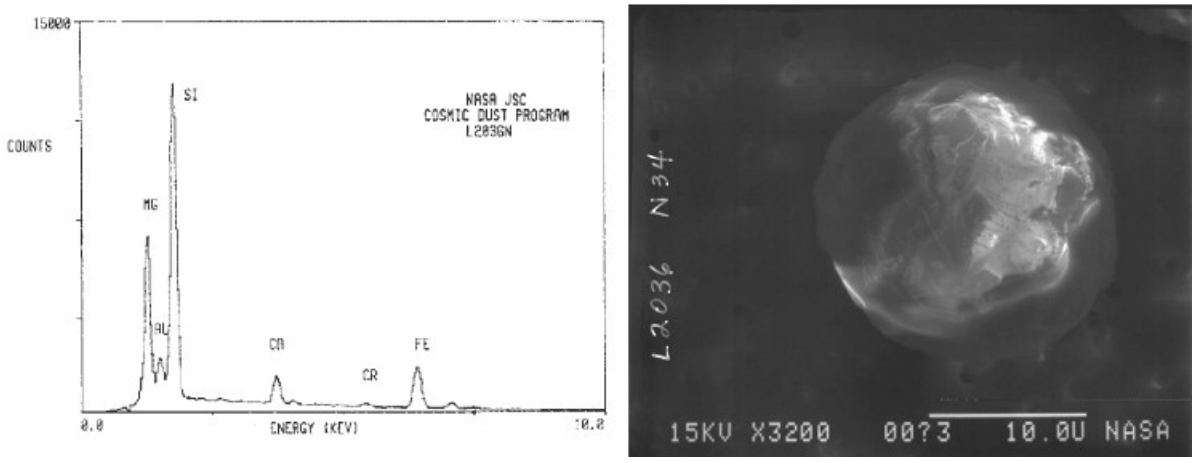

Figure 5.88 IDP collected by NASA IDP program (Catalogue vol.15) classified as Cosmic

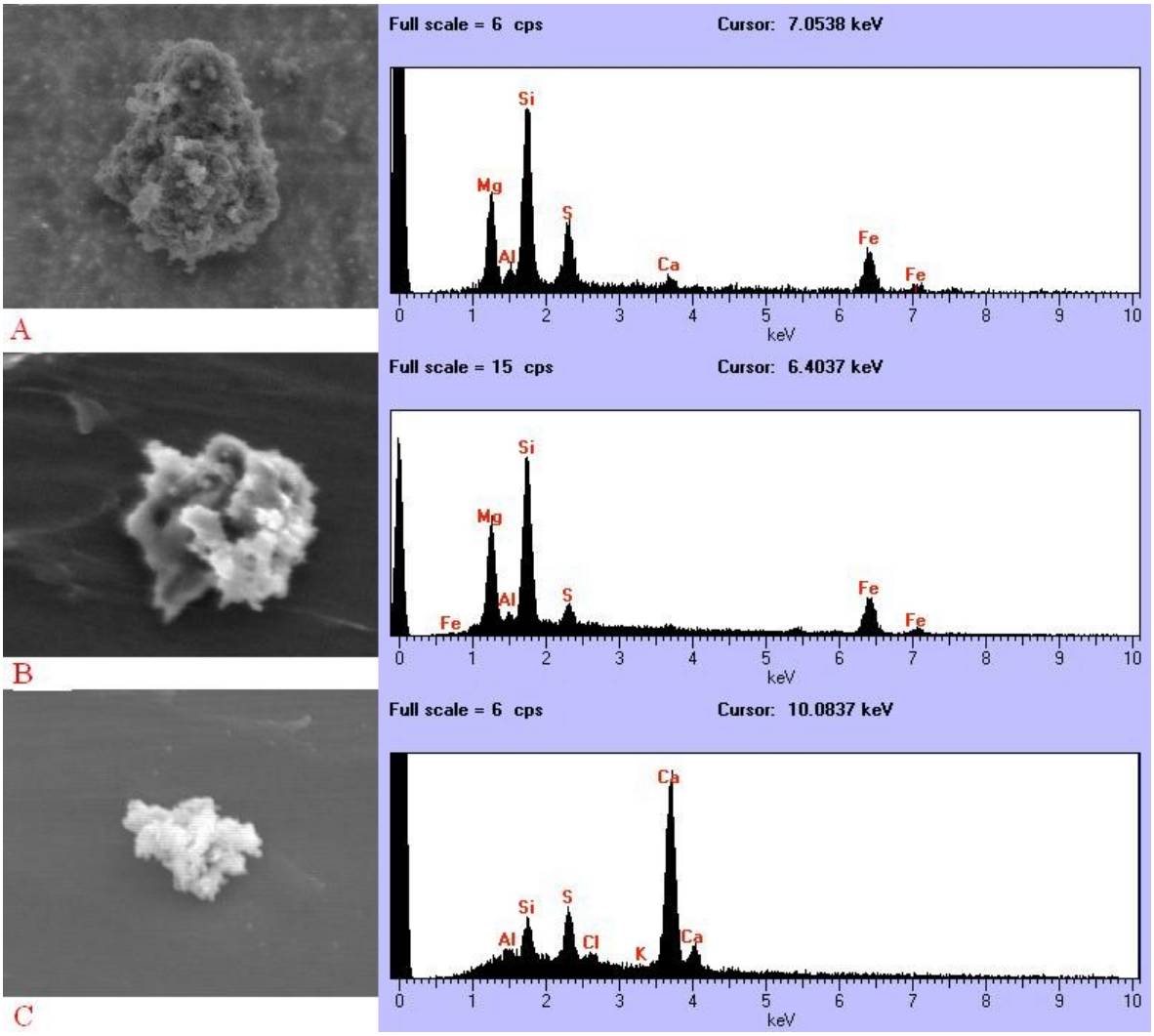

Figure 5.89 Particles collected by NASA IDP program during Tagish Lake fireball. All the particles are clssified like Cosmic. The size of the particle in the picture are: A) (28x22) µm; B) 10 µm; C) (18x13) µm.

Conclusions

In Table 5.48 are summarized the size range and the properties of stratospheric particles above and below 30 km altitude and the particles collected by DUSTER instrument.

As discussed in the previous section, analyzing morphology and composition of particles collected by DUSTER they fit with both sources, they could be from either terrestrial or extraterrestrial sources.

The DUSTER particles can be divided into two different populations: the silica rich particles, and the carbonate rich particles (Figure 5.79).

The carbonate rich population is composed of crystalline fragments and particles produced by vapour condensation (D08C_031 and D08C_029).

This population can have extraterrestrial origin.

The silica rich population consists in: the two big spheres (D08C_001, D08C_002) and a single fragment (D08C_011). The spheres also have attached on the surface fragments that are not indigenous to the spheres.

The presence of fragments attached on the spheres surface suggests a possible formation in an high dust density environment, both these two formation scenarios are plausible:

- the silica rich population is produced by the same extraterrestrial event of the carbon rich population;
- the silica rich population has a terrestrial origin, formed during a volcano eruption or the product of a power plant.

The first scenario connected to the extraterrestrial event can be excluded for silica rich population because of the high sodium content present in the particles, in particular the spheres (see section 5.5).

Coming to the second scenario I exclude the volcano ejecta, because no volcanic events have been registered close to the period of DUSTER collection.

Therefore I think that the most probable origin of the silica rich population is a coal combustion environment. In this case they could have been collected on Svalbard skies as in Longyerabien there is an active coal power plant.

6 DUSTER2009 instrument improvements and July 2009 campaign

In this chapter the improvements of the instrument for July 2009 campaign are discussed, in particular:

- the new mechanical structure;
- new configuration of sample holder, for better performances of transmission analyses;
- the flight campaign and the new performances of the instrument;
- a brief introduction of the preliminary particles detection and sources of contaminations.

6.1 The instrument

In July 2009 DUSTER had a new flight opportunity from Longyearbyen (Svalbard Island, Norway). The instrument was a piggy back of the SoRa (Sounding Radar) instrument; the flight from Longyearbyen airport to Baffin Island (Figure 6.1) was initiated on the 1st of July and had a duration of 4 days, during which the instrument was in operative mode for 55 h at an average altitude of 38 km.

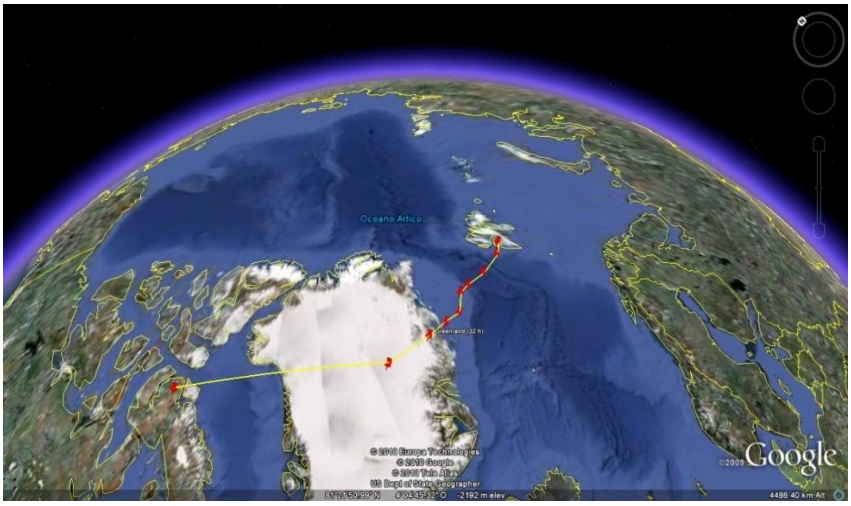

Figure 6.1 Trajectory of the SORA balloon; DUSTER2009 was piggy-back onboard (July 2009)

DUSTER 2009 (Figure 6.2) has some structural differences from DUSTER 2008. The box is still made of aluminium bars (Bosh Rexroth), the external panels being not anymore in aluminum but in Teflon, in order to preserve the thermal equilibrium; they cover the five sides not in contact with SoRa structure. The solar panels are still four but they are positioned on SoRa external box and not in cylindrical structures along the flight train, as it was made for the previous flight.

Some subsystems inside the box have been changed in order to better control the contamination and to improve performances. DUSTER2009 has 12 thermometers instead of 8 used for DUSTER2008 thermal control. The 2 sets of carbon vane volumetric micro-pumps are replaced with only one set; after good results from pump reliability testing, it was decided to have 6 pumps in hot redundancy instead of two sets of 6 pumps in cold redundancy. The gate valve, which isolates the collecting chamber from the pumping system, is replaced with a butterfly high vacuum valve commanded by a stepper motor identical to the one which opens and closes the gate valve between the inlet tube and the collecting chamber. In this way the butterfly valve can be closed before the landing procedures instead of doing it by hand during the recovery procedures, as made for DUSTER2008 flight.

The big change between DUSTER 2008 and 2009 is the presence of an antenna and an IRIDIUM 9601 SBD (Short Burst Data) Transceiver. It has been used to implement a

telecommand/telemetry (TC/TM) system allowing operations control from ground through commanding and housekeeping data transmission. The Iridium SBD service provides: mobile Originated (instrument) messages up to 340 bytes; low uniform global latency (less than 1 minute); mobile Terminated (experimenter) messages up to 270 bytes; global coverage. In this way DUSTER can be perfectly independent from the gondola or the host instrument.

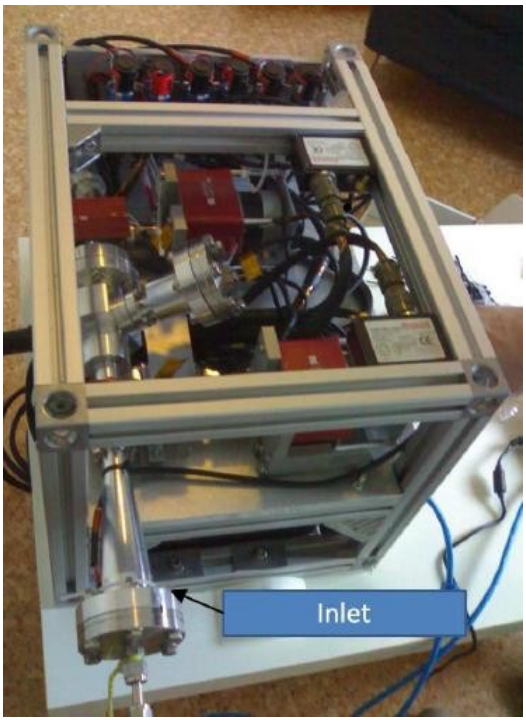

Figure 6.2 DUSTER 2009 instrument

6.1.1 Sample holders

In order to have an easy dismountable sample holder and to be able to perform analyses of the collected sample in transmission mode, the sample holder used during 2009 flight has been totally changed.

It has the same dimensions of the previous collector, but it is totally in stainless steel except for the TEM grids that are still 300 mesh, made in gold and covered with holey carbon thin film. The sample holder is compose of: a round base (0.5 cm thick and 2.3 cm in diameter) with a pin allowing accommodation in the FE-SEM chamber; a thin plate (0.05 cm) pierced with 13 holes not perfectly round, but with a little buttonhole each, to better manipulate the TEM grids; a thin plate (0.05 cm) pierced with 13 holes that has the aim to fix the TEM grids in their positions (Figure 6.3).

Comparing this configuration with the one used on DUSTER 2008, the problem of dismount procedure is solved, with one TEM grid less and without the FE-SEM dedicated smooth area (that was anyhow not used in the DUSTER 2008 data analysis).

Assembling the sample holder still requires adopting all precautions foreseen in a clean room. The sample holder assembling procedure is reported below.

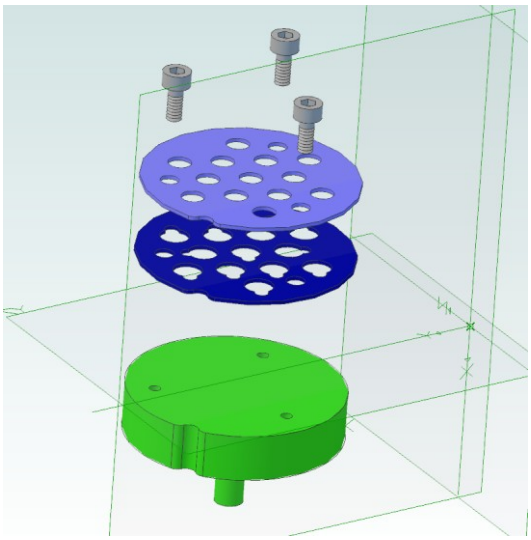

Figure 6.3 DUSTER 2009 sample holder

Assembling procedure

To mount this version of the sample holder the experimenter needs a support (Figure 6.4) designed to help in the assembling procedure and to give the right orientation to the sample holder. In the previous type of collector we had the smooth gold surface defining an orientation of the sample holder, while in this new type we define it with reference to the indentation of the rim. The indentation has to be on the right and the grids are named from up to down and from left to right as shown in Figure 6.5.

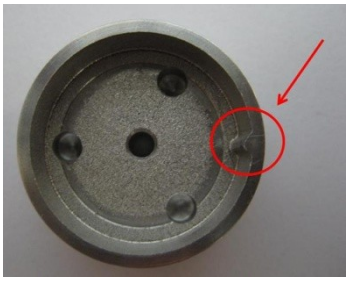

Figure 6.4 Cylinder support. In the red circle is highlighted the reference to orient the sample holder.

Figure 6.5 Sample holder orientation with named grids

Before sample holder assembling, the experimenter has to be sure that all the parts are cleaned with isopropyl alcohol and the procedure has to be done in a laminar flux bench, ensuring a clean controlled environment.

First of all, the cylinder support has to be positioned as shown in Figure 6.4 then the base with the pin and over it the plate with the buttonholes are inserted (Figure 6.6).

Figure 6.6 Cylinder support with the base and the plate with buttonholes

Then, the 13 TEM grids are accommodated in the holes using the micro-tweezers and helping with the buttonhole (Figure 6.7).

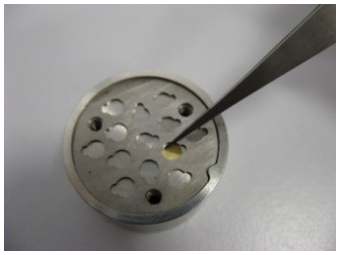

Figure 6.7 Accommodation of TEM grids

The last pierced plate is positioned, being careful not to move the TEM grids and fix all with the 3 screws (Figure 6.8).

Figure 6.8 Fixing procedure of the sample holder

Helping with a screwdriver or an hex key, the sample holder is extracted from the cylinder support (Figure 6.9). Now it is ready for SEM scanning and to be accommodate in the collecting chamber.

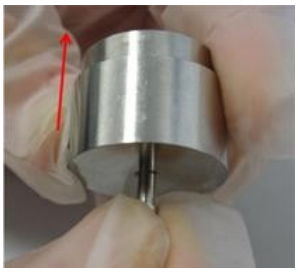

Figure 6.9 Extraction procedure of the sample holder from the cylinder support

6.2 Characterization

The results of DUSTER 2008 flight are affected by two limitations: the instrument is able to collect particles from 0.1 µm size, but the scanning resolution allowed to detect only particles larger than 0.5 µm; the second limitation is due to the gaps that sometimes occurred during scanning (see Chapter 4).

To solve these problems the scanning procedure has been changed, adapting it to the most probably collecting areas, and overlapping the scanning areas by 10% in order to not miss important data. The central area with the highest probability to collect particles is represent from the grids number 3, 4, 6, 7, 8, 10, and 11. These grids were scanned in different areas with different resolution: an area of (20x20) meshes was scanned at 6500 magnifications, each image corresponding to an area of (46x34) µm and a resolution of 0.045 µm each pixel. This scanning needs $4x3^{h}$ per grid, being divided into 4 areas of (10x10) meshes (Figure 6.10).

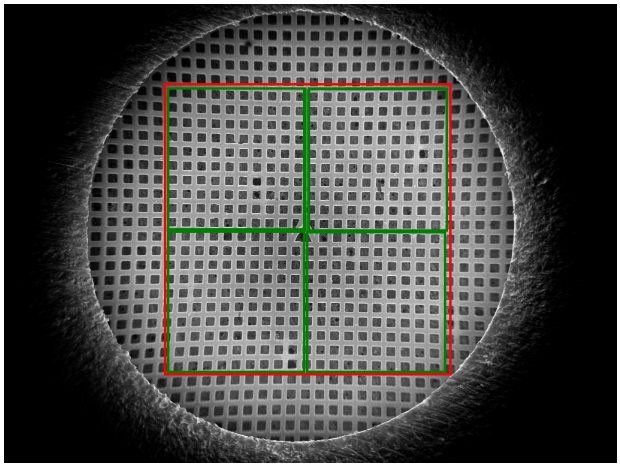

Figure 6.10 Example of TEM grid. The red squere is the area (20x20) meshes, the green squares are the areas (10x10) meshes scanned at 6500 magnifications.

To have a better resolution of most probable collecting areas, the central grids are scanned in the diagonal areas (5x5) meshes at 17000 magnifications (Figure 6.11) corresponding to an image area of (17x13) µm and a resolution of 0.016 µm each pixel; each scanning needs $3^{h}20^{m}$. The remnants areas of the central grids were scanned at 3250 magnifications in few minutes.

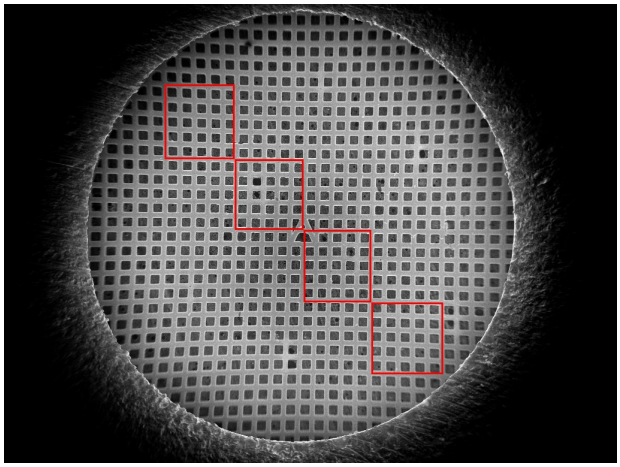

Figure 6.11 Example of TEM grid, the red squares are the (5x5) meshes areas scanned at 17000 magnification.

The lateral grids (1, 2, 5, 9, 12, and 13) were scanned on the entire surface at 3250 magnifications, corresponding to an image area of (92x69) µm and a resolution of 0.090 µm each pixel; this scanning needs $3^{h}50^{m}$.

The sample holder used like Blank has only four grids, three of them are scanned at 3250 magnifications and one is scanned with the same criteria of the Collector's central grids.

6.3 Preliminary results (contamination and collected particles identification)

The results from this campaign are still a work in progress. Only half of the grids are compared and at a preliminary analysis we can see that DUSTER2009 surely collected particles, but at the same time on the collector there is a lot of contamination.

This last one is composed in large amount by soot structures (Figure 6.12) due to a fire developed after landing and involving the main payload of the flight. DUSTER was not directly involved in the fire, but during the landing impact it loose the inlet tube (the only part protruding from the box envelope) and this violent braking caused a leakage in the gate valve, letting some smoke enter.

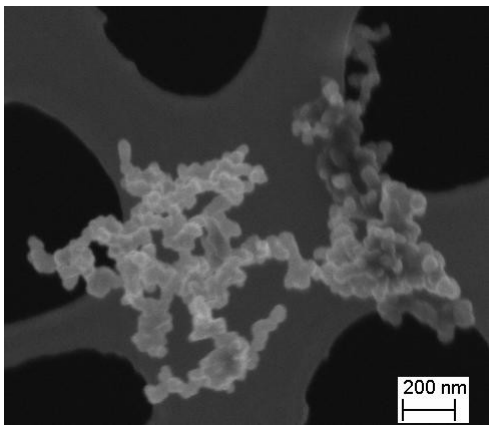

Figure 6.12 Soot structure on DUSTER2009 collector.

For this reason all the soot structures will be consider contamination. They seem to be easy to recognize, but this risks to be a lost if DUSTER2009 had collected extraterrestrial particles that has the same morphology of soot of fire (Figure 6.13).

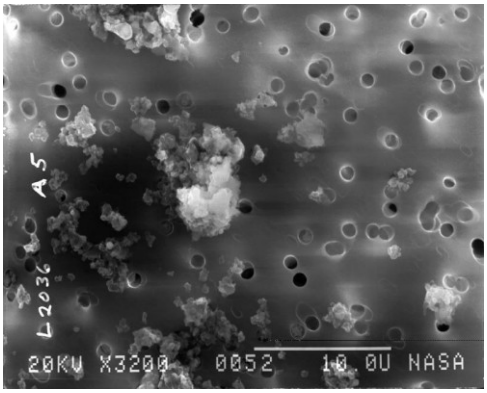

Figure 6.13 IDP NASA collected, Catalogue Vol.15 Johnson Space Centre

The new particles recognized until now, looking at the morphology could be aggregates of condensed particles or dust embedded with soot contamination (Figure 6.14); only compositional analyses will define the origins of these particles. Up to now we haven't identify particles of the size and shape of the two spheres collected during DUSTER 2008 campaign, this would be a proof that particles larger than 100 μm size (too big for DUSTER flow rate) were fortuitous collected.

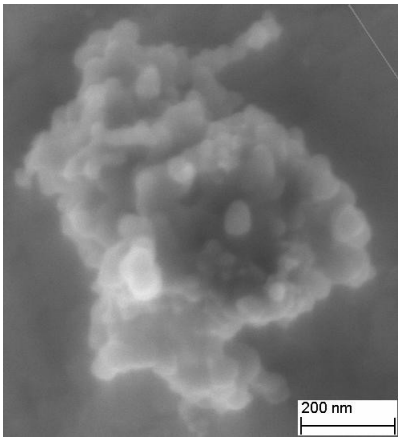

Figure 6.14 Collected particle on DUSTER2009 collector, it could be a fragment embedded with soot structures or an aggregate of condensed.

Conclusions

DUSTER2009 is really autonomous with respect to the 2008 instrument tanks to the own telemetry, and it is designed to better preserve the samples from contamination thanks to the second stepper motor that seal the collecting chamber before the landing procedure. The sample holder is perfectly dismountable and do not damage the TEM grids. From the structural point of view the instrument is improved and it is made autonomous.

For what concern the capability to collect particles, this version of the instrument is more performing than the previous one, but this need to be confirmed based on evaluation of collected particles. Future FESEM-EDX analyses will tell us what kinds of particles have been collected and their size distribution.

Conclusions and future developments

DUSTER is an instrument able to collect dust in the upper stratosphere (30 – 40 km). In the last three years it performed two flights successfully completed. My work was mainly focused on the study of the sample holder structure, in order to facilitate the analyses, preserve the contamination control, and to respect the scientific requirements, and on the analysis of the collected particles. The results concern mainly the DUSTER2008 campaign.

The particles recognized as collected during the DUSTER2008 campaign are 25 in the size range (0.5 – 7.0) μm and two spheres of more than 100 μm . The size range has a main bias in the inferior limit due to the limitation in scanning automatic procedures that not allow to detect particle less than 0.5 μm. Another bias source is due to the holey carbon film substrate, if a particle goes through the holes of the carbon film it is not possible to detect it.

The analyses (FESEM-EDX, FT-IR and Raman) shown silica-rich and calcium carbonates particles. The morphological study suggests that the particles were collected in a dust high density environment probably created by a single source.

Two different scenarios are possible:

1. a terrestrial sources, for example a volcanic ejection or an efficient power plant;
2. an extraterrestrial event that create a lot of fragment, such as a fireball as Tagish Lake (18^{th} January 2000).

The analyses cannot exclude one of the two sources, the only things sure is that in the period of DUSTER collection there were not volcanic ejection except for Chaitén (Chile) in May 2008, but it is in the Southern hemisphere and is improbable that its volcanic ashes reached the Northern stratosphere.

The possibility of the two alternative explanations (terrestrial or extraterrestrial origin) highlight the importance to study the composition of the stratospheric dust above 30 km. The study of the extraterrestrial dust component could provide information on the Solar System origins. The terrestrial component gives information on the terrestrial (natural or anthropogenic) contamination of the stratosphere.

The upper stratosphere is a boundary atmospheric layer where terrestrial and extraterrestrial components coexist, and both have to be studied as determinant factors for climate changing, in local and global scale.

DUSTER2009 was the second successful campaign performed during the last three years. We have not yet final results, the collected particle identification work is in progress. This flight opportunity was the occasion to test the new sample holders configuration. They had a good behavior and preserve the integrity of the TEM grids, by laboratory tests it is proved that they are easily dismountable to allow transmission analyses. A future work for sample holders structure is to find a material to have a smooth surface in order to have a collection surface dedicated to the FESEM analysis.

Another open point for future works is to elaborate a procedure for automatic comparison of the images taken by FESEM to characterize the sample holders pre and post flight, to shorten the collected particles identification phase.

Next DUSTER flight opportunity will be next February (2011) from Kiruna (Sweden), with the CNES (Centre National d'Études Spatiales) support. DUSTER will fly again in a piggy-back configuration demonstrating that the instrument is sufficiently small and light to be guest by a spread variety of balloon campaign.

The final aim of this project is that DUSTER could become a long-term program for high stratospheric dust collection, of terrestrial and extraterrestrial origin. The results of this collection program would be of critical interest for a wide interdisciplinary community.

Bibliography

Anders E., & Grevesse N.,1989.Abundance of the elements: Meteoritic and Solar. Geochem and Cosmochem Acta Vol. 53 Issue 1 pp. 197-214.

Angell J.K., 1997. Stratospheric worming due to Agung, El Chichon, and Piatubo taking into account quasi-biennial oscillation. J Geophys Res Vol.102.

Berthet G., Renard J.B., Brogniez C., Robert C., Chartier M., Pirre M., 2002. Optical and physical properties of stratospheric aerosols from balloon measurements in the visible and near-infrared domains. I. Analysis of aerosol extinction spectra from the AMON and SALOMON balloonborne spectrometers. Applied Optics, Vol.41.

Biermann U.M., Presper T., Koop T., Möinger J., Crut-zen P.J., Peter T., 1996. The unsuitability of meteoritic and other nuclei for polar stratospheric cloud freezing. Geophysical Research Letters. Vol. 23, pp. 1693 – 1696.Brownfield M.E., Affolter R.H., Cathcart J.D., Meeker G.P., Rice C.A., Zielinski R.A., Hower J.C., 2002. Characterization and Models of Occurrence of Elements in Feed Coal and Fly Ash - An integrated approach. USGS Fact Sheet-038-02 May.

Bigg E.K., Ono A., Thompson W.J., 1970. Aerosols at altitudes 20 and 37 km. Tellus XXII, 5, pp.550-563.

Bigg E.K., Kviz Z., Thompson W.J., 1971. Electron microscope photographs of extraterrestrial particles. Tellus XXIII, 3, pp.247-260.

Brenninkmeijer C.A.M., Zahn A., Maiss M., Crutzen P.J., Cuijpers H., Van Velthoven P.F.J., 1998. The ^{13}C, ^{14}C, and ^{18}O isotope composition of CO at 10 km between the tropics and the mid-latitudes; results from the CARIBIC project. American Geophysical Union (AGU), fall meeting, San Francicso, 6-10 December.

Brown P.G, Hildebrand A.R., Zolensky M.E., Grady M., Clayton R.N., Mayeda T.K., Tagliaferri E., Spalding R., MacRae N.D., Hoffman E.L., Mittlefehldt D.W., Wacker J.F., Bird J.A., Campbell M.D., Carpenter R., Gingerich H., Glatiotis M., Greiner E., Mazur M.J., McCausland P.JA., Plotkin H., Mazur T.R., 2000. The Fall, Recovery, Orbit, and Composition of the Tagish Lake Meteorite: A New Type of Carbonaceous Chondrite. Science Vol.290, pp. 320-325.

Brownlee D.E., Hodge P.W., 1973. Ablation debris and primary micrometeoroids in stratosphere. Space Res Vol.13.

Brownlee D.E., Ferry G.V., Tomandl D., 1976. Stratospheric aluminium oxide. Science Vol.191.

Chandra S., 1993. Changes in stratospheric ozone and temperatures due to the eruptions of Mt. Pinatubo. Geophys Res Lett Vol.20.

Curtius J., Weigel R., Vossing H.J., Wernli H., Werner A., Volk C.M., Konopka P., Krebsbach M., Schiller C., Roiger A., Schlager H., Dreiling V., Borrmann S., 2005. Observations of meteoritic

material and implications for aerosol nucleation in the winter Arctic lower stratosphere derived from in situ particle measurements. Amos Chem Phys Discuss Vol.5.

Cziczo D.J., Thomson D.S., Murphy D.M., 2001. Ablation, Flux, and Atmospheric Implications of Meteors Inferred from Stratospheric Aerosol. Science Vol.291.

Dahl K. and Buchardt B., 2006. Monohydrocalcite in the arctic Ikka Fjord, SW Greenland: First reported marine occurrence. Joural of Sedimentary Research, Vol. 76, 460-471.

Della Corte V., Palumbo P., De Angelis S., Ciucci A., Brunetto R., Rotundi A., Rietmeijer F.J.M., Zona E., Bussoletti E., Colangeli L., Esposito F., Mazzotta Epifani E., Mennella V., Peterzen S., Masi S., Ibba R., (2010). DUSTER (Dust in the Upper Stratosphere Tracking Experiment and Retrieval): a balloon-borne dust particle collector. (in press)

Deshler, T., Hervig, M.E., Hofmann, D.J., Rosen, J.M., Liley, J.B., 2003. Thirty years of in situ stratospheric aerosol size distribution measurements from Laramie, Wyoming (41°N), using balloon-borne instruments. Journal of Geophysical Research 108 (D5.), 4167.

Deshler, T., 2008. A review of global stratospheric aerosol: Measurements, importance, life cycle, and local stratospheric aerosol. Atmospheric Research 90, 223–232.

Di Sarra A., Cacciani M., Fiocco G., Fuà D., Jørgensen T.S., 2002. Lidar observations of polar stratospheric clouds over northern Greenland in the period 1990–1997. Journal of Geophysical Research Vol.107, No. D12, pp. 4152-4167.

Dutton E.G., Christy J.R., 1992.Solar radiative forcing at selected locations and evidence for global lower tropospheric cooling following the eruption of El Chichon and Pinatubo. Geophys Res Lett Vol.19.

Flynn G.J., 1997. Collecting interstellar dust grains. Nature, Vol.387.

Genge M.J., Engrand C., Gounelle M., Taylor S. 2008. The classification of micrometeorites. Meteoritics & Planetary science Vol. 43, No 3, 497 – 515.

Gieré R., Carleton L.E., Lumpkin G.R., 2003. Micro- and nanochemistry of fly ash from coal-fired power plant. American Mineralogist, Vol. 88, pp.1853 – 1865.

Grün E., Zook H.A., Fechtig H., Giese R.H., 1985. Collisional balance of the meteoritic complex. Icarus, Vol. 62, No 244.

Grün E., Gustafson B., Mann I., Baguhl M., Morfill G.E., Staubach P., Taylor A., Zook H.A., 1994. Interstellar dust in the heliosphere. Astronomy and Astrophysics, Vol. 286, pp. 915-924.

Hanson D.R., Lovejoy E.R., 1995. The reaction of ClONO2 with submicrometer sulfuric acid aerosol. Science 267, 1326–1328.

Hofmann D.J., Rosen J.M., Harder J.W., Hereford J.V., 1989. Balloon-borne measurements of aerosol condensation nuclei, and cloud particles in the stratosphere at McMurdo Station, Antarctica, during the spring of 1987. J Geophys Res Vol.94.

Hofmann D.J., 1990. Measurement of the condensation nuclei profile to 31 km in the Arctic in January 1989 and comparison with Antarctic measurements. Geophys Res Lett Vol.17.

Hofmann D.J., Oltmans S.J., Harris J.M., Komhyr W.D., Lathrop J.A., Defoor T., Kuniyuki D., 1993. Ozone sonde measurements at Hilo, Hawaii following the eruption of Pinatubo. Geophys Res Lett Vol.20.

Hunten D.M., Turco R.P., Toon O.B., 1980. Smoke and dust particles of meteoritic origin in the Mesosphere and Stratosphere. J Amos Sci Vol.37.

Junge C.E., Chagon C.W., Manson J.E., 1961. Stratospheric Aerosols. Journal of Meteorology Vol.18.

Kent G.S., Farrukh U.O., Wang P.H., Deepak A., 1988. SAGE I and SAM II measurements of 1 μm Aerosol Extinction in the free Troposphere. Journal of applied meteorology, Vol.27.

Kerr R.A., 1983. El Chichon climate effect estimated. Science 219.

Landgraf M., Baggaley W.J., Grun E., Kruger H., Linkert G., 2000. Aspects of the mass distribution of interstellar dust grains in the solar system from in sit measurements. Journal of Geophysical Research, Vol.105, No. A5, pp10343-10352.

Love S.G. and Brownlee D.E., 1994. Peak atmospheric entry temperatures of micrometeorites. Meteoritics 29, pp. 67-70.

Luo K., Xu L., Li R., Xiang L., 2002. Fluoine emission from combustion of steam coal of North China Plate and Northwest China. Chinese Science Bulletin, Vol. 47, No. 16, pp. 1346 – 1350.

Martinsson B.G., Nguyen H.N., Brenninkmeijer C.A.M., Zahn A., Heintzenberg J., Hermann M., van Velthoven P.F.J., 2005. Characteristics and origin of lowermost stratospheric aerosol at northern midlatitudes under volcanically quiescent conditions based on CARIBIC observations. Journal of Geophysical Research, Vol.110, No. D12201.

Mateshvili N. and Rietmeijer F.J.M., 2002. Stratospheric dust loading from early 1981 to September 1985 based on the twilight sounding method and stratospheric dust collections. J Volcanol Geother Res Vol 120.

Mateshvili N., Fussen D., Vanhellemont F., Bingen C., Kyrola E., Mateshvili I., Mateshvili G., 2005. Twilight sky brightness measurements as a useful tool for stratospheric aerosol investigations. J Geophys Res Vol.110.

McDonnell J.A.M., Berg O.E., 1975. Space Research Vol. 15, No. 555.

Meckinnon I.D.R, McKay D.S., Nace G., Isaacs A.M., 1982. Classification of the Johnson Space Center Dust Collection. Proceedings of the thirteenth lunar and planetary science conference , part1 Journal of geophysical research, vol.87, supplement, pages A413-A421, November 15.

McCormick M.P., Hamill P., Pepin T.J., Chu V.P., Swissler T.J., McMaster L.R., 1979. Satellites studies of the stratospheric aerosol. Bull Amer Meteor Soc vol.60.

McCormick, M.P., Thomason, L.W., Trepte, C.R., 1995. Atmospheric effects of the Mt. Pinatubo eruption. Nature 373, 399.

Murphy D.M., Thomson D.S., Mahoney M.J., 1998. In Situ Measurements of Organics, Meteoritic Material, Mercury, and Other Elements in Aerosols at 5 to 19 Kilometers. Science Vol.282.

Parker D.E., Brownscombe J.L., 1983. Stratospheric worming following the El Chichon volcanic eruption. Nature Vol.301.

Pitari G., 1993. A numerical study of the possible perturbation of stratospheric dynamics due to Pinatubo aerosols – Implication for tracer transport. J Atmos Sci Vol.50.

Plane J.M.C., 2003. Atmospheric Chemistry of Meteoric Metals. Chem. Rev. Vol. 103, pp. 4963-4984.

Pueschel R. F, Kinne S.A., 1995. Physical and radiative properties of Arctic atmospheric aerosols. The Science of the Total Environment, Vol. 160, pp. 811 – 824.

Qing Sun, Guoqiang Chu, Jiaqi Liu, Denyi Gao, 2006. A 150 – year Record of Heavy Metals in the Varved Sediments of Lake Bolterskardet, Svalbard. Arctic, Antarctic, and Alpine Research, Vol. 38, No. 3, pp. 436 – 445.

Renard J.-B., Ovarlez J., Berthet G., Fussen D., Vanhellemont F., Brogniez C., Hadamcik E., Chartier M., Ovarlez H. 2005. Optical and physical properties of stratospheric aerosols from balloon measurements in the visible and near-infrared domains. III. Presence of aerosols in the middle stratosphere. Applied Optics, Vol.44, No.19, pp. 4086 – 4095.

Rietmeijer F.J.M., 1989. Tin in a chondritic interplanetary dust particle. Meteoritical society 24, 43 - 47.

Rietmeijer F.J.M. (1993) Volcanic dust in the stratosphere between 34 and 36 km altitude during May, 1985. J. Volc. Geothermal Res. 55, 69-83.

Rietmeijer F.J.M., 2000. Interrelationships among meteoric metals, meteors, interplanetary dust, micrometeorites, and meteorites. Meteoritics Planet Science, Vol. 35, pp. 1025 – 1041.

Rietmeijer F.J.M., 2002. The Earliest Chemical Dust Evolution in the Solar Nebula. Chemie der Erde, Geochemistry, 62, 1, pp. 1-88.

Rodhe H., 1985. The transport of sulphur and nitrogen through the remote atmosphere. *The Biochemical Cycling of Sulphur and Nitrogen in the Remote Atmosphere*, Galloway J.N. et al., Eds., NATO ASI Series C, Vol. 159, 105 – 124.

Rotundi A., Rietmeijer F.J.M., Brucato J.R., Colangeli L., Mennella V., Palumbo P., Bussoletti E., 2000. Refractory comet dust analogues by laser bombardment and arcdischarge production: a reference frame for ``dusty experiments'' on-board ROSETTA. Planetary and Space Science, Vol. 48, pp.371-384.

Saxena V.K., Shaocai Yu, Anderson J., 1997. Impact of stratospheric volcanic aerosols on climate: evidence for aerosol shortwave and longwave forcing in the southeastern U.S. Atmospheric Environment, Vol. 31, No. 24, pp. 4211-4221.

Taylor S., Lever J.H., Harvey R.P., 2000. Numbers, types and compositions of an unbiased collection of cosmic spherules. Meteoritics & Planetary science 35, 651 – 666.

Testa Jr.J.P., Stephens J.R., Berg W.W., Cahill T.A., Onaka T., 1990. Collection of microparticles at high balloon altitudes in the stratosphere. Earth and Planetary Science Letters, Vol.98.

US Standard Atmosphere 1976. U.S. Government Printing Office, Washington, D.C., 1976

Vassilev S.V. and Vassileva C.G., 1997. Geochemistry of coals, coal ashes and combustion wastes from coal-fired power stations. Fuel processing technology 51, 19-45.

Wilson J.C., Stolzenburg M.R., Clark W.E., Loewenstein M., Ferry G.V., Chan K.R., 1990. Measurement of condensation nuclei in the airborne Arctic stratospheric expedition: Observations of particle production in the polar vortex. Geophys Res Lett, Vol.17.

Wilson J.C., Stolzenburg M.R., Clark W.E., Loewenstein M., Ferry G.V., Chan K.R., Kelly K.K. 1992. Stratospheric sulfate aerosol in and near the Northern Hemisphere polar vortex: The morphology of the sulfate layer, multimodal size distributions, and the effect of denitrification. J Geophys Res Vol.97.

Xu, L., Okada, K., Iwasaka, Y., Hara, K., Okuhara, Y., Tsutsumi, Y., Shi, G., 2001. The composition of individual aerosol particle in the troposphere and stratosphere over Xianghe (39.45°N, 117.0°E), China. Atmospheric Environment, 35.

Zolensky M.E. and Mackinnon I.D.R., 1985. Accurate stratospheric particles size distribution for a flat plate collection surface. J Geophys Res.

Zolensky M.E., McKay D.S., Kaczor L.A., 1989. A tenfold increase in the abundance of large solid particles in the stratosphere, as measured over the period 1976-1984. J Geophys Res Vol.94.

Zolensky M.E. and Warren J.L., 1994. Collection and curation of interplanetary dust particles recovered from the stratosphere. Conf Proc Workshop on Analysis of IDPs.

Acknowledgements

I wish to thank Prof. Pasquale Palumbo, Prof. Alessandra Rotundi and Ing. Della Corte Vincenzo, for the support they gave me with theirs advices and to be a guide during these last three years.

I wish to sincerely express my gratitude to Prof. Frans J.M. Rietmeijer to be a lighthouse in the darkness.

A special thank to all my family that support me in every step of my life.

A particular thanks goes to the marvelous friends, to be near me in each good and bad moment, thanks to Mauro, Michele, Simone and Vincenzo.

Thanks also to all the group of 'Laboratorio di Fisica Cosmica e Planetologia' and to Antonella Continanza.

Last but not least thanks to Prof. Antonio Moccia for his valuable availability as coordinator of the Aerospace Engineer PhD school.

I apologize if I forgot someone.